

Dissertation zur Erlangung des Doktorgrades
der Fakultät für Chemie und Pharmazie
der Ludwig-Maximilians-Universität München



Iron-polyphenol peptide nanoparticles for intracellular delivery

Faqian Shen

aus

Chizhou, Anhui, China

2023

Erklärung

Diese Dissertation wurde im Sinne von § 7 der Promotionsordnung vom 28. November 2011 von Herrn Prof. Dr. Ernst Wagner betreut.

Eidesstattliche Versicherung

Diese Dissertation wurde eigenständig und ohne unerlaubte Hilfe erarbeitet.

München, 05.07.2023

.....
Faqian Shen

Dissertation eingereicht am: 19.07.2023

1. Gutachter: Prof. Dr. Ernst Wagner

2. Gutachter: Ass.-Prof. Dr. Ulrich Lächelt

Mündliche Prüfung am: 14.09.2023

To my family

致家人

Do not, for one repulse, give up the purpose that you resolved to effect.

— **William Shakespeare, British dramatist**

Table of Contents

1	Introduction.....	3
1.1	Iron-based MPNs for drug delivery.....	3
1.1.1	Iron-based MPNs.....	3
1.1.2	Iron-based MPNs for cancer therapy with synergistic ROS effect.....	4
1.2	Peptide therapeutics.....	6
1.2.1	Current state.....	6
1.2.2	Advantages and disadvantages of peptide therapeutics.....	9
1.2.3	Strategies for overcome the shortcoming of peptides.....	11
1.2.4	Peptides as a platform for drug delivery.....	12
1.3	Aim of this thesis.....	13
2	Materials.....	15
2.1	Chemicals.....	15
2.2	Cell lines.....	15
3	Methods.....	16
3.1	Nuclear magnetic resonance (NMR):.....	16
3.2	MALDI-TOF mass spectrometry:.....	16
3.3	ESI mass spectrometry:.....	16
3.4	Analytical reversed-phase high performance liquid chromatography (RP-HPLC):.....	16
3.5	Transmission electron microscopy (TEM):.....	17
3.6	X-ray photoelectron spectroscopy (XPS):.....	17
3.7	X-ray diffraction (XRD):.....	17
3.8	Dynamic light scattering (DLS) and zeta-potential measurements:.....	17
3.9	Thermogravimetric analysis (TGA):.....	18
3.10	UV-Vis spectroscopy:.....	18
3.11	Synthesis of 3,4,5-tri-O-(tert-butoxycarbonyl)-gallic acid.....	18
3.12	General synthesis of peptides.....	19
3.13	Synthesis of iron-gallic acid peptide nanoparticles (IGPNs).....	20
3.14	Investigation of the stability of IGPNs in different media.....	20
3.15	Methylene blue assay.....	20

3.16	Cell culture.....	21
3.17	Evaluation of ROS generation by flow cytometry	21
3.18	Evaluation of ROS generation by confocal laser scanning microscopy (CLSM)	21
3.19	Evaluation of cellular uptake by flow cytometry	22
3.20	Evaluation of cellular uptake by confocal laser scanning microscopy (CLSM).....	23
3.21	Evaluation of cell viability (CellTiter-Glo assay).....	23
3.22	Apoptosis assay	24
4	Results and discussion.....	25
4.1	Synthesis of gallic acid-tagged peptides	25
4.2	Synthesis and characterization of Iron Gallic Acid Nanoparticles (IGPNs).....	27
4.3	Cellular uptake of IGPNs	38
4.4	ROS production of IGPNs	40
4.5	Bioactivity of IGPNs	42
5	Summary	47
6	Abbreviations	48
7	Analytical data	50
8	References	71
9	Publication	86
10	Acknowledgements	87

1 Introduction

In this part, a concise description of the recent progress in iron-based MPNs (metal-phenolic networks) for drug delivery and peptide therapeutics with their strategies for the intracellular delivery of peptides is given.

1.1 Iron-based MPNs for drug delivery

This part will focus on the introduction of iron-based MPNs and its purpose for cancer therapy with a synergistic ROS enhancement effect.

1.1.1 Iron-based MPNs

Over the past decade, MPNs entered into the realm of therapeutics research gradually, such as antibacterial therapy and antitumor therapy.^{1,2} MPNs are three-dimensional stable supramolecular organic-inorganic hybrid networks formed through coordination between various metal ions and polyphenolic ligands. Polyphenolic compounds possess inherent properties, such as metal chelation, pH reactivity, redox potential, polymerization, and photo-absorption. These networks exhibit similarities to metal-organic framework (MOF) materials.³ However, compared with MOF nanomaterials, MPNs possess several advantages, including excellent safety, faster and cost-effective preparation methods, and environmental friendliness.^{4,5} Nanoparticles based on MPNs take advantages of the interactions between metal ions and phenolic molecules to confer favorable characteristics, such as exceptional thermal stability and pH sensitivity.^{4,6,7} As studied by Xu, et al., by adjusting the multimodal iron coordination involving catechol, carbonyl, and hydroxyl groups within the MPNs, it is feasible to manipulate a wide range of physicochemical characteristics, such as size control, selective permeability by fluorescein isothiocyanate (FITC)-dextran within the range of 20-2000 kDa, and pH-dependent degradability.⁸ The utilization of natural polyphenols and molecules that possess catechol or galloyl groups, such as tannic acid (TA), gallic acid (GA), and epigallocatechin gallate (EGCG), dopamine (DOPA) have been reported as the phenolic

ligand for MPNs.⁹⁻¹³ Meanwhile, metal ions like Fe^{3+} , Cu^{2+} , Zn^{2+} , Mn^{2+} , Ni^{2+} , and Co^{3+} were successfully applied to coordinate with polyphenols to create MPNs.^{14,15}

Iron (Fe) is one of the common essential trace elements found in the human body, playing a crucial role in various physiological processes. It exhibits a particularly strong connection with the immunity, enhancing the body's ability to resist infections and low biotoxicity.¹⁶ Hence, iron stands out as a promising candidate for therapeutic applications. In addition, the polyphenolic compound gallic acid (GA) features several favorable characteristics for biomedical applications, such as antioxidant, anti-inflammatory, antimicrobial, and antitumoral properties and is suggested as beneficial agent for the treatment of diabetes and cardiovascular diseases.¹⁷⁻²² These properties enable GA to serve as building blocks for developing iron-based MPN materials with multiple functionalities.

1.1.2 Iron-based MPNs for cancer therapy with synergistic ROS effect

To date, cancer is one of the leading threats of human health behind the heart and circulatory disorders.²³ Various cancer treatments such as surgical resection, chemotherapy, radiotherapy, and immunotherapy have been developed and demonstrated some efficacy in suppressing tumor growth.²⁴⁻²⁹ Nonetheless, due to their lack of tumor specificity, potential development of therapeutic resistance, and challenging tumor microenvironments (TME), these existing cancer treatments are still hindered by limited therapeutic effectiveness and severe side effects.¹ Therefore, there is an urgent need to develop innovative strategies that can achieve more potent and safer cancer treatments.

Recently, iron-based nanoparticle systems, such as iron nanometallic glasses, iron oxide, and metal polyphenol networks (MPNs), have been utilized as drug delivery vehicles and as agents that generate reactive oxygen species (ROS) for the purpose of treating cancer.³⁰⁻³² ROS, including peroxide (O_2^{2-}), $\text{O}_2^{\cdot-}$, hydroxyl radical ($\text{HO}\cdot$), and singlet oxygen ($^1\text{O}_2$), play crucial roles in cell signaling and homeostasis during various biological processes.^{33,34} The Fenton reaction, contained in iron-based MPNs, can transform hydrogen peroxide (H_2O_2) into free radicals with the help of iron.³¹ Moreover, polyphenol

could accelerate the conversion from Fe(III) (low catalytic efficiency) into Fe(II) (high catalytic efficiency), resulting in a significantly enhanced Fenton reaction.³⁵ High level of ROS within the organism can induce oxidative harm to cellular components and impair proper cellular metabolism.³⁶ To be specific, the concept of the ROS threshold is used to elucidate the varying vulnerability of tumor cells and non-tumor cells to approaches that produce reactive oxygen species (ROS). While a certain level of ROS is necessary for cell survival, an excessive amount of ROS leads to cell death. Non-tumor cells typically generate lower levels of ROS and possess robust antioxidant mechanisms. When therapeutic approaches elevate ROS levels, tumor cells surpass the threshold for cell death sooner, making them more susceptible to elimination. This distinction provides an opportunity for ROS-promoting therapies.³⁷ Thus, the induction of ROS from external sources represents a promising strategy for cancer treatment.

Multiple polyphenols and their derivatives can be employed to coordinate with Fe for cancer therapy with ROS synergistic effect. In order to discover new pathways for overcoming multidrug resistance (MDR) of cancer, Guo et al. prepared the dendrimer (Den)-doxorubicin (DOX)-tannic acid-Fe³⁺ (DDTF) nanocomplex by mixing the metal-phenolic network formed by tannic acid and Fe³⁺ with the DOX-loaded Den, which can combat MDR of cancer cells via an apoptosis/ferroptosis hybrid pathway.³⁸ Dong et al. developed a kind of ultras-small nanocomplexes composed of gallic acid-ferrous (GA-Fe(II)), serving as catalysts for the Fenton reaction and facilitating the continuous conversion of H₂O₂ into highly cytotoxic hydroxyl radicals (HO•). This process effectively amplifies intracellular oxidative stress, leading to cancer cell death.³⁹ Yu et al. formed another versatile nanotherapeutic agent, called FeEP-NPs, through a one-pot self-assembly technique based on the coordination between Fe and (-)-epigallocatechin gallate (EGCG), with poly(vinylpyrrolidone) serving as a stabilizer. The engineered FeEP-NPs demonstrated efficient generation of the toxic hydroxyl radical (HO•) through the Fenton reaction, thereby enabling effective chemodynamic therapy (CDT).¹² Additionally, to address challenges such as multidrug resistance (MDR) and minimizing drug toxicity in normal tissues, Chen et al. designed and fabricated a core structure comprised of glucose

oxidase (GOx)-attached Fe₃O₄ nanoparticles, while their shell layer consists of PEGylated metal-phenolic networks (MPNs) loaded with the prodrug form of doxorubicin (pDOX).⁴⁰

To sum up, iron-based MPNs act not only as the carriers for antitumor drugs, but also as the reactive oxygen species (ROS) enhancing agent through Fenton reaction. Therefore, the exploration of Iron-based MPNs presents a highly promising approach for the combination therapy against cancer.

1.2 Peptide therapeutics

In recent years, there has been a revival of interest and scientific progress in the field of peptide drug discovery. The pharmaceutical industry has recognized the significant potential of peptide therapeutics in addressing unmet medical needs. This class of compounds is now seen as an excellent complement or even a preferable alternative to small molecule and biological therapeutics.

1.2.1 Current state

Peptides are a distinctive category of biomolecules that have found a therapeutic niche due to their unique biochemical and therapeutic properties. The intermediate nature between small molecule drugs and therapeutic biologics enables peptides to combine their benefits while avoiding their respective drawbacks.⁴¹ By virtue of their molecular weight, peptides were defined by the IUPAC and US FDA as a polymer composed of less than 50 amino acids (500-5000 Da), between small chemical molecules (< 500 Da) and biologics (> 5000 Da).^{27,42} Nevertheless, the boundary of 50 residues is not an absolute rule, and some scientists differentiate peptides from proteins based on their synthetic feasibility.⁴³ However, recent advances in synthesis techniques have also made it possible to synthesize small proteins.⁴⁴

The impact of peptides on the modern pharmaceutical industry has been significant, and they have played a crucial role in advancing the fields of biological and chemical science. In first half of the 20th century, the study of the structures and physiological functions of

peptide hormones like insulin, oxytocin, gonadotropin-releasing hormone, and vasopressin had a profound impact on the fields of pharmacology, biology, and chemistry, as well as other technologies that were crucial for modern drug discovery. These fundamental investigations acted as a catalyst for numerous major advancements.⁴⁵ Towards the end of 20th century, there was a notable emergence of a new category of peptides therapeutics that differed significantly from small molecule drugs in size. This progress was driven by advancements in recombinant protein expression and other molecular biology tools, improved protein purification techniques and analysis tools, and the discovery that proteins possess exceptional potency and selectivity towards their molecular targets.²⁷ Contemporarily, particular attention was attracted on peptide therapeutics, with a strong emphasis on macrocyclic peptides. These peptides possess a distinct size and extensive binding surface area, which allows them to effectively target protein-protein interactions (PPI) and other challenging, hard-to-treat targets.^{46,47}

Over the past two decades, there has been a notable surge in the exploration of peptide-based drugs. Over 60 new, non-insulin peptide drugs (Table 1) were approved worldwide since 2000, with several achieving significant market success.^{48,49} All these peptide drugs have found extensive use in various therapeutic fields, including pain management, oncology, urology, respiratory, metabolic disorders, cardiovascular diseases, and antimicrobial treatments.⁵⁰ Currently, more than 170 peptides are undergoing active clinical development, and numerous others are being studied in preclinical research.⁵⁰ During the transition from Phase II to Phase III of drug development, peptides are demonstrating superior performance compared to small molecules, with a success rate of 42% for peptides compared to 29% for small molecules.⁵¹ This favorable performance of peptides, as well as their advantageous characteristics and recent innovative advancements in their discovery, have generated significant interest in peptides as a promising class of drugs.^{27,52,53}

Table1. Non-insulin Peptides Approved in the Years 2000–2022

Peptide name	Year of approval	Approved indication(s)	Peptide name	Year of approval	Approved indication(s)
Atosiban	2000	obstetrics	Angiotensin II	2017	hematology
Taltirelin	2000	Central nervous system	Semaglutide	2017	metabolic disease
Aviptadil	2000	urology	Etelcalcetide	2017	hemodialysis
Carbetocin	2001	obstetrics	Macimorelin	2017	endocrinology
Nesiritide	2001	cardiovascular	¹⁷⁷Lu Dotatate	2018	oncology
Teriparatide	2002	osteoporosis	Edotreotide	2019	oncology
Enfuvirtide	2003	antiinfective	Gallium Ga-68		
Abarelix	2003	oncology	Bremelanotide	2019	endocrinology
Ziconotide	2004	pain	Afamelanotide	2019	hematology
Pramlintide	2005	metabolic disease	Enfortumab Vedotin	2019	oncology
Exenatide	2005	metabolic disease	Polatuzumab Vedotin	2019	oncology
Icatibant	2008	hematology	Trastuzumab Deruxtecan	2019	oncology
Romiplostim	2008	hematology	Setmelanotide	2020	metabolic disease
Degarelix	2008	oncology	⁶⁴Cu-Dotatate	2020	imageology
Mifamurtide	2009	oncology	Gallium (⁶⁸Ga) Gozetotide	2020	oncology
Liraglutide	2009	metabolic disease	Belantamab Mafodotin	2020	oncology
Tesamorelin	2010	antiinfective	Pegcetacoplan	2021	metabolic disease
Lucinactant	2012	pulmonary	Vosoritide	2021	achondroplasia
Peginesatide	2012	hematology	Melphalan-Flufenamid	2021	oncology
Pasireotide	2012	endocrinology	Voclosporin	2021	lupus nephritis
Carfilzomi	2012	oncology	Dasiglucagon	2021	hypoglycemia
Linaclotide	2012	gastroenterology	Piflufolastat-F18	2021	imageology
Teduglutide	2012	gastroenterology	Difelikefalin	2021	hemodialysis
Lixisenatide	2013	metabolic disease	Odevixibat	2021	metabolic disease
Albiglutide	2014	metabolic disease	Tisotumab Vedotin	2021	oncology
Oritavancin	2014	antiinfective	Loncastuximab Tesirine	2021	oncology
Dulaglutide	2014	metabolic disease	Terlipressin	2022	hepatorenal syndrome
Afamelanotide	2014	dermatology	Daxibotulinumt-oxinA	2022	glabellar lines
			Olipudase Alfa	2022	endocrinology

Lxazomib Ninlar	2015	multiple myeloma	Tebentafusp	2022	melanoma
Abaloparatide	2017	osteoporosis	Sutimlimab	2022	cold agglutinin disease
Plecanatide	2017	chronic idiopathic constipation	Faricimab	2022	metabolic disease

Data taken from ^{45,48,49}.

On the other hand, the remarkable and simultaneous success of recombinant biologics have prompted a reconsideration of the peptide field for potential prospects, given their common biological traits and scientific advancements that are applicable to both areas.⁴⁵ Furthermore, methods, employed to produce peptides, play an important role in the widely application of peptide therapeutics. Since Merrifield introduced solid-phase peptide synthesis (SPPS) in 1963,⁵⁴ and recent advances in flow-SPPS,⁴⁴ chemical synthesis was revolutionized by offering rapid and reliable access to peptides and small proteins, while convergent synthesis in solution and chemical ligation are for large-scale production or peptides larger than 50 amino acids. Enzymatic synthesis is among other strategies, as well as the utilization of expression systems such as cell-free or recombinant systems, transgenic animals, and plants.⁵⁵ As a result of these accomplishments, pharmaceutical corporations have been motivated to make substantial enhancements in their investments towards the discovery of peptide-based drugs.

1.2.2 Advantages and disadvantages of peptide therapeutics

Small molecule drugs are renowned for their extensive history of therapeutic use, and possess inherent benefits such as economical production and sale, oral delivery, and favorable membrane permeability.⁵⁶ Both naturally derived and chemically manufactured small molecules offer cost competitiveness when compared to peptides and biologics (which include proteins or antibodies).^{57,58} Nonetheless, their small structure makes it challenging to effectively modulate extensive surface interactions, such as protein-protein interactions (PPIs). PPIs play significant role in numerous cellular processes and influence biological functions by causing changes in protein characteristics, including enzymatic activity, subcellular localization, and/or binding properties.⁵⁹ Typically, PPIs cover an interaction area of 1500-3000 Å², whereas small molecules can embrace only 300-1000

A² of the protein surface, owing to their restricted molecular size.⁶⁰ The clinical use of small molecules is also limited by their low specificity compared with peptide drugs.⁶¹ When compared to small molecules, peptides provide heightened potency, selectivity, and specificity, while displaying diminished off-target toxicity and reduced potential for drug-drug interactions. On the other hand, in contrast to proteins, peptides exhibit enhanced activity per unit mass, superior tissue penetration, reduced immunogenic potential, and lower manufacturing expenses (synthesis for small peptides as opposed to recombinant production for proteins).⁶² Moreover, peptides generally exhibit moderate molecular weights, and feature structural diversity and conformational flexibility at the same time which can be tuned to specific bio-interactions.⁴¹ From the physicochemical perspective, bioactive peptides fill the gap between small molecule drugs and large macromolecular biologics, which can mediate therapeutic effects by interference with cellular process and interactions with target receptors.⁶³ It was demonstrated that these remarkable biomolecules are suitable to treat cancer, vascular diseases and microbial infection.⁶⁴ Furthermore, their design flexibility and feasible modification enables generation of sequences with favorable solubility, target selectivity, low toxicity and immunogenicity leading to safe and economic therapeutics.^{65,66}

Nevertheless, certain limitations hinder the broad clinical application of peptides, such as short half-life and susceptibility to enzymatic degradation. In addition, the membrane impermeability of polar, macromolecular peptides generally restricts applicability to extracellular targets, such as cell surface receptors, ion channels, or secreted proteins.^{42,67}, posing significant obstacles in the development of peptide drugs.

- i. Peptides have poor biological stability. While natural peptides are composed of amino acids linked by amide bonds, they do not possess the stability that results from secondary or tertiary structures.⁵⁰
- ii. Peptides are membrane impermeable. Several factors, including the length and amino acid composition of peptides, affect their ability to permeate the membrane. Peptides usually face difficulty in crossing the cell membrane to reach intracellular targets, which restricts their potential use in drug development.⁵³

The inherent pros and cons of peptides pose obstacles for peptide drug development, but they also offer prospects and pathways for the refinement and customization of peptide drug design.

1.2.3 Strategies for overcome the shortcoming of peptides

Advanced chemical and nanoengineering methods have been employed to conquer biological barriers. To unravel the full potential of peptide drugs and extend the pharmacological space of 'druggable' targets toward the intracellular environment, diverse strategies were developed, such as peptide cyclization, variation of the sequence length and side chains and conjugation to cell-penetrating peptides (CPPs).⁶⁸ Specifically, the methods can be classified into two categories - the direct enhancement of the properties of the therapeutic compound that change its chemical structure, while the employment of nanoparticles that address certain drawbacks without modifying the peptide's structure.^{44,69-72} These cutting-edge technologies signify a promising shift in the approach towards developing peptides as effective therapeutic agents and distinctive molecular tools.

In the realm of peptides, cyclization methods have been extensively utilized and accomplished through various approaches, such as cyclization from head to tail, from head/tail to side chain, or from side chain to side chain.^{73,74} Cyclization can tackle protein-protein interactions, enhance affinity, extend the target's retention period, and consequently prolong the half-life.^{75,76}

Recently, many research papers focused on directly modifying amino acids were published.^{46,50,75,77} As an instance, substituting L-amino acids with D-amino acids (L-Trp to D-Trp).⁷⁸ Another promising avenue for modification is increasing the size of the side chain which leads to greater stability due to the disruption of enzyme recognition, but without assist for cell permeability.⁷⁹ Furthermore, recent advancements in chemical and enzymatic synthesis technologies have significantly improved the accessibility of synthetic non-natural amino acids. As a result, peptides can now be engineered with unprecedented precision and control, thereby expanding their potential applications. For example, the

incorporation of reactive side chains into peptides enables the formation of covalent crosslinks, which can enhance their stability and binding affinity towards target molecules.⁸⁰⁻⁸² However, non-natural chemical building blocks as side chains may bring the risk of side effects, such as toxicity or immunogenicity.⁸³

When assessing renal clearance, it is important to take into account the total net charge of a peptide sequence. Peptides that have a net negative charge tend to have a longer half-life than those with a net positive charge.⁸⁴ Moreover, there are many other approaches to prolong plasma stability, such as by modifications at the N- and C-terminus,⁷⁹ and to slow down the renal clearance, by conjugation of peptides with larger molecules (such as HSA), PEGylation,⁸⁵ PASylation.⁷⁷

1.2.4 Peptides as a platform for drug delivery

Peptides present a versatile platform that can deliver cargos to designated targets while also exhibiting biological activity. Consequently, they have emerged as a promising tool for developing targeted therapeutics, particularly in the field of oncology. PDC (peptide-drug conjugates) presents a versatile approach that provides an excellent opportunity for delivering payloads and imaging agents, enabling the identification of the tumor location or determination of tumor progression.^{86,87} However, PDCs suffer from the same limitations as peptides, namely poor stability in circulation and rapid renal clearance, which are one of their primary drawbacks. The utilization of nanoparticles presents a promising solution to overcome the poor stability in circulation and rapid renal clearance associated with PDCs and peptides.^{88,89} Nanoparticles have been extensively studied for their ability to improve drug delivery, primarily due to their unique physical and chemical properties. They have a high surface area-to-volume ratio, which allows for increased drug loading, and their physiological property enables them to penetrate tissues more efficiently.⁹⁰ Moreover, nanoparticles can be designed to have specific surface properties that enable them to evade the body's immune system, leading to longer circulation times and enhanced accumulation at the tumor site.

1.3 Aim of this thesis

Considering economic synthesis and retention of activity, nanoparticles (NPs) play an increasing role for the delivery of biomacromolecules into cells, including therapeutic peptides.⁹¹⁻⁹⁵ Several researchers have confirmed that encapsulation of peptides into NPs significantly improves proteolytic stability and cellular uptake.^{96,97} However, in contrast to nucleic acids which can be encapsulated by nanocarriers via electrostatic interactions almost quantitatively, the diverse physicochemical properties of peptides impede the development of generic strategies for a facile, flexible and efficient cargo loading. Consequently, the general lack of active loading mechanisms frequently leads to low encapsulation efficiencies and loading capacities. Therefore, new concepts for delivery of bioactive peptides with facile and high loading efficiency, for instance via self-assembly is still a challenging task.

The aim of this thesis has been to develop a novel generic platform for the quantitative assembly of peptides into nanoparticles and efficient cellular delivery. More specifically, a protected gallic acid (GA) derivative 3,4,5-tris((tert-butoxycarbonyl)oxy)benzoic acid⁹⁸ was planned to be used for the preparation of GA-functionalized peptides via solid-phase synthesis, which should assemble into iron-gallic acid peptide nanoparticles (IGPNs) via coordinative interaction with Fe^{3+} . In view of potential applications in cancer therapy, pro-apoptotic peptides^{99,100} had to be encapsulated into IGPNs. It was expected that multi-leveled anti-tumor effects could be achieved by the combination effect with intrinsic ROS generation enhanced by the nanomaterial. $\text{Fe}^{2+}/\text{Fe}^{3+}$ can catalyze the conversion of endogenous H_2O_2 into highly reactive hydroxy radical ($\text{HO}\cdot$) through Fenton reaction (Figure 1).^{9,101} In this process, polyphenols contribute by accelerating the reduction of Fe^{3+} to Fe^{2+} .³⁵ It was the hope that this strategy would lead to therapeutic nanoparticles exclusively composed of functional components: bioactive peptides as well as ROS generating Fe^{3+} and gallic acid. In this research, the feasibility to assemble different peptides into IGPNs and trigger intracellular effects had to be systematically investigated. If successful, the proposed platform provides a promising therapeutic direction for delivery

of antitumoral peptides accompanied by synergistic chemodynamic effects via intracellular ROS generation.

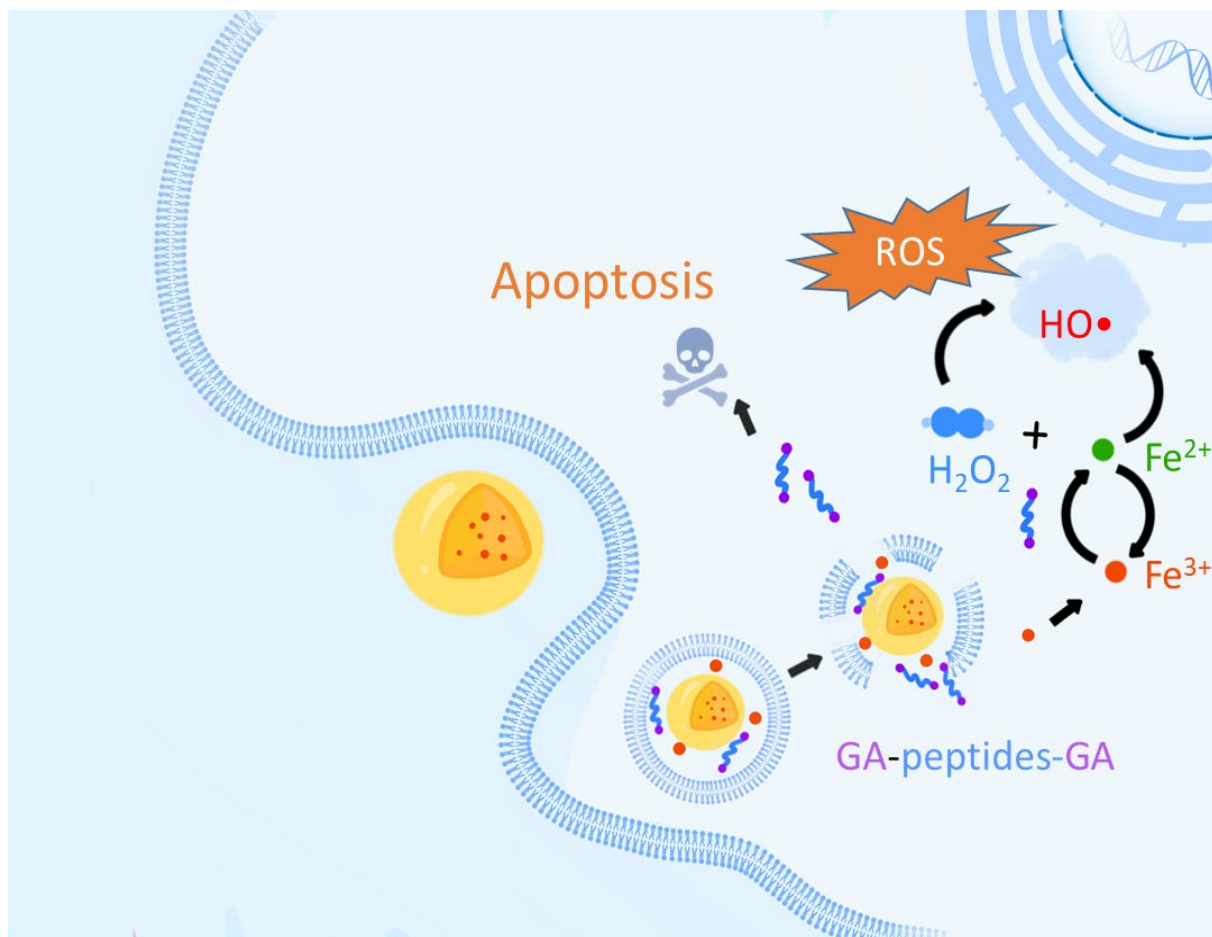


Figure 1. Illustration of combined antitumoral affects mediated by IGPNs containing gallic acid (GA) modified apoptotic peptides and Fe³⁺.

2 Materials

2.1 Chemicals

Gallic acid (Sigma-Aldrich, Burlington, MA, USA), anhydrous DCM AcroSeal® (Acros Organics, Geel, Belgium), di-tert-butyl dicarbonate (DIBOC, Sigma-Aldrich), *N,N*-diisopropylethylamine (DIPEA, Iris Biotech), ethyl acetate (Sigma-Aldrich), 4-(dimethylamino)pyridine (DMAP, Sigma-Aldrich), 2-chlorotriyl chloride resin (Iris Biotech), Fmoc-L-Lys(Boc)-OH, Fmoc-L-Lys(Dde)-OH, Fmoc-L-Ala-OH, Fmoc-L-Thr(tBu)-OH, Fmoc-L-Gln(Trt)-OH, Fmoc-L-Pro-OH*H₂O, Fmoc-L-Val-OH, Fmoc-L-Leu-OH, Fmoc-Gly-OH, Fmoc-L-Glu(tBu)-OH*H₂O (Iris Biotech), 1-hydroxybenzotriazole (HOBT, Sigma-Aldrich), benzotriazole-1-yl-oxy-tris-pyrrolidino-phosphonium hexafluorophosphat (PyBOP, Multisynthet GmbH, Witten, Germany), methanol anhydrous AcroSeal® (Acros Organics), *N,N*-dimethylformamide (DMF, Iris Biotech, Marktredwitz, Germany), dichloromethane (DCM, Bernd Kraft, Nordrhein-Westfalen, Germany), *N*-methyl-2-pyrrolidone (NMP, Iris Biotech), trifluoroacetic acid (TFA, Thermo Scientific, Waltham, MA, USA), piperidine (Iris Biotech), hydrazinium hydroxide (Sigma-Aldrich), methyl-tert-butyl ether (Brenntag Mülheim/Ruhr, Mülheim, Germany), *n*-hexane (Brenntag Mülheim/Ruhr), deuterium oxide (Sigma-Aldrich), dimethyl sulfoxide-*d*₆ (Eurisotop, Saint-Aubin, France), iron (III) chloride hexahydrate (Grüssing GmbH, Filsum, Germany), polyvinylpyrrolidone (PVP10, average mol wt 10 kDa, Sigma-Aldrich), 2',7'-dichlorodihydrofluorescein-diacetate (H₂DCFDA, Thermo Fisher Scientific), CellROX™ Green Flow Cytometry Assay Kit (Thermo Fisher Scientific), CellTiter-Glo® (Promega, Madison, WI, USA), methylene blue (Sigma-Aldrich).

2.2 Cell lines

Name	Description	Application
N2A	Mouse neuroblastoma cell lines	Cytotoxicity
WT-HeLa	Human cervix carcinoma cell lines	Cytotoxicity

3 Methods

3.1 Nuclear magnetic resonance (NMR):

¹H-NMR spectroscopy was performed with an Advance III HD 400 MHz Bruker BioSpin (400 MHz) with CryoProbe™ Prodigy probe head. Each sample was prepared by dissolving 5-7 milligram of the material in 600 µL D₂O or DMSO-d₆ in NMR tubes (Hilgenberg, standard 5 mm).

3.2 MALDI-TOF mass spectrometry:

MALDI-TOF mass spectra were measured with a Autoflex II mass spectrometer (Bruker Daltonics, Germany). The matrix solution was composed of 10 mg/mL Super-DHB (90/10 m/m mixture of 2,5-dihydroxybenzoic acid and 2-hydroxy-5-methoxybenzoic acid) in 69.93/30/0.07 (v/v/v) H₂O/acetonitrile/trifluoroacetic acid. 1.5 µL of matrix solution was spotted on a MTP AnchorChip (Bruker Daltonics, Germany). After crystallization of the matrix solution, 1.5 µL of sample solution (1 mg/mL in water) was added onto the matrix spot. Data was recorded either in positive or negative ion mode, depending on chemical structure.

3.3 ESI mass spectrometry:

ESI mass spectra were recorded with a Thermo scientific LTQ FT Ultra Fourier transform ion cyclotron with IonMax source. All the samples were dissolved in water or 30% acetonitrile in water at a concentration of 1 mg/mL.

3.4 Analytical reversed-phase high performance liquid chromatography (RP-HPLC):

RP-HPLC was carried out with a VWR-Hitachi Chromaster 5160 pump system VWR-Hitachi Chromaster 5260 autosampler and a VWR-Hitachi Chromaster 5430 diode array detector (VWR, Darmstadt, Germany) at 280 nm detection wavelength. As a column either

a YMC Hydrosphere 302 C18 (YMC Europe, Dinslaken, Germany) or a Waters Sunfire C18 (Waters, Milford, MA, USA) was used. A gradient from 1% to 100% acetonitrile containing 0.1% trifluoroacetic acid in 30 min was applied.

3.5 Transmission electron microscopy (TEM):

For Transmission electron microscopy (TEM) and energy dispersive X-ray (EDX) spectroscopy, a Titan Themis (FEI) equipped with a Super-X EDX detector, operated at 300 kV was used. Samples were prepared by drying sample droplets on a plasma activated thin carbon film supported by a copper grid.

3.6 X-ray photoelectron spectroscopy (XPS):

The XPS measurements were carried out by using a VSW TA10 X-ray source providing non-monochromatized Al K α radiation ($h\nu = 1486.6$ eV) set at 15 mA and 12 kV and a VSW HA100 hemispherical analyzer. The spectra were recorded with a pass energy of 22 eV and a dwell time of 0.1 s per measurement point. The samples were applied onto a silica wafer and subjected to overnight oven drying, resulting in the formation of a residual dry film on the wafer.

3.7 X-ray diffraction (XRD):

Powder X-ray diffraction (PXRD) measurements were carried out on a Bruker D8 Discover with Ni-filtered Cu K α radiation and a LynxEye position-sensitive detector in Bragg-Brentano geometry. K β radiation was attenuated with a 0.0125 mm Ni filter. All samples were prepared by fixating the dried samples between two polymer foils.

3.8 Dynamic light scattering (DLS) and zeta-potential measurements:

DLS and zeta potential were measured using the Nano-ZS Zetasizer equipped with DTS-1070 folded capillary cuvettes (Malvern Instruments, Malvern, Worcestershire, United Kingdom). All samples were dispersed in deionized water and measured three times with

at least six subruns each to get respective z-averages, PDIs. Zeta potential measurements were performed in the solution of 10 mM NaCl in water as triplicates with 10-15 subruns, respectively.

3.9 Thermogravimetric analysis (TGA):

Thermogravimetric analysis (TGA): TGA was carried out with a thermo-microbalance (Netzsch, STA 449 C Jupiter) by applying a heating rate of 10 °C/min from room temperature up to 900 °C. Approximately 10 mg of material was heated under synthetic air (N₂/O₂ mixture).

3.10 UV-Vis spectroscopy:

UV-Vis measurements were carried out using a Cary 3500 UV-Vis multicell spectrophotometer system. All the samples were diluted with the respective solvent to a total volume of 1 mL or 3 mL.

3.11 Synthesis of 3,4,5-tri-O-(tert-butoxycarbonyl)-gallic acid

4-Dimethylaminopyridine (DMAP) (61 mg, 0.5 mmol, 0.5 eq.), di-tert-butyl decarbonate (DIBOC) (237 mg, 1.08 mmol, 4.0 eq.) and pyridine (474 mg, 6 mmol, 6.0 eq.) was added in sequence to a stirred suspension of gallic acid (170 mg, 1 mmol, 1.0 eq.) in dichloromethane (20 mL) under nitrogen atmosphere. After stirring at room temperature overnight, the reaction mixture was quenched with water (20 ml) and washed with 3 × 1 M HCl, 3 × water and dried over anhydrous MgSO₄. The solvent was evaporated at reduced pressure, to give the crude product. Purification by column chromatography with n-hexane:ethyl acetate 9:1 (v/v) as eluent yielded the product 3,4,5-tri-O-(tert-butoxycarbonyl)-gallic acid (231 mg, 47.1%) as a light yellow oil, ¹H NMR (400 MHz, DMSO-*d*₆) δ 7.78 (d, J = 0.6 Hz, 2H), 1.49 (s, 18H), 1.48 (s, 9H); MS (ESI) *m/z* 469.2 [(M-H)⁻].

3.12 General synthesis of peptides

2-Chlorotrityl chloride resin was used as solid support for all peptide syntheses. In case of GA modified peptides, Fmoc-Lys(Dde)-OH was loaded onto the peptide resin. Amino acids were sequentially coupled from C- to N-terminus under standard Fmoc solid phase peptide synthesis (SPPS) conditions in 10 mL syringe reactors. Coupling of α -amino acids were carried out with 4 eq Fmoc L-amino acid (relative to loaded amines), 4 eq 1-hydroxybenzotriazole (HOBt), 4 eq PyBOP and 8 eq N, N-diisopropylethylamine (DIPEA) dissolved in a mixture of DCM-DMF 4:3 (7 mL per g resin), followed by 1 h incubation under agitation at room temperature. Fmoc deprotection was carried out by 4 \times 10 min incubation with 20% piperidine in DMF (7 mL per g resin) at room temperature. After each coupling and deprotection step, the resin was washed 2 \times DMF and 3 \times DCM (7 mL per g resin), and a Kaiser test was performed to confirm quantitative conversion. In case of double-GA modified peptides, the sequence was terminated by coupling of Fmoc-Lys(Dde)-OH, followed by Fmoc deprotection and Boc protection (10 eq DIBOC and 10 eq DIPEA in DCM, 1 h reaction time) of the lysine α -amine. Dde protecting groups were removed by 15 \times 2 min incubation with 2% hydrazinium hydroxide in DMF (7 mL per g resin) at room temperature. 3,4,5-tri-O-(tert-butoxycarbonyl)-gallic acid (Boc-protected GA) was then coupled to the deprotected lysine ϵ -amines with a solution containing 3 eq. of the building block, 3 eq PyBOP, 3 eq HOBt and 12 eq DIPEA in DMF for 30 min at 50 °C (Biotage SP Wave) and for 30 min at room temperature.

Finally, peptides were cleaved from the resin by incubation with trifluoroacetate-triisopropylsilane-H₂O 95:2.5:2.5 (7 mL per g resin) for 90 min at room temperature. The cleavage solution was dropped into 45 mL of pre-cooled methyl-tert-butylether (MTBE)-n-hexane 1:1 and centrifuged. The supernatant was discarded and precipitated peptide was collected. Peptide purification was carried out by preparative RP-HPLC with a Pure C-830 chromatography system (BÜCHI, Flawil, Switzerland), a semi-preparative C18 RP-HPLC column (Waters, Milford, US) and a gradient from 99:1 to 0:100 (water / acetonitrile) within 25 min. All peptides were lyophilized and analyzed by analytic RP-HPLC, ¹H-NMR and mass spectrometry (MALDI-MS or ESI-MS).

3.13 Synthesis of iron-gallic acid peptide nanoparticles (IGPNs)

For the synthesis of FePVP nanoparticles, a solution of $\text{FeCl}_3 \cdot 6\text{H}_2\text{O}$ in H_2O (0.2 mL, 0.6 M) was added to 10 mL PVP solution (10 mg mL^{-1} in H_2O) and agitated for 1 h. The peptide solution (1 mL, 0.6 M in H_2O) was added to the mixture and stirred overnight. Fe nanoparticles were synthesized in a similar way, but without addition of PVP. The following day, obtained nanoparticles were dialyzed (MWCO = 10K) against deionized water for 24 h and stored at 4 °C for further use.

3.14 Investigation of the stability of IGPNs in different media

In order to evaluate the stability of IGPNs over time, IGPNs were incubated in water, PBS, 50% serum and artificial lysosomal fluid (ALF 1 L contains: 3.21 g NaCl, 6.00 g NaOH, 20.80 g citric acid, 0.097 g CaCl_2 , 0.179 g sodium phosphate heptahydrate, 0.039 g Na_2SO_4 , 0.106 g $\text{MgSO}_4 \cdot 6\text{H}_2\text{O}$, 0.059 g glycerine, 0.077 g sodium citrate dihydrate, 0.09 g sodium tartrate dihydrate, 0.085 sodium lactate, 0.086 sodium pyruvate, 1 mL formaldehyde, topped to 1L by double distilled water). 50 μL of the freshly prepared IGPNs were added into each cuvette, followed by dilution with 2 mL of the individual medium (water, PBS, 50% serum and ALF). The four samples were monitored under agitation for 6 hours (25 °C, 700 rpm) at 550 nm using a Cary 3500 UV-Vis Spectrophotometer. The absorbance of each sample was recorded every 5 minutes.

3.15 Methylene blue assay

MB assays were used to measure the $\text{HO}\cdot$ production efficacy of IGPNs. IGPNs (36 μg Fe^{3+}) were mixed with MB (1.5 mL, 10 μg L^{-1}), H_2O_2 (1 mL) and H_2O was added to a final volume 3 mL. The absorbance at 664 nm was recorded every 5 minutes over 6 h or 24 h using a Cary 3500 UV-Vis Spectrophotometer.

3.16 Cell culture

HeLa cells were grown in Dulbecco's Modified Eagle Medium (DMEM)-low glucose (1 g/L glucose) supplemented with 10% fetal bovine serum (FBS), 100 U/mL penicillin, and 100 µg/mL streptomycin. The cells were cultured in ventilated flasks at 37 °C and 5% CO₂ in an incubator with a relative humidity of 95%. The cells were passaged at a confluency of 80-90%.

3.17 Evaluation of ROS generation by flow cytometry

The CellROX™ Green Flow Cytometry Assay Kit (Thermo Fisher Scientific) was used to detect ROS in living cells by flow cytometry. HeLa cells were seeded in 24-well plates at a density of 50000 cells/well one day prior to the treatment. On the next day, the medium was replaced with 450 µL of fresh medium. 50 µL of peptides or IGPNs (100 µM) was added to each well resulting in a final concentration of 10 µM peptides, and the cells were incubated for 24 h. Afterwards, the medium was removed, and the cells were harvested, washed, and re-suspended in PBS containing 10% FBS. The CellROX™ Green reagent was added to each sample resulting in a final concentration of 800 nM. Then, the cells were incubated for 45 min at 37 °C in the dark. Subsequently, 0.6 µL of the 5 µM SYTOX® Red Dead Cell stain solution was added to each sample. After another 15 min incubation, the cells were analyzed by flow cytometry as described above. The CellROX™ Green signal was measured with 488 nm excitation and 530 nm emission. The SYTOX® Red signal was assayed with 639 nm excitation and 660 nm emission. Ten thousand of isolated live cells were counted.

3.18 Evaluation of ROS generation by confocal laser scanning microscopy (CLSM)

HeLa cells were seeded in 8-well Ibidi µ-slides (Ibidi GmbH, Germany) at a density of 20000 cells/well 24 h prior to the treatment. On the next day, the medium was replaced with 270 µL of fresh medium. 30 µL of IGPNs and peptides was added to each well resulting in a final concentration of 10 µM peptides, and the cells were incubated for 24 h.

As a positive control, tert-butyl hydroperoxide solution (TBHP, 200 μ M) was added, and the cells were incubated for 30 min. Afterwards, the cells were washed twice with PBS followed by 30 min of staining with DCFH-DA (10 μ M) in the dark. Next, the DCFH-DA solution was discarded, and 300 μ L of PBS was added per well for CLSM imaging. Images were recorded on a Leica-TCS-SP8 confocal laser scanning microscope equipped with a HC PL APO 63 \times 1.4 objective (Germany). DCFH-DA signal was recorded with emission at 520 nm. All images were analyzed using the LAS X software from Leica.

3.19 Evaluation of cellular uptake by flow cytometry

The peptides were labeled using 5-carboxyfluorescein NHS ester. Peptides (5 mg) were dissolved in 0.5 mL of HEPES buffer (pH 7.4) and the pH was adjusted to 8.3 using 1 M NaOH. The solution of 5-carboxyfluorescein NHS ester (10 mg/mL) DMSO was prepared. Afterwards, the solution of reactive dye was mixed with peptides solution, with molar ratio of 0.75(dye):1(peptide). After 4 h reaction time at room temperature, the peptide-carboxyfluorescein conjugate was purified by dialysis (MWCO = 1 KDa) and lyophilized for further use.

One day prior to the cellular uptake experiments, HeLa cells were seeded into 24-well plates at a density of 30000 cells/well. On the next day, the medium in each well was replaced with 450 μ L of fresh medium. Peptides (20% carboxyfluorescein labeled) and IGPNs were prepared as described above. 50 μ L of the nanoparticles was added to each well resulting in a final concentration of 10 μ M peptides, and the cells were incubated for 4 h. Subsequently, the cells were harvested, washed with PBS, and re-suspended in PBS containing 10% FBS. Subsequently, trypan blue (0.04%, w/v) was added to quench the fluorescence of carboxyfluorescein-labeled peptides adsorbed on the cell membrane, and the cells were incubated for 1 min. Then, 1 ng/ μ L DAPI was added directly to each sample before the measurement to differentiate between live and dead cells. The samples were analyzed by flow cytometry with a CytoFLEX S flow cytometer (Beckman Coulter, CA, USA). The DAPI fluorescence was detected with 405 nm excitation and 450 nm emission. The FITC signal was measured with 488 nm excitation and 530 nm emission. Ten thousand of isolated live cells were counted and evaluated. The data were analyzed using

FlowJo 7.6.5 by FlowJo, LLC (Becton, Dickinson and Company, USA). All experiments were performed in triplicate.

3.20 Evaluation of cellular uptake by confocal laser scanning microscopy (CLSM)

HeLa cells were seeded in 8-well Ibidi μ -slides (Ibidi GmbH, Germany) at a density of 20000 cells/well 24 h prior to the experiment. On the next day, the medium was replaced with 270 μ L of fresh medium. 30 μ L of carboxyfluorescein-labeled IGPNs was added to each well corresponding to a final concentration of 10 μ M peptides. The medium was removed after 4 h incubation, and the cells were washed twice with 300 μ L of PBS followed by 40 min of fixation with 4% PFA at RT. Afterwards, the cells were washed twice with PBS again, and the cell nuclei were stained with 2 ng/ μ L DAPI. The DAPI solution was discarded after 20 min incubation, and the cells were further washed with trypan blue (0.04%, w/v). Afterwards, 300 μ L of PBS was added per well for CLSM imaging. Images were recorded on a Leica-TCS-SP8 confocal laser scanning microscope equipped with a HC PL APO 63 \times 1.4 objective (Germany). DAPI and carboxyfluorescein emission were recorded at 450 nm and 520 nm, respectively. All images were analyzed using the LAS X software from Leica.

3.21 Evaluation of cell viability (CellTiter-Glo assay)

CellTiter-Glo[®] Luminescent Cell Viability Assay was performed to determine the viability of HeLa cells after treatment with IGPNs or the individual components. One day prior to the treatments, HeLa cells were seeded into 96-well plates at a density of 5000 cells/well. On the next day, the medium in each well was replaced with 90 μ L of fresh medium. Afterwards, 10 μ L of nanoparticles or control solutions (free peptides, Fe, FePVP) was added to each well corresponding to the specified final concentrations of peptide or Fe³⁺, respectively. The supernatant was removed after 72 h incubation, and 25 μ L of medium as well as 25 μ L of CellTiter-Glo reagent (Promega, Mannheim, Germany) were added to each well. The plate was gently agitated for 30 min at RT, and the luminescence signal (relative light units, RLU) was recorded by a Centro LB 960 plate reader luminometer

(Berthold Technologies, Bad Wildbad, Germany). The relative cell viability (in percentage) was calculated relative to control wells treated with HBG buffer as $([RLU] \text{ test}/[RLU] \text{ control}) \times 100\%$. All experiments were performed in triplicate.

3.22 Apoptosis assay

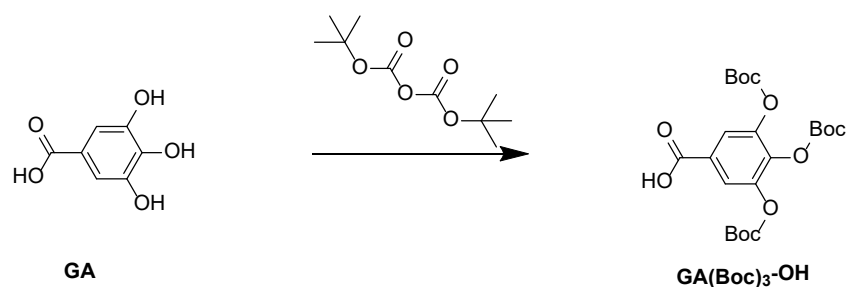
Cell apoptosis was assessed by flow cytometry using an Annexin V-FITC Apoptosis Detection Kit (BioVision, USA). HeLa cells were seeded into 24-well plates at a density of 30000 cells/well one day prior to the experiment. On the next day, the medium in each well was replaced with 450 μL of fresh medium. 50 μL of IGPNs or controls was added to each well corresponding to a final concentration of 10 μM peptides (or Fe in case of FeCl_3 and FePVP). After 48 h incubation, the cells were trypsinized, collected, and re-suspended in 500 μL of Annexin V-FITC binding buffer (1 \times). Next, 5 μL of Annexin V-FITC and 5 μL of propidium iodide (PI, 50 $\mu\text{g}/\text{mL}$) were added to each sample, and the samples were incubated for 5 min at RT in the dark. Afterwards, the cells were washed, re-suspended, and analyzed by flow cytometry as described above. The FITC signal was measured with 488 nm excitation and 530 nm emission. The PI fluorescence was assayed with 488 nm excitation and 640 nm emission. All experiments were performed in triplicate.

4 Results and discussion

This section was adapted from: F Shen, Y Lin, M Höhn, X Luo, M Döblinger, E Wagner, U Lächelt (2023) Iron-Gallic Acid Peptide Nanoparticles as a Versatile Platform for Cellular Delivery with Synergistic ROS Enhancement Effect. *Pharmaceutics* **15** (7), 1789.

4.1 Synthesis of gallic acid-tagged peptides

Basis for the assembly of peptides into IGPNs is the integration of gallic acid (GA) into the peptide sequences. To enable GA functionalization during peptide synthesis, a Boc-protected derivative was synthesized following a procedure developed by Florimond et al (Scheme 1): gallic acid was converted into 3,4,5-tri-O-(tert-butoxycarbonyl)-gallic acid (GA(Boc)₃-OH) by reaction with di-tert-butylidicarbonate in presence of pyridine and 4-dimethylaminopyridine.⁹⁸



Scheme 1. Synthesis of Boc-protected gallic acid. Reagents and conditions: DIBOC (4 eq), pyridine (6 eq), DMAP (0.5 eq), DCM, RT, 2 h.

Standard Fmoc solid-phase peptide synthesis conditions were used for the assembly of a series of GA modified peptides (Table 2). The sequences were designed for a systematic assessment of the following peptide sequence parameters: (1) number of GA moieties, (2) physico-chemical peptide characteristics, and (3) bioactivity. The different peptides can be grouped into six series: minimal GA peptide motif, neutral model peptides, positively charged model peptides, negatively charged peptides, pro-apoptotic SIO peptides and pro-apoptotic AVP peptides. Each sequence was conjugated with one or two gallic acid moieties via amide formation at the side-chain of N- and C-terminal lysines serving as molecular adaptors. The purity, molecular weights and structures of all

synthesized peptides were confirmed by analytic RP-HPLC, ESI- or MALDI-TOF mass spectrometry and NMR (cf. Analytical Material).

Table 2. Gallic acid-tagged functional units used for the assembly of IGPNs.

Code	Sequence ^a	Molecular Weight (Da)	Function
K*	K(GA)	298.3	minimal peptide motif
K**	GA-K(GA)	450.0	
A ₄	AAAA	300.2	neutral model peptides
A ₄ *	AAAAK(GA)	582.6	
A ₄ **	K(GA)AAAAK(GA)	862.4	
(KA) ₂	KAKA	416.3	cationic model peptides
(KA) ₂ *	KAKAK(GA)	696.8	
(KA) ₂ **	K(GA)KAKAK(GA)	977.1	
(EA) ₂	EAEA	418.4	anionic model peptides
(EA) ₂ *	EAEAK(GA)	698.7	
(EA) ₂ **	K(GA)EAEAK(GA)	979.0	
SIO	QPK	371.4	pro-apoptotic SIO peptides
SIO*	QPK(GA)	523.5	
SIO**	K(GA)QPK(GA)	803.8	
AVP	AVPIAQK	725.9	pro-apoptotic AVP peptides
AVP*	AVPIAQK(GA)	878.0	
AVP**	K(GA)AVPIAQK(GA)	1158.3	

^a Peptide sequences are ordered from N- to C-terminus. * indicates one gallic acid (GA) conjugated to the side chain of the C-terminal lysine (K); ** indicates two GA conjugated to the side chains of the C- and N-terminal K.

4.2 Synthesis and characterization of Iron Gallic Acid Nanoparticles (IGPNs)

IGPNs were synthesized by adaption of previously published procedures for the generation of iron-GA coordination polymers.¹⁰² With each peptide, two different types of nanoparticles were assembled, either by direct interaction of GA modified peptides with Fe^{3+} in solution or after initial pre-complexation of Fe^{3+} with polyvinyl pyrrolidone (PVP) (Figure 2, 3). FeCl_3 was dissolved in bidistilled water for preparation of Fe nanoparticles, while for FePVP nanoparticles FeCl_3 and PVP were agitated for 1 hour initially. Then, equimolar amounts of peptides were added to assemble IGPNs via coordinative interactions between GA and Fe^{3+} .

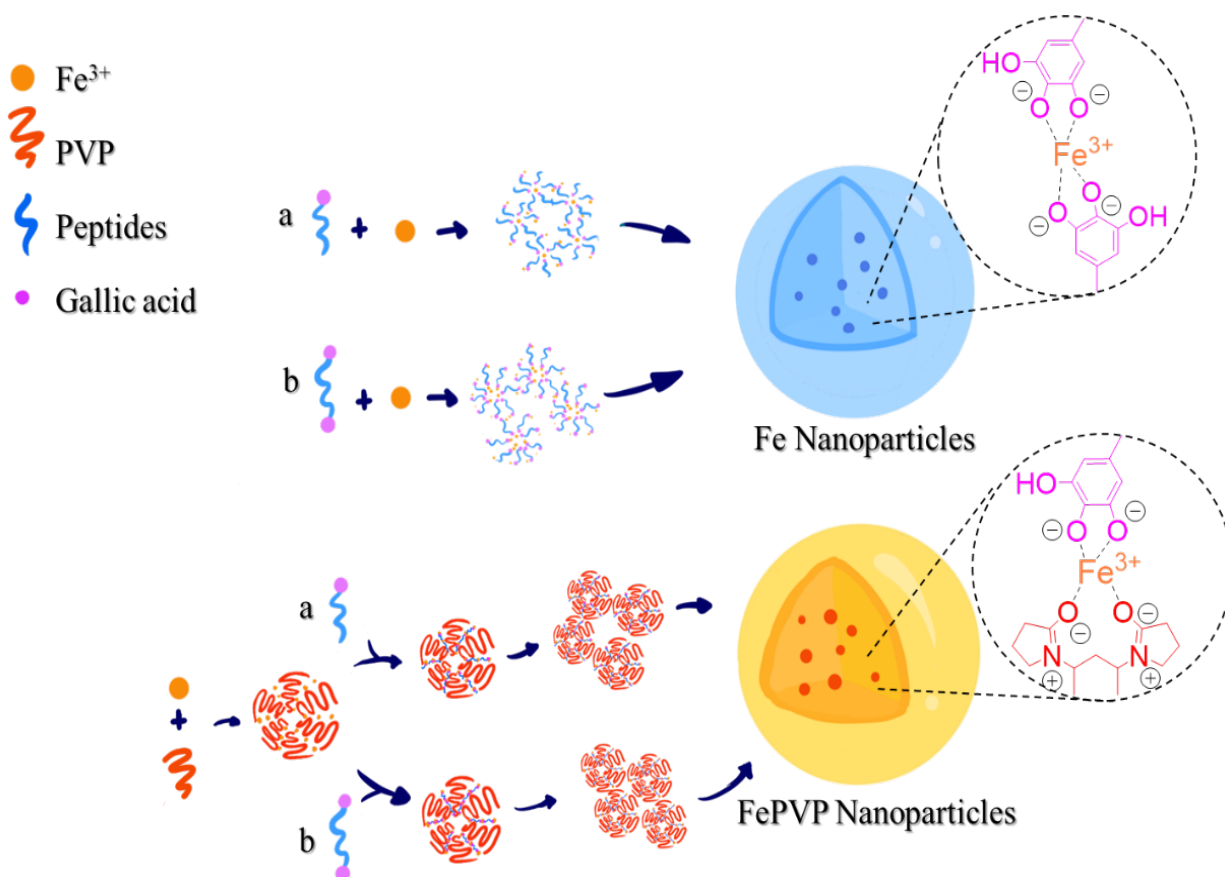


Figure 2. Assembly of IGPNs. Synthesis of IGPNs by coordinative interaction of mono- (a) or di-functionalized (b) gallic acid peptides with Fe^{3+} (Fe Nanoparticles),¹⁰³ and by initial pre-complexation of Fe^{3+} with PVP (FePVP Nanoparticles).¹⁰⁴

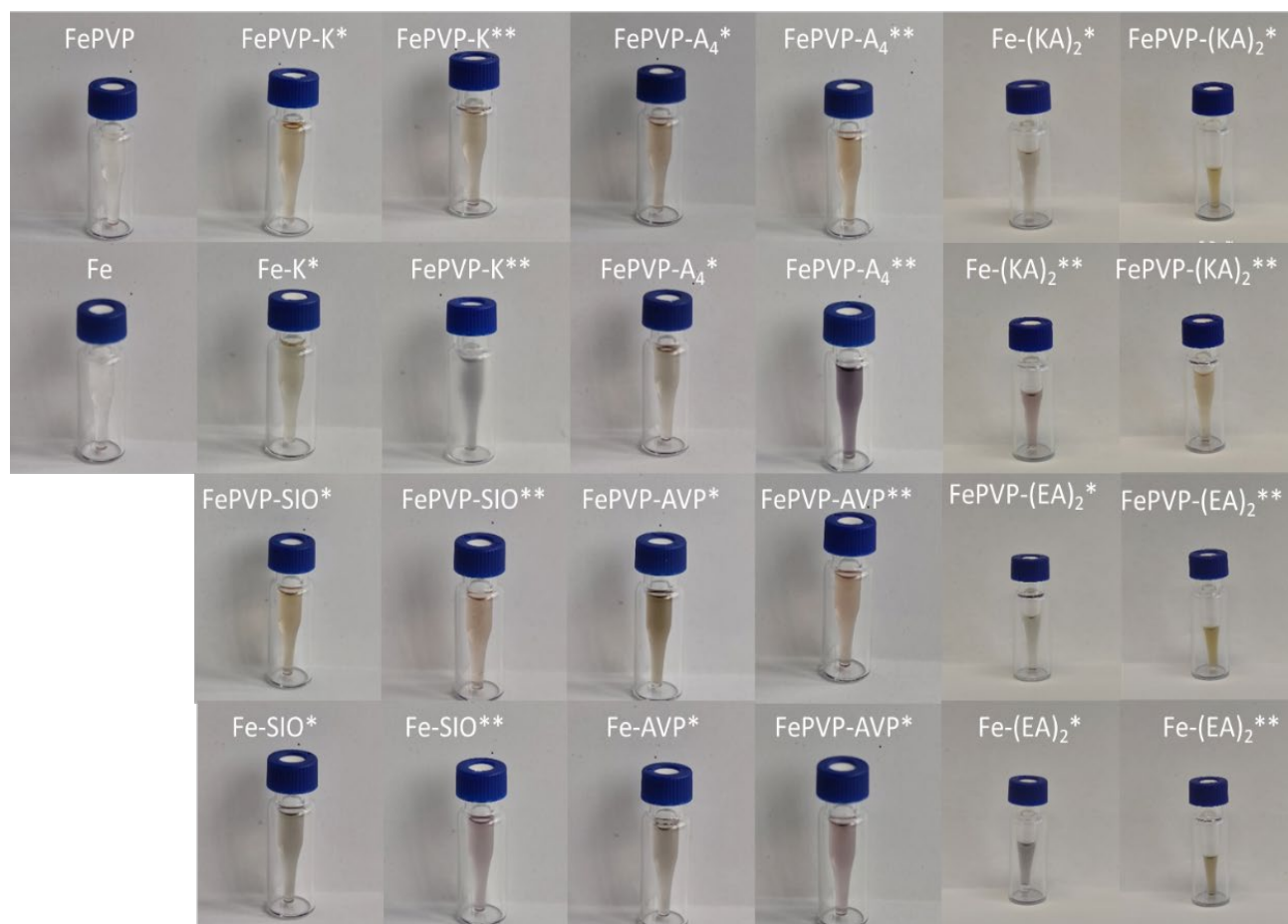


Figure 3. Photographs of IGPN suspensions in water.

The systematic evaluation showed that formation of IGPNs depended on GA modification: native peptides without GA did not form particles with Fe^{3+} , whereas peptides with one (*) or two (**) GA moieties at the termini showed assembly. Measurements of particles size distribution (hydrodynamic diameter), polydispersity index (PDI) and ζ -potential of the generated IGPN suspensions were carried out by dynamic and electrophoretic light scattering (DLS, ELS) (Figure 4A, Table 3) and revealed mean z-averages between 86.5 ± 2.7 nm and 384.4 ± 22.4 nm and ζ -potential values in the range between -25.2 mV to 2.2 mV. It was found that the length or charge of investigated peptide sequences as well as the number of attached GA modifications did not change the size significantly, However, in case of positively or negatively charged peptide sequences a strong reduction of PDI was achieved with the PVP mediated synthesis procedure. Accordingly, an evaluation of

the size distribution (Figure 4B) suggests favorability of the PVP assembly approach due to a reduction of IGPN aggregation in aqueous environment.

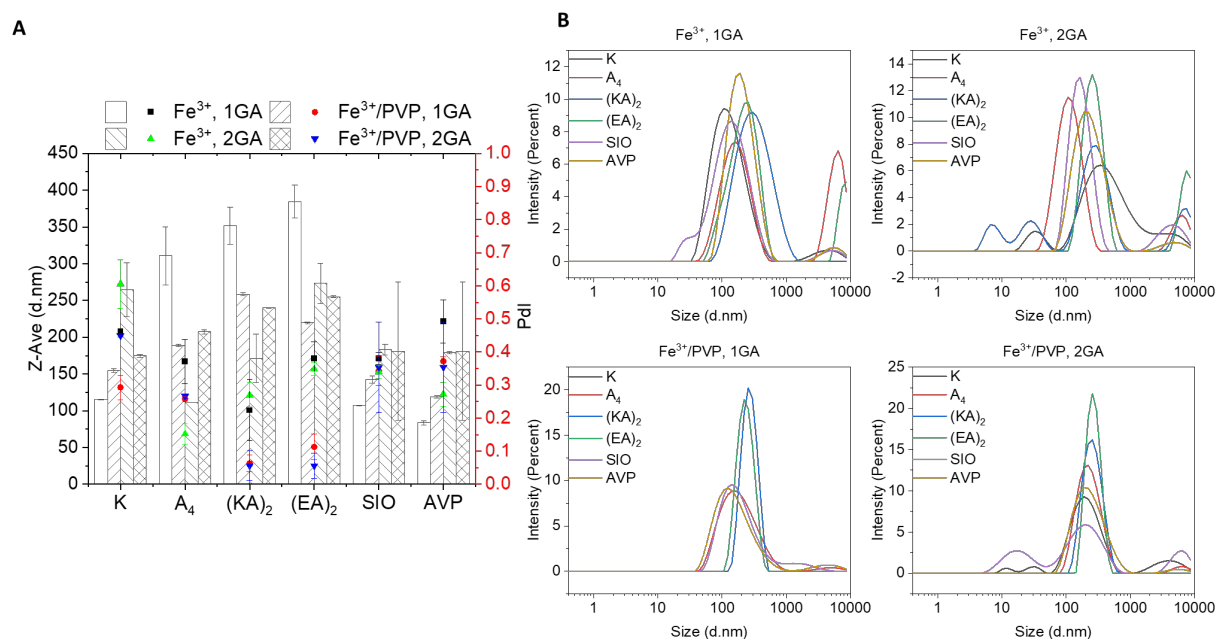


Figure 4 Characterization of nanoparticles. (A) Hydrodynamic size (z-average, columns) and polydispersity index (PDI, dots) of IGPNs as determined by DLS. (B) Particle size distribution of IGPN suspensions in water.

Table 3. Size (Z-Ave), Polydispersity Index(PDI), zeta-potential (ZP) and Conductivity (Cond) measurements by dynamic light scattering(DLS).

Nanoparticles	Z-Ave(d.nm)	Pdi	ZP(mV)	Cond(mS/cm)
Fe-K*	115.3±0.26	0.46±0.01	-25±2.48	1.19±0.05
FePVP-K*	154.9±2.25	0.29±0.04	-0.3±0.2	1.4±0.08
Fe-K**	264.7±36.4	0.61±0.07	-16.8±3.35	1.21±0.05
FePVP-K**	174.7±2.22	0.45±0	0.88±0.12	1.55±0.08
Fe-A₄*	310.7±39.29	0.37±0.07	-3.92±0.21	1.4±0.06
FePVP-A₄*	188.6±1.7	0.26±0.01	2.54±0.04	1.36±0.07
Fe-A₄**	111.51±2.68	0.15±0.03	-11.9±2.77	1.14±0.05
FePVP-A₄**	207.3±0.24	0.27±0.01	-5.06±0.85	1.07±0.05

<i>Fe-(KA)₂*</i>	351.7±25.45	0.23±0.09	-2.77±0.2	1.19±0.05
<i>FePVP-(KA)₂*</i>	258.3±2.14	0.06±0.03	2.17±0.1	1.71±0.08
<i>Fe-(KA)₂**</i>	171.2±32.91	0.27±0.04	-3.6±3.42	1.25±0.07
<i>FePVP-(KA)₂**</i>	239.9±0.49	0.06±0.05	2.83±0.25	1.53±0.07
<i>Fe-(EA)₂*</i>	384.4±22.35	0.38±0.05	-2.13±0.76	1.16±0.05
<i>FePVP-(EA)₂*</i>	219.5±1.22	0.11±0.04	-0.77±0.11	1.79±0.09
<i>Fe-(EA)₂**</i>	273.3±27.16	0.35±0.02	-18.6±2.27	1.1±0.05
<i>FePVP-(EA)₂**</i>	255.2±1.13	0.06±0.04	1.16±0.2	1.8±0.09
<i>Fe-SIO*</i>	107.3±0.61	0.38±0.02	-11.2±0.17	1.19±0.06
<i>FePVP-SIO*</i>	142.2±4.82	0.34±0.04	2.74±0.53	1.48±0.08
<i>Fe-SIO**</i>	183.4±7.29	0.34±0.02	-10.7±1.48	1.12±0.05
<i>FePVP-SIO**</i>	181±93.98	0.35±0.14	-13.1±1.37	1.18±0.05
<i>Fe-AVP*</i>	83.45±3.01	0.49±0.07	-21.6±0.72	1.24±0.05
<i>FePVP-AVP*</i>	118.97±1.85	0.37±0.01	-25.2±2.06	1.34±0.05
<i>Fe-AVP**</i>	179±1.78	0.27±0.04	-2.53±0.39	1.12±0.05
<i>FePVP-AVP**</i>	181±93.98	0.35±0.14	-13.1±1.37	1.14±0.06

* indicates one gallic acid (GA) conjugated to the side chain of the C-terminal lysine (K);

** indicates two GA conjugated to the side chains of the C- and N-terminal K.

In a dry dispersed state, transmission electron microscopy (TEM) determined similar appearance of Fe and FePVP nanoparticles built from neutral model peptides (*Fe-A₄***, *FePVP-A₄***, Figure 5).

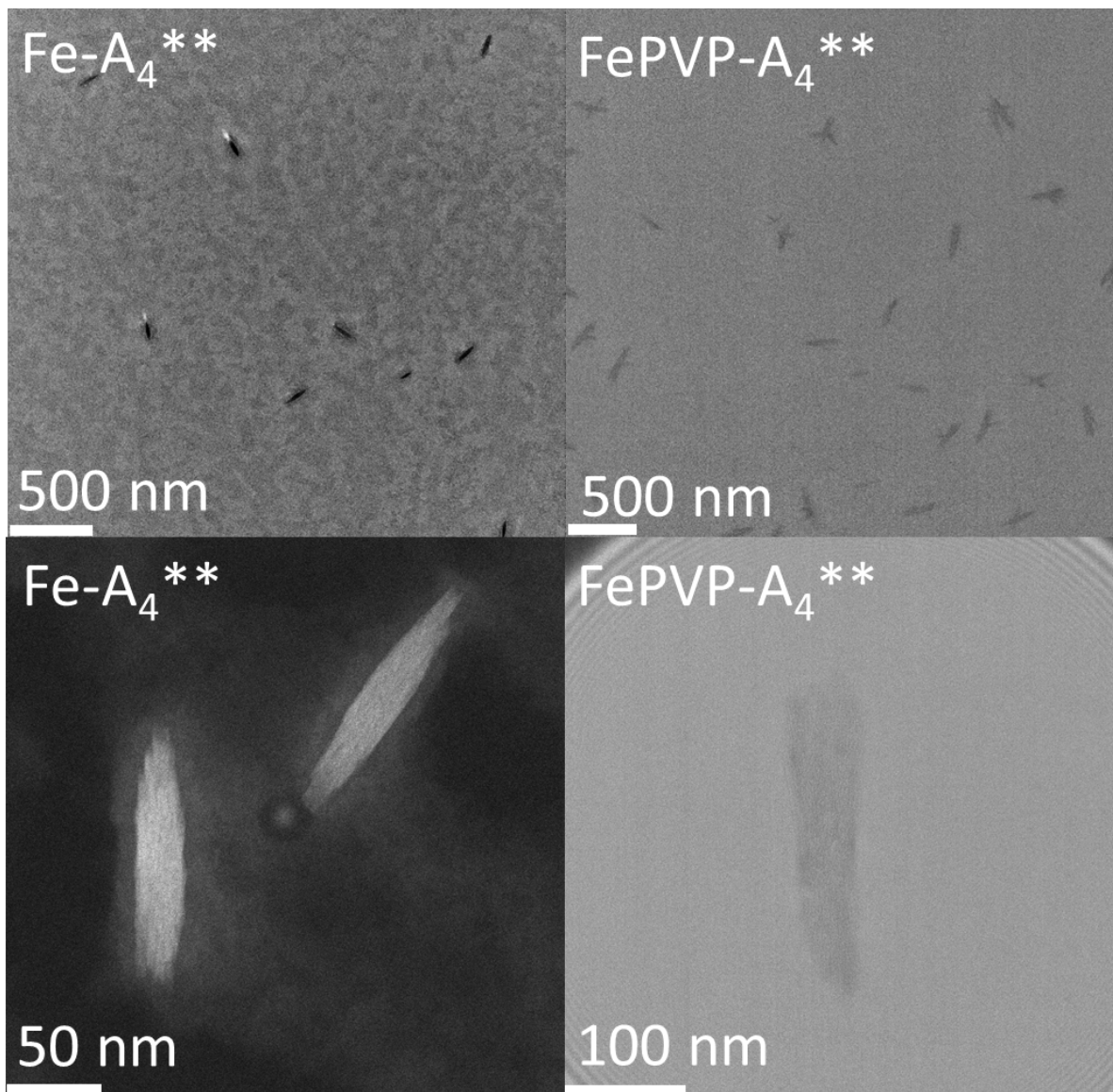


Figure 5. TEM micrograph of Fe-A₄** and FePVP-A₄** . Measurement performed by Markus Döblinger (Department of Chemistry, LMU München).

X-ray diffraction (XRD) experiments with Fe-A₄*, FePVP-A₄*, Fe-A₄**, FePVP-A₄** did not show distinct diffraction patterns (Figure 6).

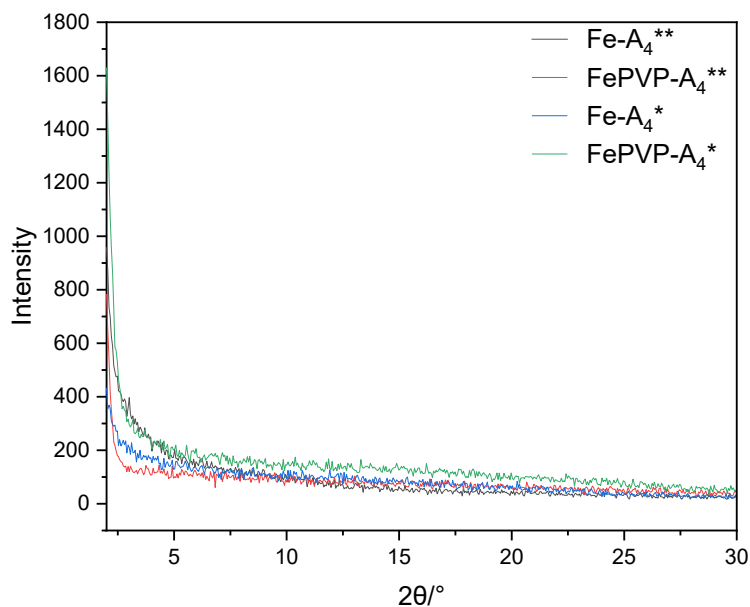


Figure 6. XRD measurements of Fe-A₄*, FePVP-A₄*, Fe-A₄**, FePVP-A₄**. Measurement performed by Tianhao Xue (Department of Chemistry, LMU München).

The XPS spectra of the iron 2p core level confirms the presence of iron in the sample. The core level for Fe(0) is expected at 707 eV. The binding energies shifted to higher values indicate higher oxidation states (Figure 7).

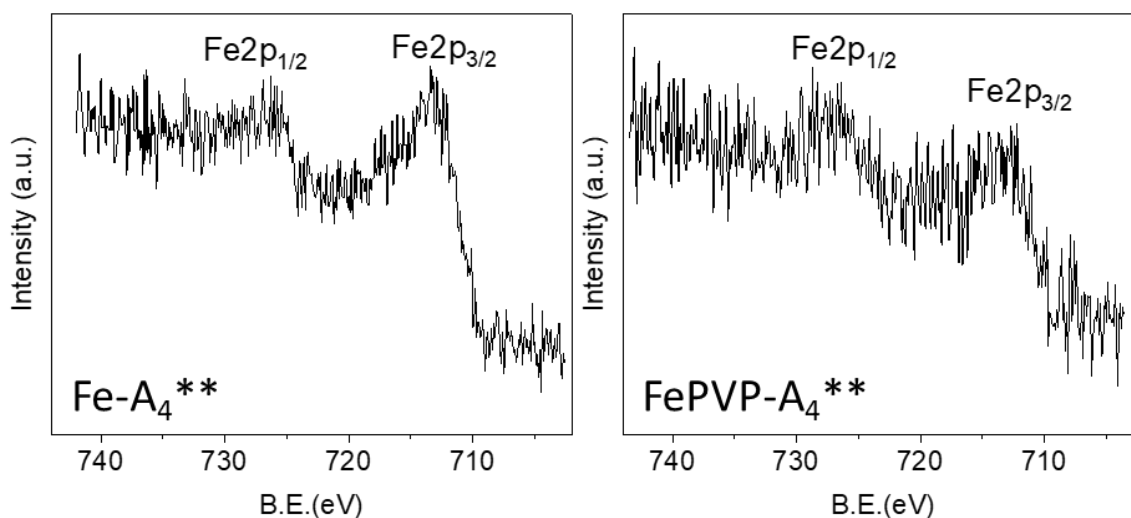


Figure 7. XPS analysis of Fe-A₄** (left) and FePVP-A₄** (right). Measurement performed by Hannah Illner (Department of Chemistry, LMU München).

Elemental mapping by energy dispersive X-ray (EDX) spectroscopy in scanning transmission electron microscopy (STEM) mode shows that iron (Fe) and Oxygen (O) are homogeneously distributed in IGPNs (Figure 8A, B), and the total iron content in Fe-A₄**^{*}, FePVP-A₄**^{*} was determined by inductively coupled plasma optical emission spectroscopy (ICP-OES) to be ~4.6% and ~3.6%, respectively.

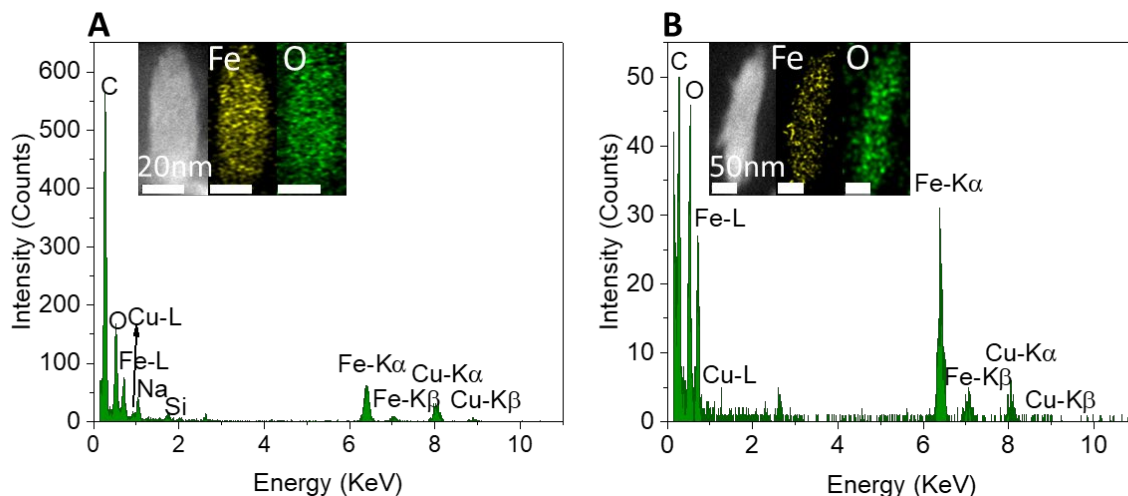


Figure 8. (A)STEM-EDX elemental map of Fe-A₄**^{*}. (B) STEM-EDX elemental map of FePVP-A₄**^{*}. Markus Döblinger (Department of Chemistry, LMU München).

Furthermore, to assess the encapsulation efficiency of integrated peptides, solid IGPNs were separated from surrounding dispersant medium with spin filters (Agilent Spin Filter, 10 kDa) via centrifugation (12500 rpm, 5 min). Free peptide solutions (A₄^{*}, A₄**^{*}, K^{*}, K**^{*}, SIO^{*}, SIO**^{*}, AVP^{*}, AVP**^{*}) served as controls and analysis via RP-HPLC showed that the GA modified peptides were encapsulated into IGPNs via Fe³⁺ chelation quantitatively (Figure 9), since in case of IGPN suspensions no distinct amounts of free peptide were detectable. The peptides were found to be quantitatively integrated in each of the four different IGPNs, providing strong evidence for an efficient assembly and encapsulation process.

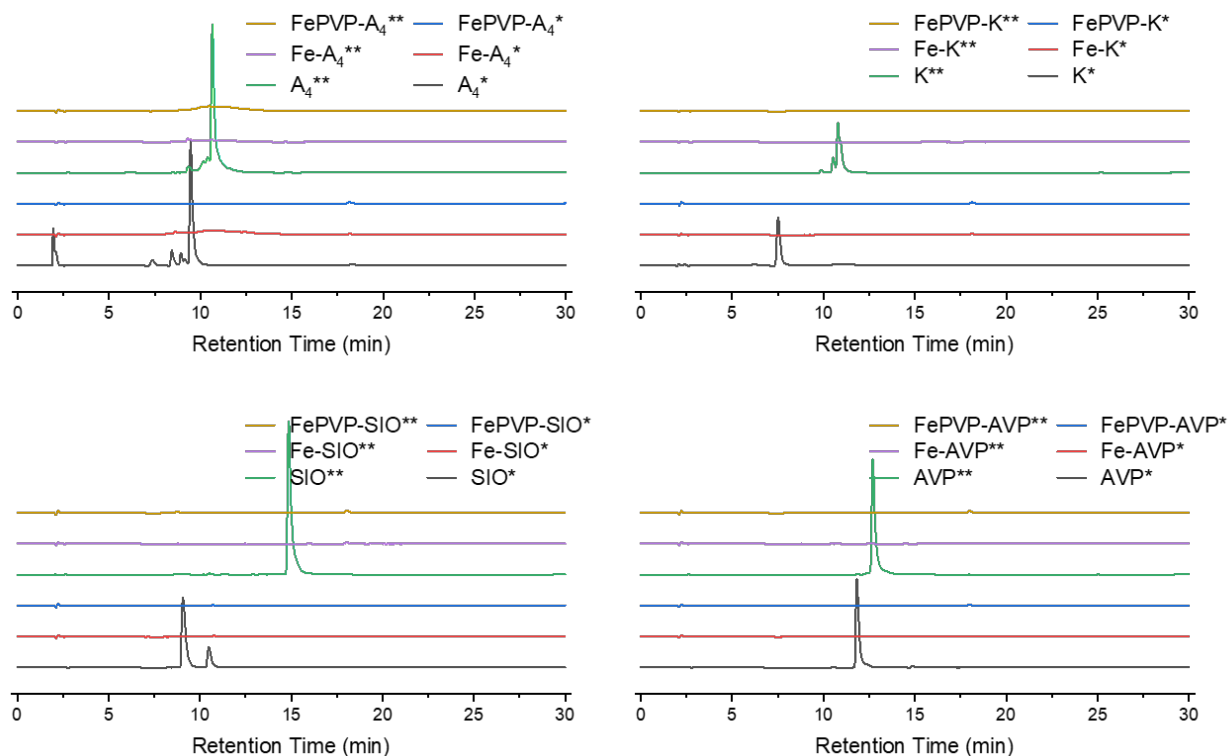


Figure 9. Determination of free peptides in filtrated solutions via RP-HPLC. Free peptide solutions (100 μ M) served as controls.

Additional characterization of IGPNs was conducted by UV-Vis spectroscopy (Figure 10). After decomposition of IGPNs at pH 1, the measurements revealed characteristic absorbance peaks of the particle components (265 nm peptide, 333 nm Fe^{3+}). Compared with Fe nanoparticles (red curve), the FePVP nanoparticles (black curve) exhibit higher absorbance at 214 nm in relation to 265 nm, which can be attributed to the introduction of PVP.

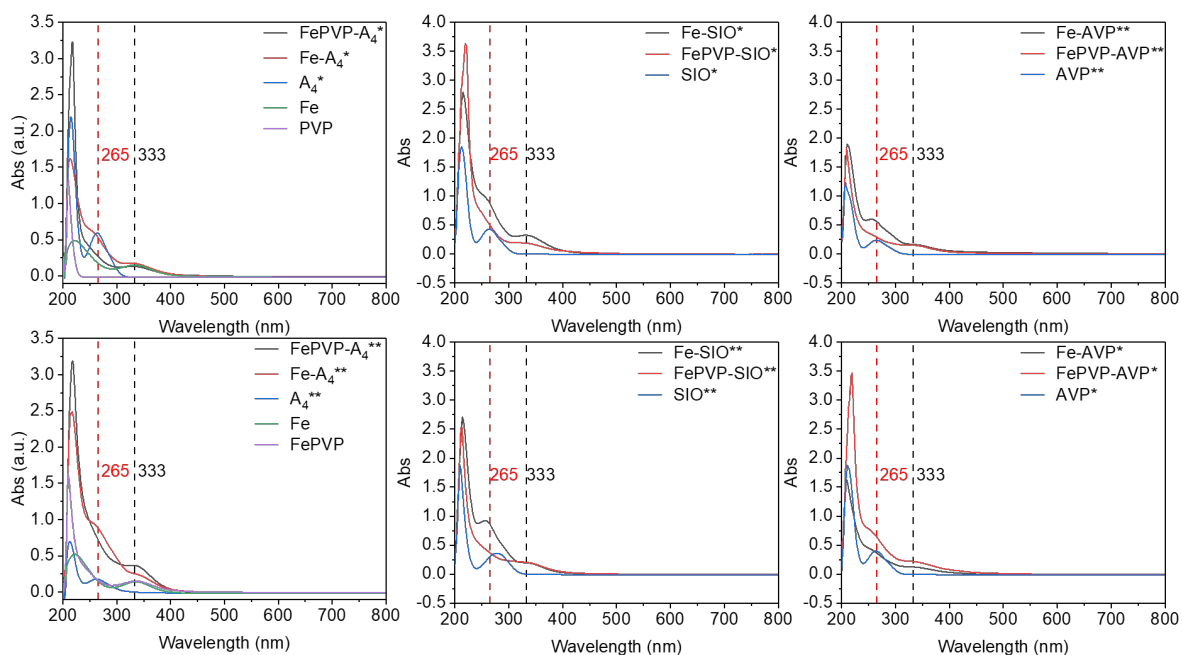


Figure 10. UV-Vis spectrometry of IGPNS.

Moreover, the decomposition resulted in the disappearance of the Ligand to Metal Charge Transfer Bands (LMCT), which confirms the supposed nature of bonding between iron and gallic acid (Figure 11).

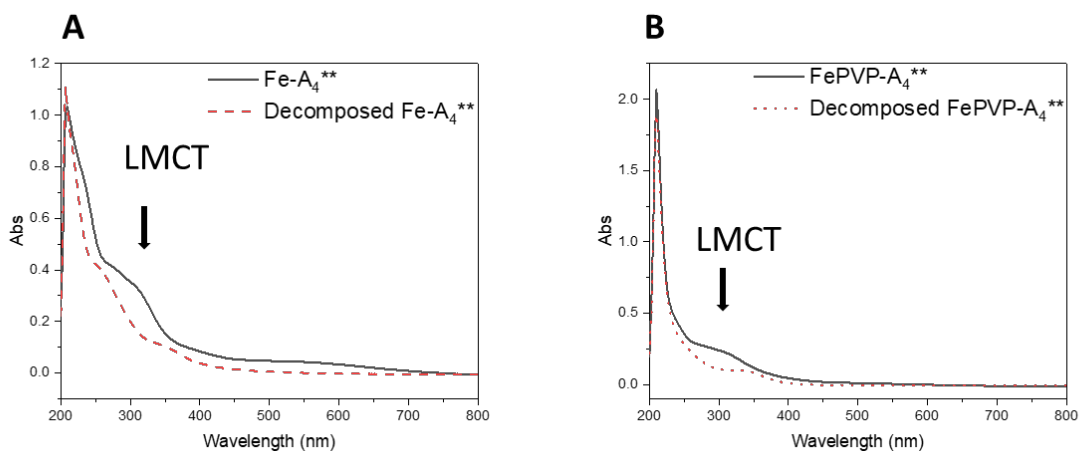


Figure 11. UV-Vis spectrometry. (A) Fe-A₄** (black), decomposed Fe-A₄** (red). (B) FePVP-A₄** (black), decomposed FePVP-A₄** (red).

Thermogravimetric analysis (TGA) showed an obvious difference between Fe-A₄** and FePVP-A₄** nanoparticles, which is consistent with a higher organic content due to the integration of PVP (Figure 12).

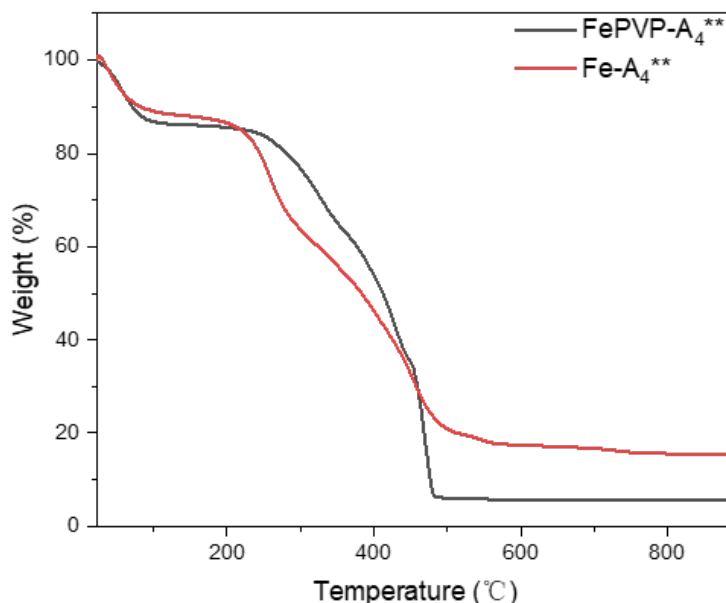


Figure 12. Thermogravimetric analysis of Fe-A₄** and FePVP-A₄**. Measurement performed by Tianhao Xue (Department of Chemistry, LMU München).

The stability of Fe-A₄*, FePVP-A₄*, Fe-A₄**, FePVP-A₄** in water, phosphate buffer (PBS), 50% serum and artificial lysosomal fluid (ALF) were investigated by monitoring the absorbance of IGPN suspensions at 550 nm by UV-Vis spectroscopy (Figure 13).

The stability of Fe-A₄*, FePVP-A₄*, Fe-A₄**, FePVP-A₄** in water, PBS, 50% serum and artificial lysosomal fluid (ALF) were investigated by monitoring the absorbance of the suspension of IGPNs at 550 nm by UV-Vis (Figure 13). ALF was prepared as previously described to simulate the environment of lysosomes, including pH, ionic strength, salts and viscosity.¹⁰⁵ The aggregation or dissolution of nanoparticles were assessed continuously over a time period of 6 hours after the treatment with above mentioned solutions. It was found, that all IGPNs remained stable in water, but dissolved rapidly in

ALF. Interestingly, Fe-A₄* and FePVP-A₄* exposed to 50% serum increased in absorbance over time presumably due to adsorption of serum proteins probably leading to the issue of peptide release. In contrast, Fe-A₄** and FePVP-A₄** remained stable, which can be attributed to the GA modification at both termini of peptide. FePVP-A₄** showed the most stable particle size, which indicates that the two-fold GA modification and PVP both improve the stability of IGPNs.

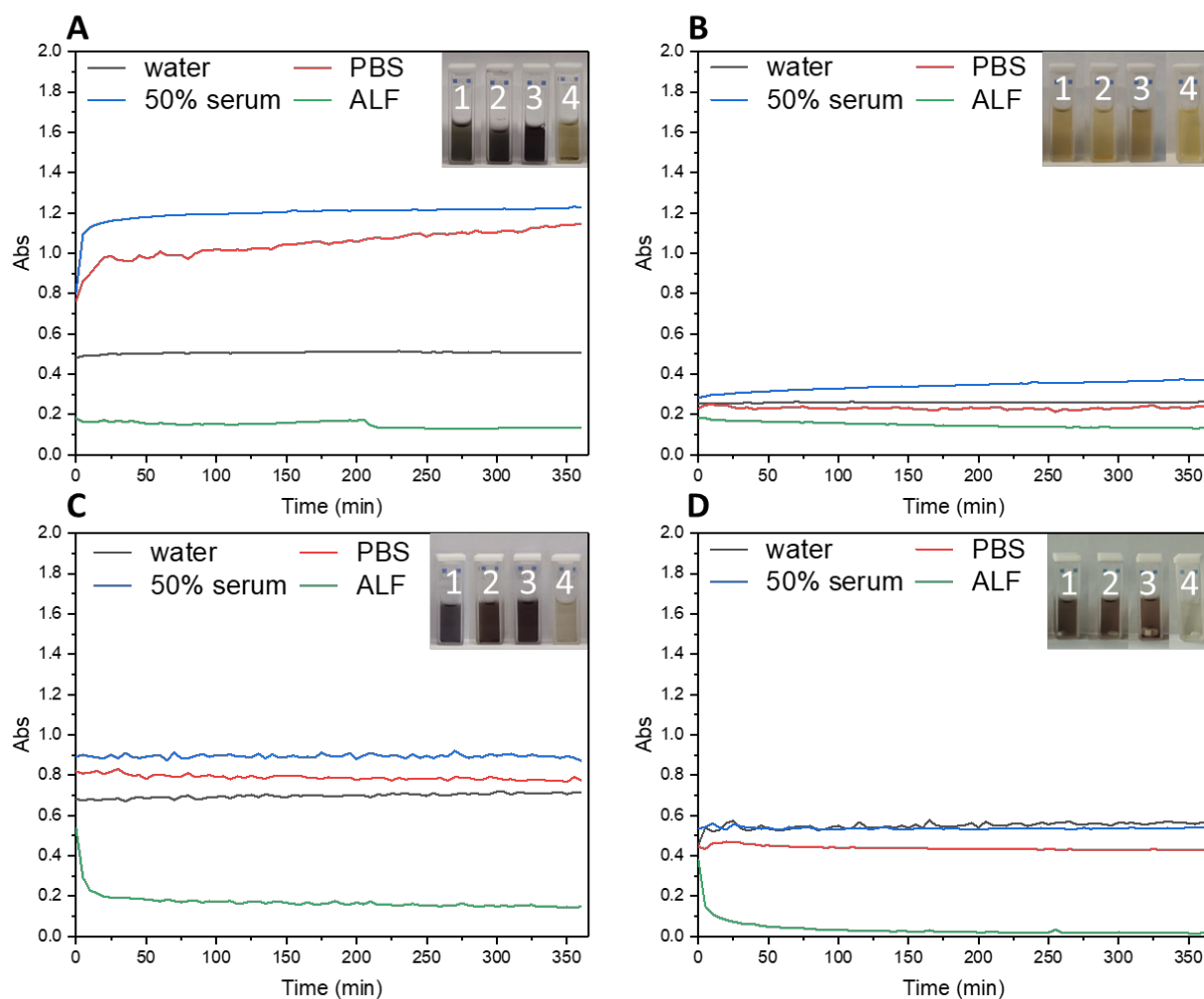


Figure 13. Absorbance of IGPNs at 550 nm in different media (1: water, 2: PBS, 3: 50% serum, 4: ALF). (A) Fe-A₄*. (B) FePVP-A₄*. (C) Fe-A₄***. (D) FePVP-A₄**.

4.3 Cellular uptake of IGPNs

The cellular uptake of IGPNs was investigated to confirm that the assembly into nanoparticles is a favorable strategy to facilitate the cellular delivery of non-permeable peptides. carboxyfluorescein-labeled derivatives of the model peptides with poor cell permeability (A_4 , A_4^* , A_4^{**} , $(EA)_2$, $(EA)_2^*$, $(EA)_2^{**}$) were used for assembly into fluorescent IGPNs ($Fe-A_4^*$, $FePVP-A_4^*$, $Fe-A_4^{**}$, $FePVP-A_4^{**}$, $Fe-(EA)_2^*$, $FePVP-(EA)_2^*$, $Fe-(EA)_2^{**}$, $FePVP-(EA)_2^{**}$) and cellular internalization was determined by flow cytometry analysis (Figure 14) and confocal laser scanning microscopy (CLSM, Figure 15 and Figure 16). As expected, cells treated with free carboxyfluorescein-labeled peptides exhibited significant fluorescence levels compared to HBG buffer treated cells. In contrast, assembly into IGPNs strongly promoted cellular delivery of A_4^* , A_4^{**} , $(EA)_2^*$ and $(EA)_2^{**}$. Moreover, the CLSM images confirm, that with IGPNs ($Fe-A_4^*$, $FePVP-A_4^*$, $Fe-A_4^{**}$ and $FePVP-A_4^{**}$) intracellular carboxyfluorescein is detectable, in contrast to the free carboxyfluorescein-labeled peptides (A_4 , A_4^* , A_4^{**}) alone. Altogether, the results demonstrate that IGPNs represent a feasible strategy for cellular peptide delivery.

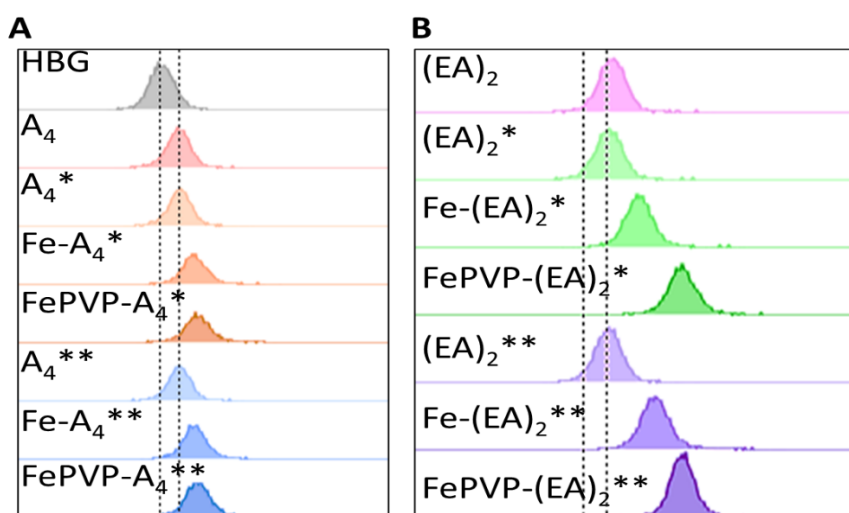


Figure 14. Flow cytometry analysis of HeLa cells treated with carboxyfluorescein-labeled peptides or derived IGPNs for 4 h. Experiments performed by Yi Lin (Pharmaceutical Biotechnology, LMU München).

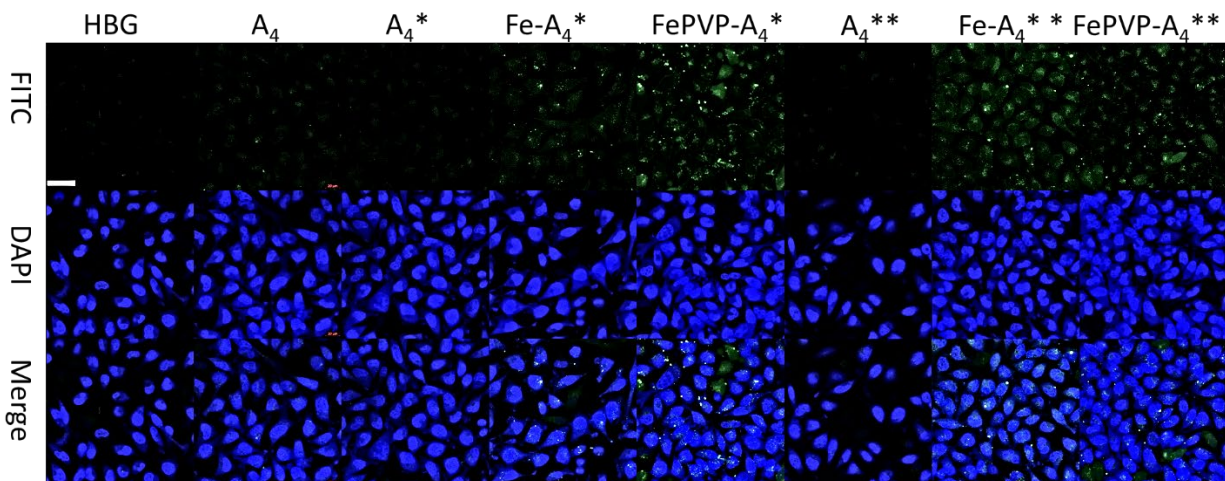


Figure 15. CLSM images of HeLa cells treated with HBG buffer, carboxyfluorescein-labeled A_4 , A_4^* , A_4^{**} , $Fe-A_4^*$, $FePVP-A_4^*$, $Fe-A_4^{**}$ or $FePVP-A_4^{**}$ for 4 h. Nuclei were stained with DAPI. Additional flow cytometry and CLSM data are provided in Figure S8-S10. Scale bar, 40 μ m. Experiments performed by Miriam Höhn (Pharmaceutical Biotechnology, LMU München) and Yi Lin (Pharmaceutical Biotechnology, LMU München).

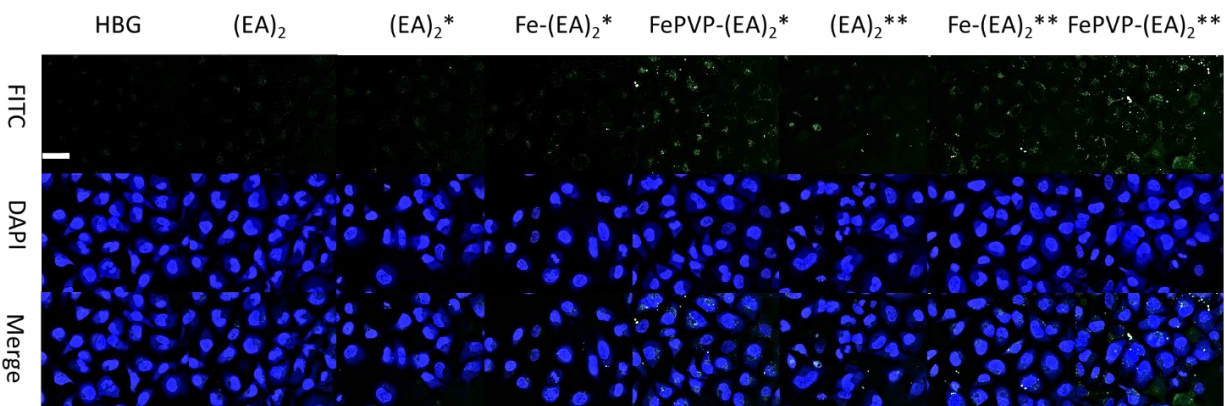


Figure 16. Cellular uptake of carboxyfluorescein-labeled peptides determined by confocal laser scanning microscopy (CLSM). HeLa cells were incubated with HBG, $(EA)_2$, $(EA)_2^*$, $(EA)_2^{**}$, $Fe-(EA)_2^*$, $FePVP-(EA)_2^*$, $Fe-(EA)_2^{**}$, $FePVP-(EA)_2^{**}$ for 4 h. Nuclei were stained with DAPI (blue), FITC channel indicates carboxyfluorescein fluorescence (green). Scale bar: 40 μ m. Experiments performed by Miriam Höhn (Pharmaceutical Biotechnology, LMU München) and Yi Lin (Pharmaceutical Biotechnology, LMU München).

4.4 ROS production of IGPNs

To verify the hypothesized Fenton reaction of IGPNs, H_2O_2 was used as a source of hydroxyl radicals ($\text{HO}\cdot$) and to simulate the tumor microenvironment. This is confirmed by monitoring the generation of $\text{HO}\cdot$ with methylene blue (MB).³¹ The degradation of MB upon exposure to H_2O_2 and different samples adjusted to the same Fe content (IGPNs or FeCl_3 solution) was monitored by UV-Vis spectrometry. At pH 4 (Figure 17A) the absorbance at 664 nm decreased rapidly in presence of Fe-A_4^{**} , FePVP-A_4^{**} or Fe^{3+} . While no different reaction rates were observed for IGPNs and Fe at the favorable acidic pH, at pH 7.4 the absorbance decline was generally slower, but much more obvious in case of IGPNs. (Figure 17B). This phenomenon could be explained by an accelerated conversion of Fe^{3+} to Fe^{2+} in presence of GA. Altogether, the above results indicate that IGPNs facilitate the generation of toxic ROS, which is expected to enhance their therapeutic effect.

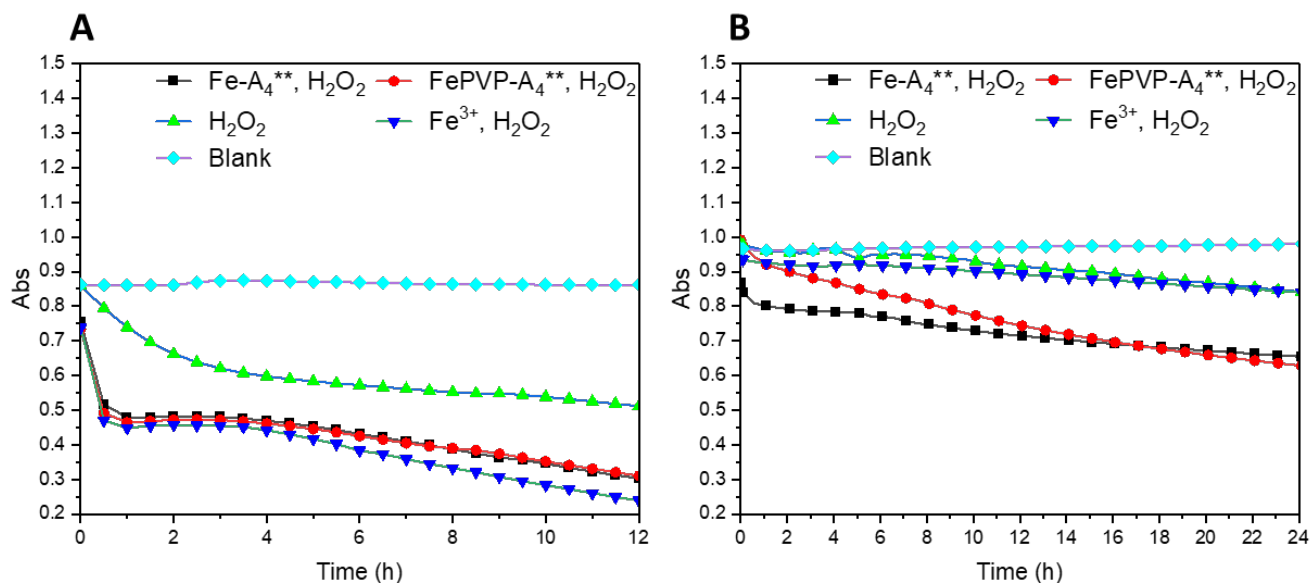


Figure 17. Determination of ROS generation by UV-Vis spectrometry. (A), (B) Detection of $\text{HO}\cdot$ at pH 4 (A) and pH 7.4 (B) by monitoring of methylene blue absorbance for 6 h at 664 nm.

To further evaluate ROS production on a cellular level, flow cytometry and confocal laser scanning microscopy (CLSM) were employed for determination. CellROX™ Green reagent, which is converted to a bright fluorescent derivative intracellularly in presence of

ROS, was incubated with HeLa cells pretreated with A_4^* , $Fe-A_4^*$, $FePVP-A_4^*$, A_4^{**} , $Fe-A_4^{**}$, $FePVP-A_4^{**}$. HBG and tert-butyl hydroperoxide (TBHP) treated cells served as negative and positive controls, respectively. After 45 min incubation, dead cells were stained with SYTOX red. After the evaluation of 10000 live cells by flow cytometry, it was found that IGPNs ($Fe-A_4^*$, $FePVP-A_4^{**}$, $Fe-A_4^{**}$, $FePVP-A_4^{**}$) mediated a distinct shift of the cell populations towards higher CellROX™ Green fluorescence, comparable to the positive control TBHP (Figure 18A). A visual confirmation of intracellular ROS generation was achieved by CLSM using the ROS imaging probe 2',7'-dichlorodihydrofluorescein diacetate (DCFDA), which is oxidized to 2',7'-dichlorofluorescein (DCF) upon intracellular exposure to ROS. Compared with the HBG group, a much stronger green fluorescence could be observed in cells after 24 h incubation with IGPNs (Figure 18B).

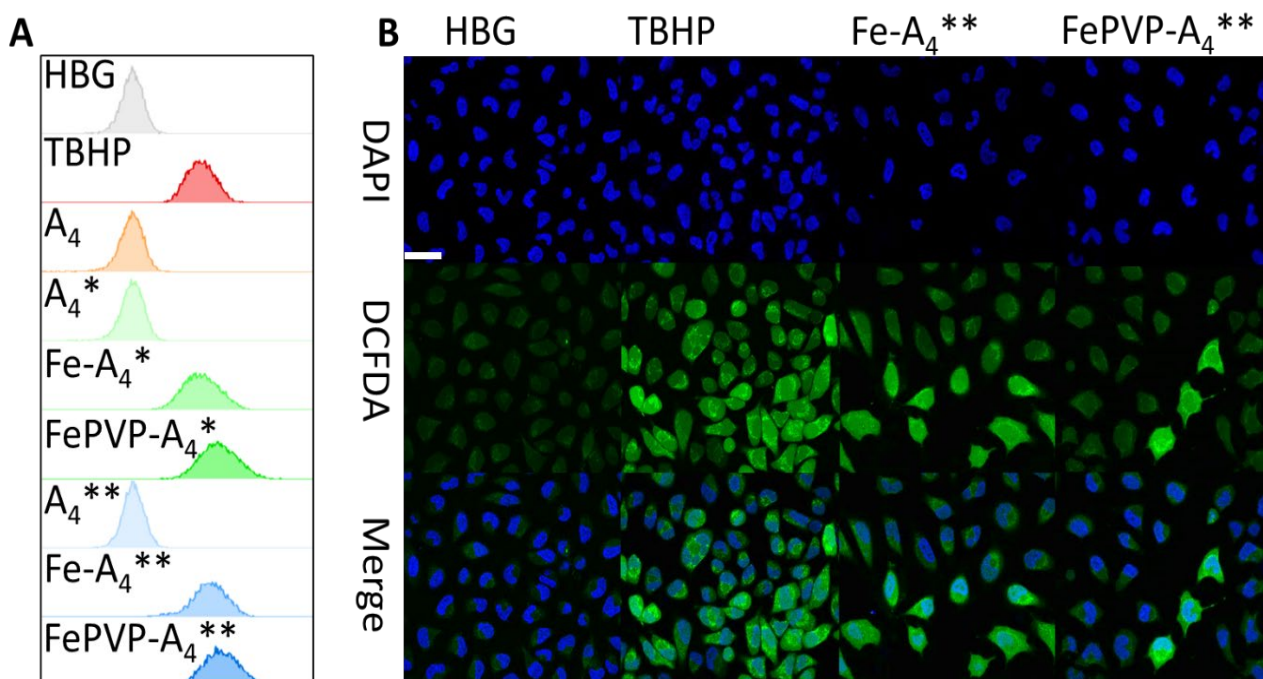


Figure 18. Determination of intracellular ROS generation by flow cytometry and confocal microscopy. (A) HeLa cells incubated with A_4 peptides and derived IGPNs (10 μ M, 24 h) followed by staining with CellROX Green. (B) HeLa cells incubated with $Fe-A_4^{**}$ and $FePVP-A_4^{**}$ (10 μ M, 24 h) followed by staining with DCFDA. TBHP was used as a positive control. Scale bar, 40 μ m. Experiments performed by Miriam Höhn (Pharmaceutical Biotechnology, LMU München) and Yi Lin (Pharmaceutical Biotechnology, LMU München).

Additional data indicates that the IPGN-triggered ROS generation is time and dose dependent (Figure 19). In sum, IPGNs demonstrated a distinct ability to generate ROS in HeLa cells, with Fe-A₄** and FePVP-A₄** being most effective.

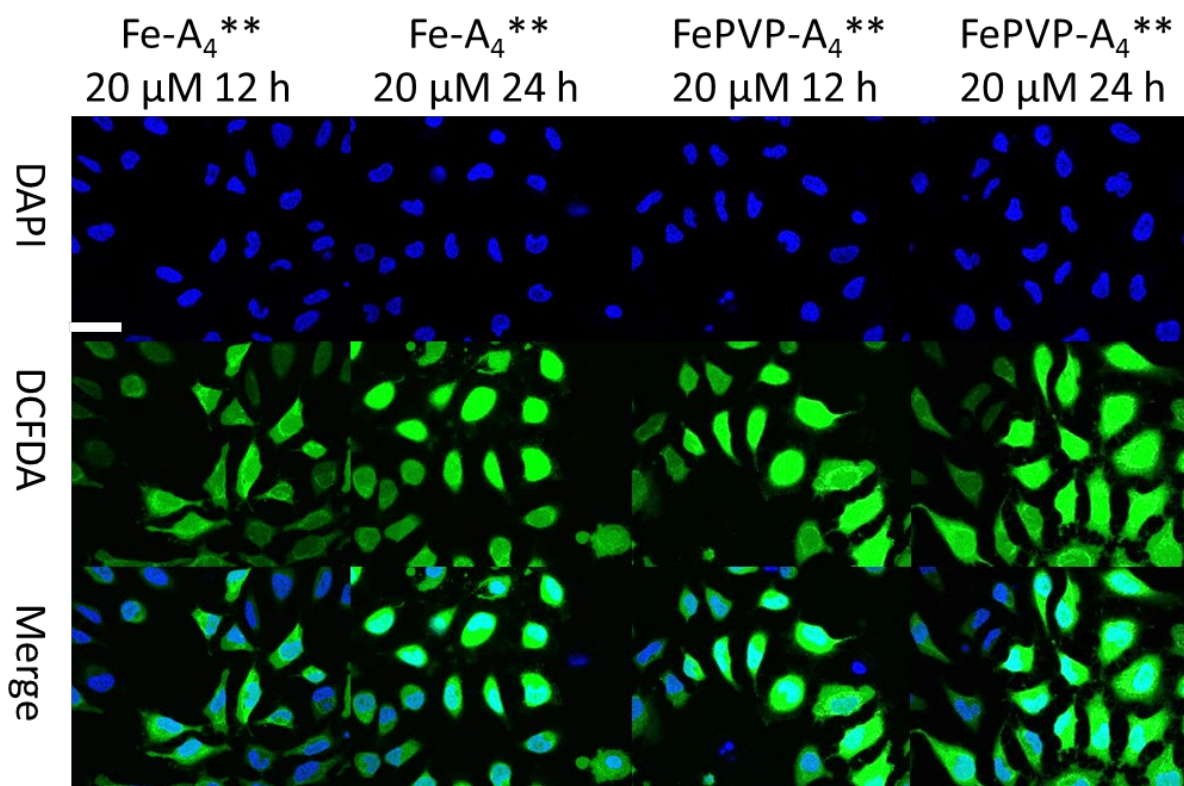


Figure 19. Determination of intracellular ROS formation. HeLa cells were incubated with Fe-A₄** (20 μM) and FePVP-A₄** (20 μM) for 12 h or 24 h, respectively. Nuclei were stained with DAPI (blue) and ROS was detected by DCFDA (green). Scale bar: 40 μm. Experiments performed by Miriam Höhn (Pharmaceutical Biotechnology, LMU München) and Yi Lin (Pharmaceutical Biotechnology, LMU München).

4.5 Bioactivity of IGPNs

The general cytotoxicity of IGPNs as well as the ability to induce biological effects by delivering bioactive peptides were evaluated by CellTiter-Glo assay in HeLa cells (Figure 20). The two pro-apoptotic peptides SIO and AVP were selected as bioactive peptide cargos. FeCl₃ solution (Fe), the complex of iron and PVP (FePVP) as well as free peptides (unmodified and coupled with gallic acid) were used as controls at the same concentration

(10 μM). The viability of cells treated with the model peptides A_4 , A_4^* and A_4^{**} indicate that the integration of gallic acid did not affect the tolerability of the derivatives. Moreover, IGPNs assembled from the inactive model peptides did not show obvious toxicity and cell viability levels remained over 80% in all cases. Also, the pro-apoptotic peptides SIO and AVP, with or without gallic acid modification, were not able to mediate significant cytotoxicity. In contrast, IGPNs assembled from double-GA modified pro-apoptotic peptides (Fe-SIO**, FePVP-SIO**, Fe-AVP**, FePVP-AVP**) induced strong tumor cell killing and reduced cell viability below 20%.

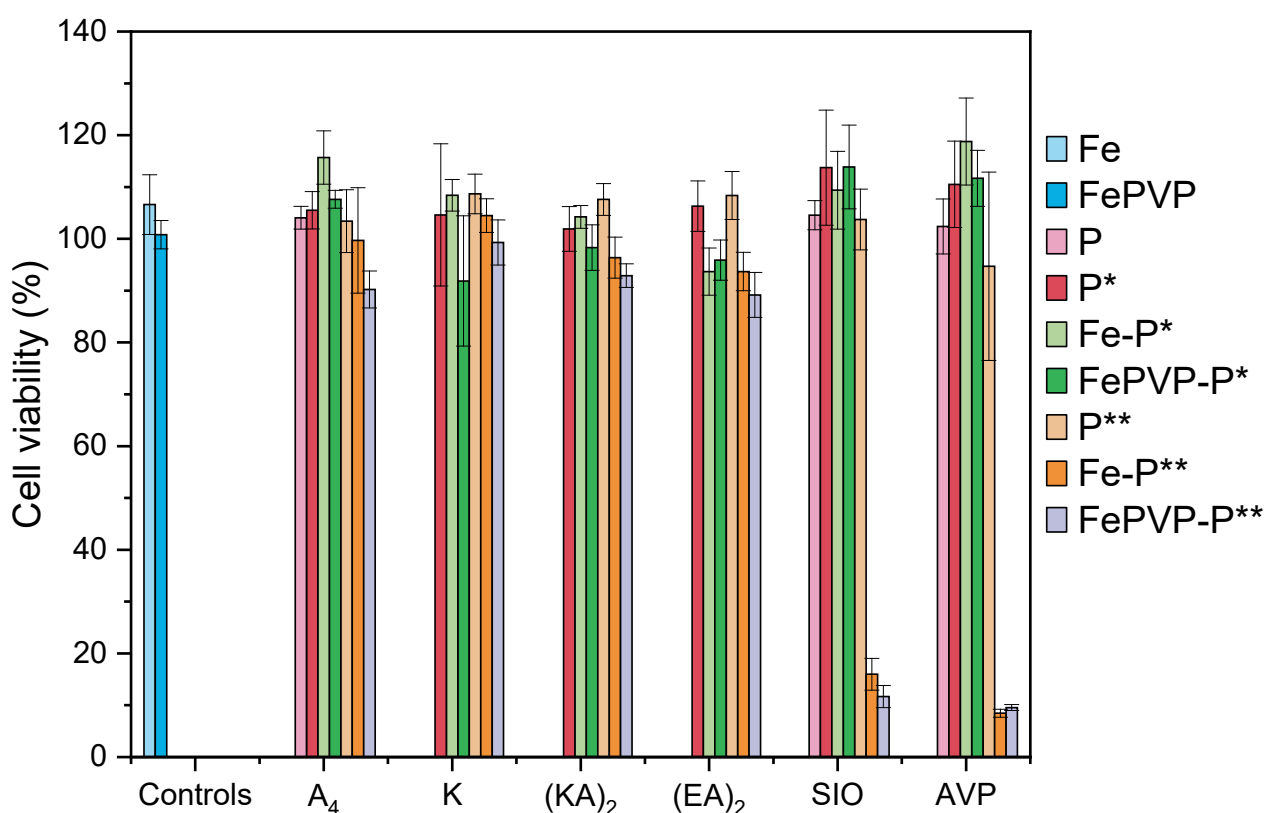


Figure 20. Cell viability of HeLa cells after treatment with peptides or IGPNs as determined by CellTiter-Glo[®] Luminescent Cell Viability Assay. HeLa cells were incubated for 72 h with Fe, FePVP, SIO, SIO*, SIO**, AVP, AVP*, AVP**, SIO**, Fe-SIO**, FePVP-SIO**, AVP**, Fe-AVP**, FePVP-AVP** at doses corresponding to 10 μM peptide content (or Fe^{3+} in case of Fe and FePVP). Experiments performed by Yi Lin (Pharmaceutical Biotechnology, LMU München).

Additional cell viability experiments with Fe-SIO^{**}, FePVP-SIO^{**} determined, that the cytotoxic effects are dose-dependent (Figure S21). To evaluate the cytotoxicity of IGPNs in another tumor cell line, the model peptide (A₄) and proapoptotic peptide (AVP) were chosen for testing in murine neuroblastoma Neuro 2A (N2a) cells. Also, in N2a cells, a pronounced cytotoxic effect was observed with Fe-AVP^{**} and FePVP-AVP^{**} at a dose corresponding to 10 μM peptide, whereas none of the other samples (free A₄ or AVP peptides, A₄-based IGPNs, Fe-AVP^{*} or FePVP-AVP^{*}) showed distinct effects on cell viability. These additional findings support the potential utility of IGPNs based on double GA-modified peptides as effective therapeutic agents against different types of tumor cells.

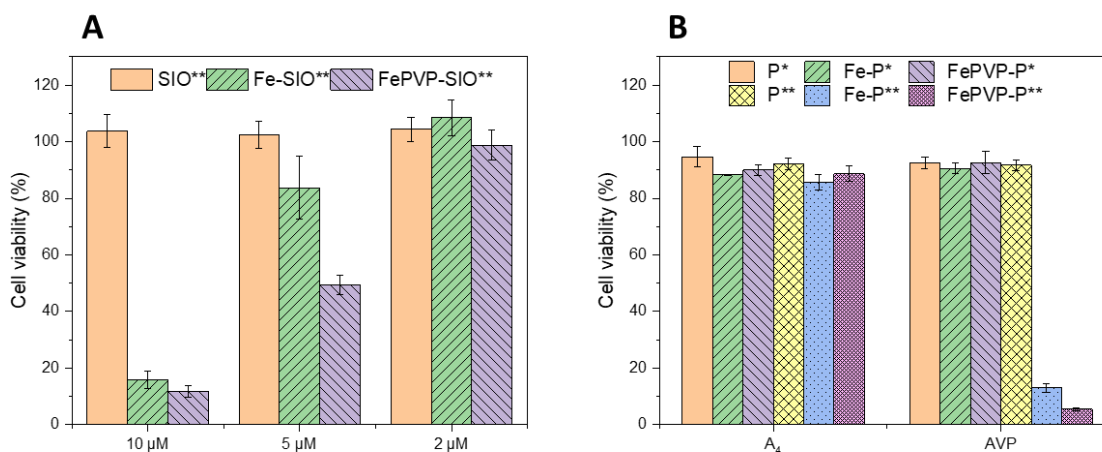


Figure 21. Cell viability determined by CellTiter-Glo Assay. (A) HeLa cells were incubated with SIO^{**}, Fe-SIO^{**}, FePVP-SIO^{**} (2, 5, and 10 μM), (B) N2a cells were incubated with IGPNs (10 μM) of A₄ and AVP for 72 h before evaluation via CellTiter-Glo[®] Luminescent Cell Viability Assay. Experiments performed by Yi Lin (Pharmaceutical Biotechnology, LMU München) and Xianjin Luo (Pharmaceutical Biotechnology, LMU München).

To elucidate the cytotoxicity mechanism of IGPNs more in detail, cell apoptosis assays were carried out via Annexin V and propidium iodide (PI) staining and flow cytometry (Figure 22, 23). Consistent with the cell viability data, none of the controls or IGPNs assembled from single-GA modified peptides resulted in obvious apoptosis induction; only the cells treated with IGPNs assembled from double-GA modified pro-apoptotic peptides showed a clear enrichment of Annexin-V-FITC positive subpopulations indicating the

occurrence of apoptotic events. These results demonstrate that double-GA modification of bioactive peptides and assembly into IGPNs is a feasible strategy for cytosolic delivery and induction of intracellular biological effects.

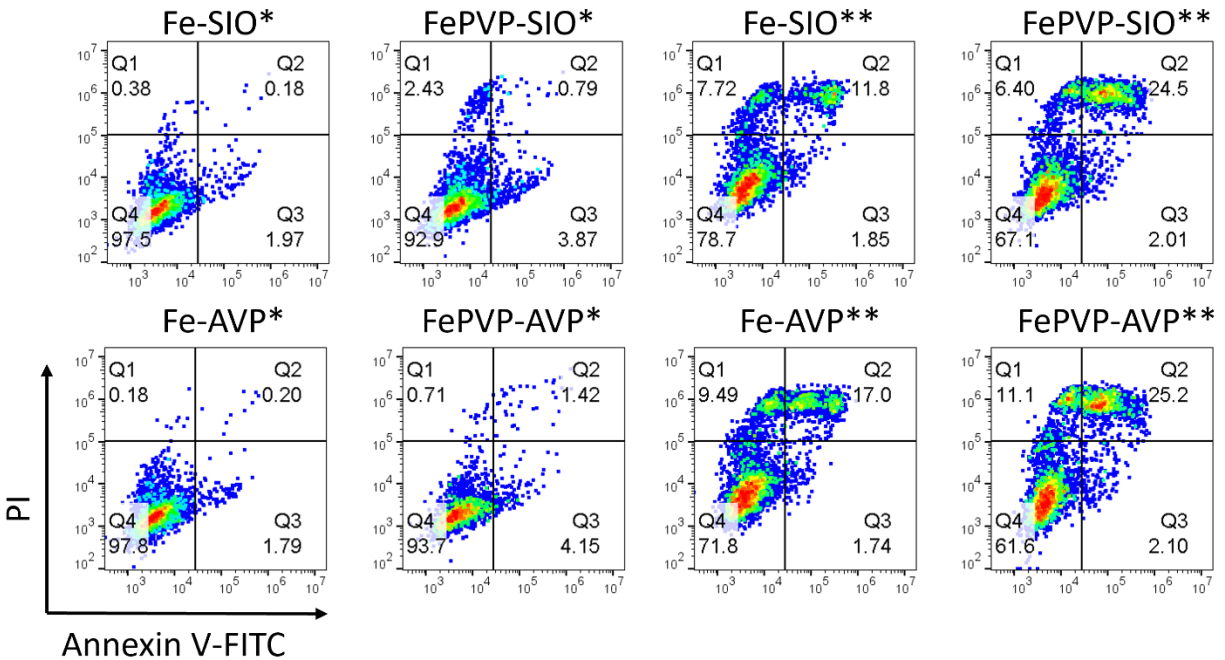


Figure 22. Evaluation of apoptotic events by PI/Annexin V-FITC staining and flow cytometry. HeLa cells were incubated for 24 h with Fe-SIO**, FePVP-SIO**, AVP**, Fe-AVP**, FePVP-AVP** at doses corresponding to 10 μ M peptide content. Experiments performed by Yi Lin (Pharmaceutical Biotechnology, LMU München).

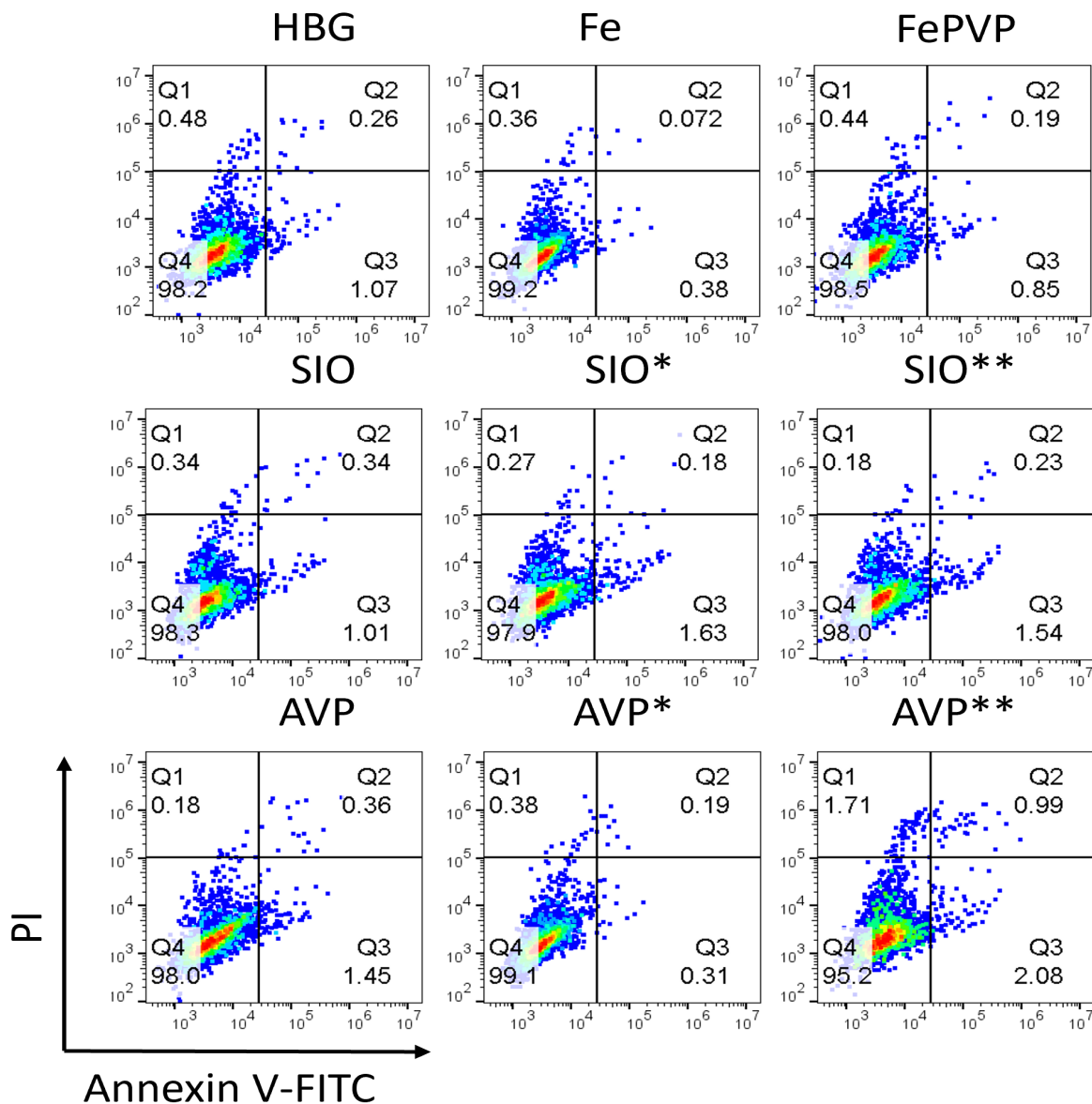


Figure 23. Evaluation of apoptotic events by PI/Annexin V-FITC staining and flow cytometry. HeLa cells were incubated for 24 h with Fe, FePVP, SIO, SIO *, SIO **, AVP, AVP*, AVP** at doses corresponding to 10 μ M peptide content (or Fe³⁺ in case of Fe and FePVP). Experiments performed by Yi Lin (Pharmaceutical Biotechnology, LMU München).

5 Summary

Cytosolic delivery of peptides is of great interest owing to their biological functions, which could be utilized for therapeutic applications. However, their susceptibility to enzymatic degradation and the multiple cellular barriers hinder their clinical applications. Integration into nanoparticles, which can enhance the stability and membrane permeability of bioactive peptides, is a promising strategy to overcome the extracellular and intracellular obstacles.

A novel generic strategy for the assembly of peptides into metallo-peptidic nanoparticles is presented. By conjugation of gallic acid (GA) to the side-chains of C- and N-terminal lysines, GA modified peptides are generated, which assemble quantitatively with Fe^{3+} or PVP-templated Fe^{3+} (FePVP) into iron-gallic acid peptide nanoparticles (IGPNs). This approach exhibits versatility in its applicability to a wide range of peptides with varying lengths, charges, and sequences. GA functions can readily be integrated into peptide sequences by the presented approach via coupling to C- and N-terminal lysine side chains. IGPNs, especially the double GA-modified FePVP NPs are stable in water, PBS and serum-containing medium, but decompose in artificial lysosomal fluid (ALF), which indicates the endolysosomal biodegradability of the particles. Although the particle appearance of dry disperse Fe and FePVP IGPNs appears similar in TEM imaging, the PVP assembly approach is considered to be favorable for higher colloidal stability in aqueous environment. It could be shown that IGPNs are able to promote generation of reactive oxygen species (ROS) from H_2O_2 via a Fenton reaction. Furthermore, the assembly into IGPNs facilitates cellular uptake of peptides with poor cellular permeability otherwise. Finally, the IGPNs integrated with double GA-tagged pro-apoptotic peptides and FePVP demonstrated a potent anti-tumoral activity with apoptosis induction and killing of HeLa and N2a cells.

In sum, the presented data describes a convenient and versatile platform for the cellular delivery of cell-impermeable peptides and highlights a potential utilization for cancer therapy by combining apoptotic peptide cargos with the intrinsic ROS generation of IGPNs.

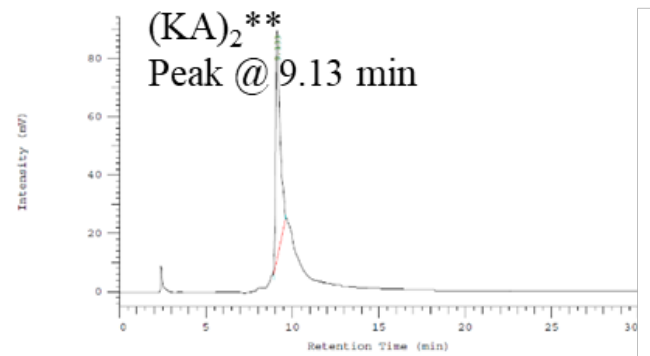
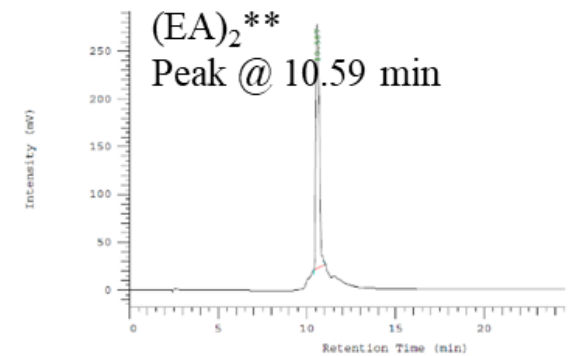
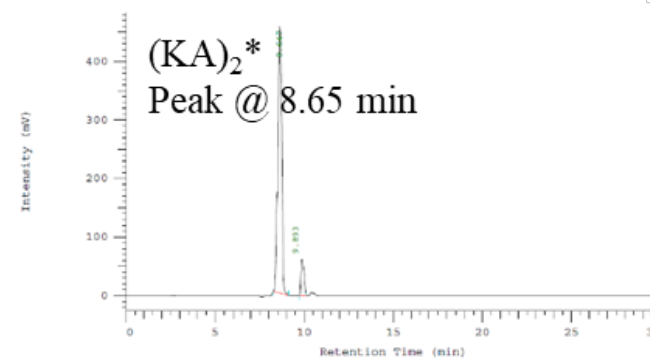
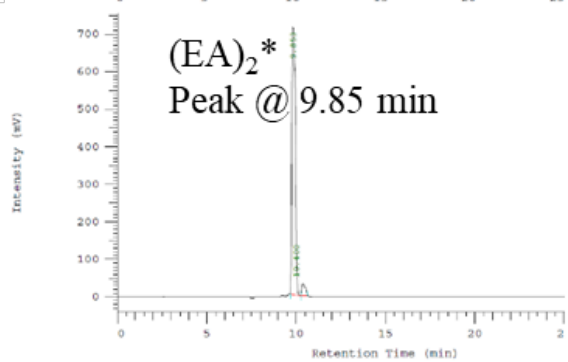
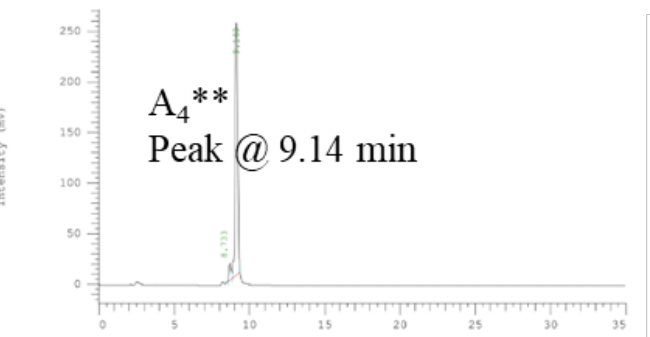
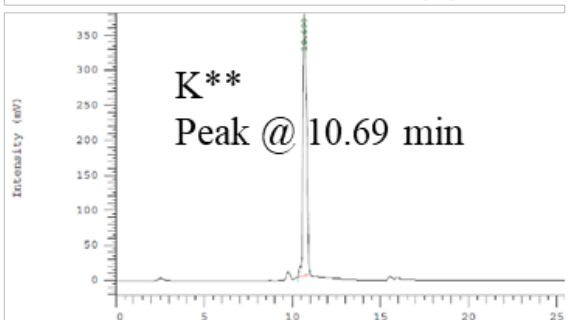
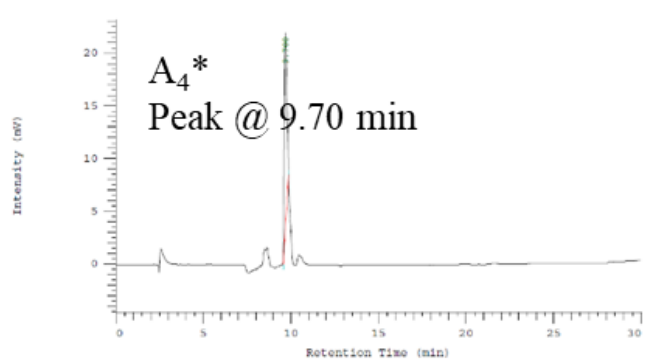
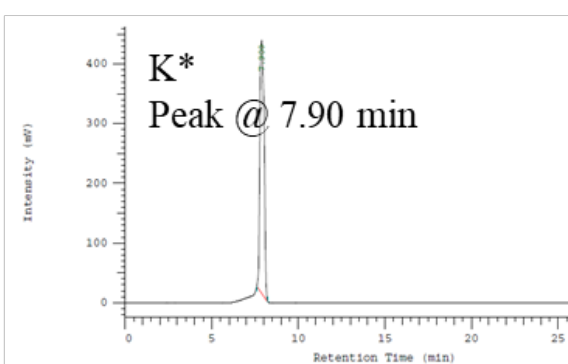
6 Abbreviations

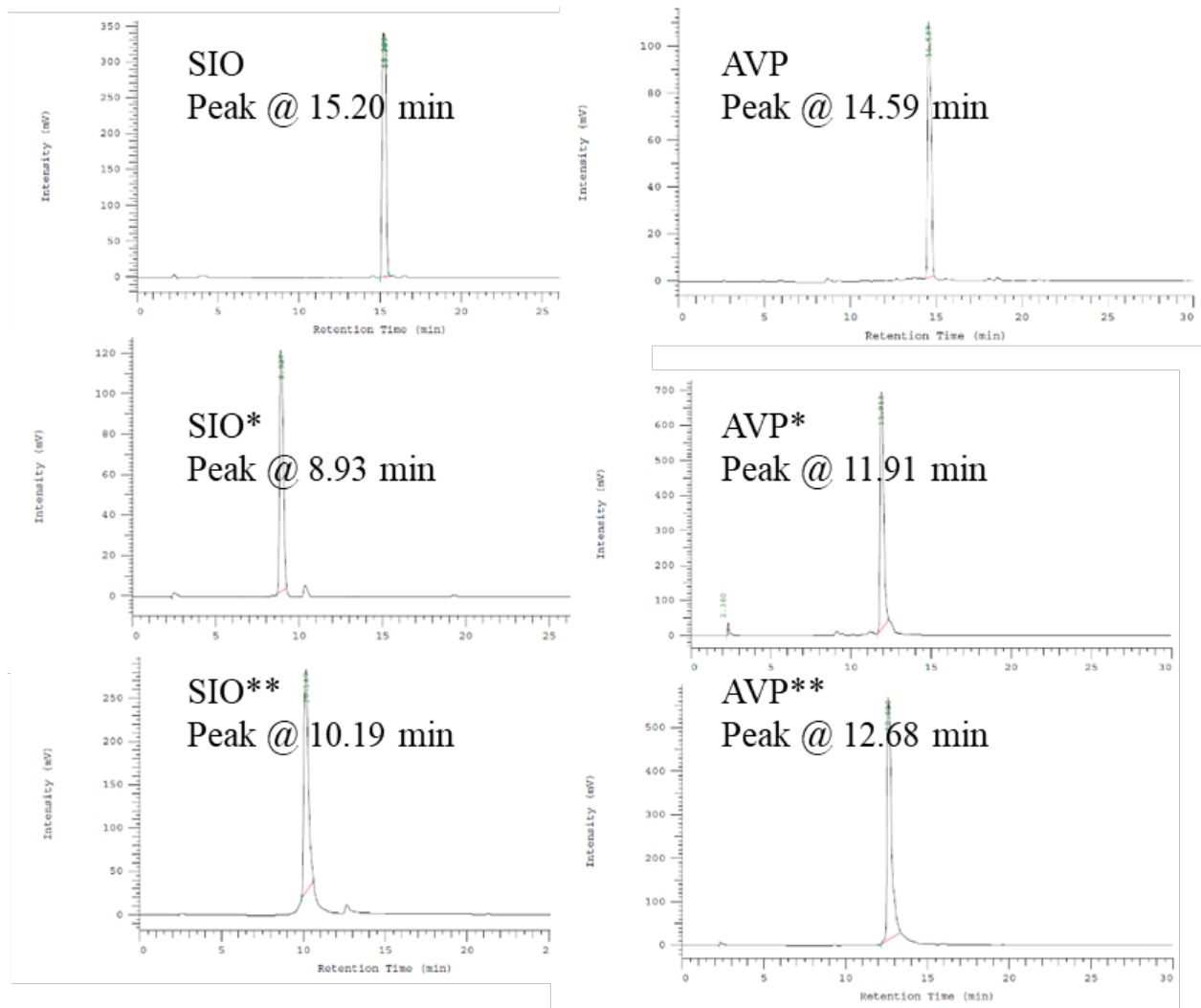
HO•	Hydroxyl radical
ADCs	Antibody-drug conjugates
ALF	Artificial lysosomal fluid
CDT	Chemodynamic therapy
CLSM	Confocal laser scanning microscopy
CPPs	Cell penetrating peptides
DCM	Dichloromethane
Den	Dendrimer
DHB	2,5-dihydroxybenzoic acid
DIPEA	<i>N,N</i> -diisopropylethylamine
DLS	Dynamic light scattering
DMAP	4-(dimethylamino)pyridine
DMF	<i>N,N</i> -dimethylformamide
DOPA	Dopamine
DOX	Doxorubicin
D-Trp	D-tryptophan
EGCG	Epigallocatechin gallate
FBS	Fetal bovine serum
FDA	Food and drug administration
FITC	Fluorescein isothiocyanate
GA	Gallic acid
Glu-PLGA	Glucose-poly(lactide-co-glycolide)
H ₂ DCFDA	2',7'-dichlorodihydrofluorescein-diacetate
HAS, HSA	Human serum albumin
HOBt	1-hydroxybenzotriazole
ICP-OES	Inductively Coupled Plasma Optical Emission spectroscopy
IGPNs	Iron-gallic acid peptide nanoparticles
IUPAC	International Union of Pure and Applied Chemistry
kDa	Kilodalton
LMCT	Ligand to Metal Charge Transfer Bands
L-Trp	L-tryptophan
MDR	Multidrug resistance
mL	Milliliter
mM	Millimolar
mmol	Millimole
MOF	Metal-organic framework
MPNs	Metal polyphenol networks
MWCO	Molecular weight cut-off

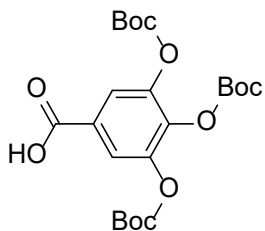
NMP	N-methyl-2-pyrrolidone
NMR	Nuclear magnetic resonance
NPs	Nanoparticles
PAS	Pro, Ala and Ser
PBS	Phosphate buffered saline
PDCs	Peptide-drug conjugates
PDI	Polydispersity index
PEG	Poly(ethylene glycol)
PK	Pharmacokinetic
PPI	Protein-protein interactions (PPI)
PVP	Poly-(vinylpyrrolidone)
PyBOP	Benzotriazol-1-yloxytripyrrolidinophosphonium hexafluorophosphate
RGD	Tripeptide - arginine, glycine, aspartic acid
ROS	Reactive oxygen species
RP- HPLC	High performance liquid chromatography
SEM	Scanning electron microscopy
SPPS	Solid-phase peptide synthesis
TA	Tannic acid
TBHP	Tert-butyl hydroperoxide solution
TFA	Trifluoroacetic acid
TGA	Thermogravimetric analysis
TME	Tumor microenvironments
UV Vis	Ultraviolet visible
XRD	X-ray diffraction
μM	Micromolar
μmol	Micromole

7 Analytical data

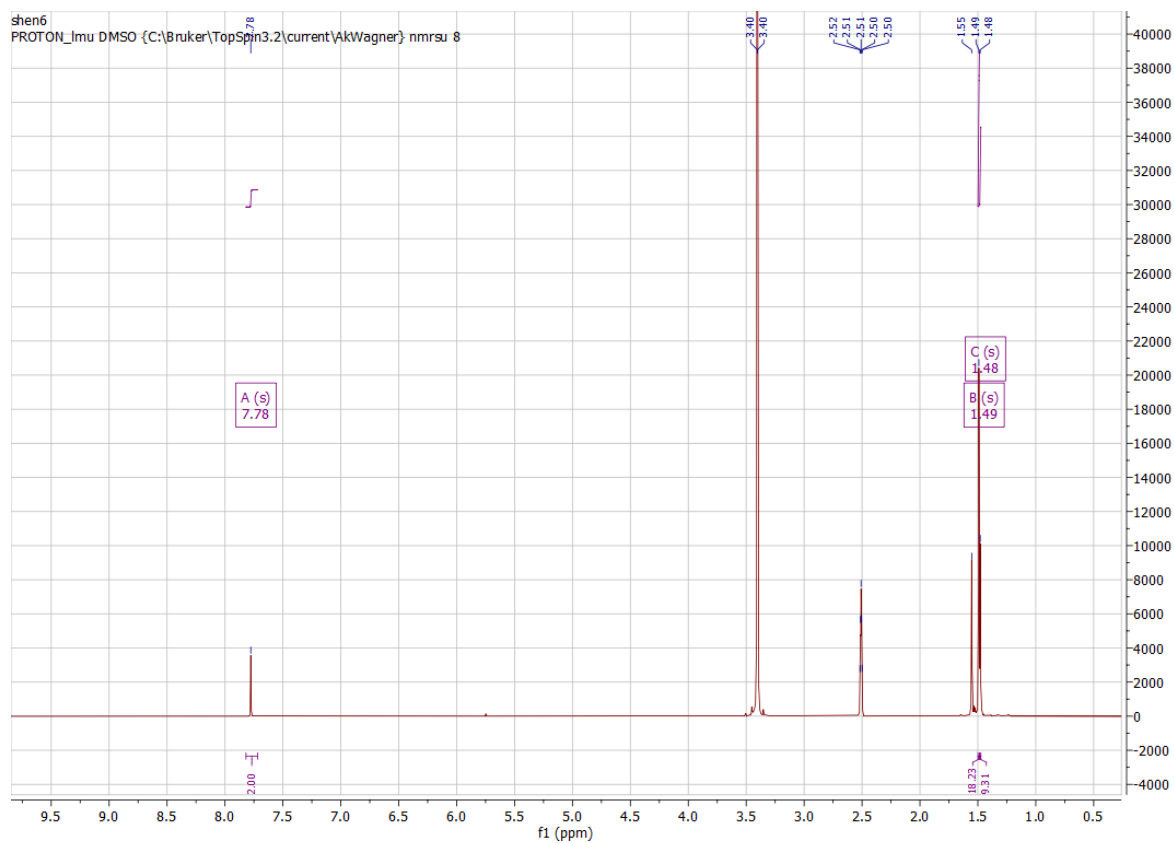
HPLC (RP-C18, detection at 280 nm)





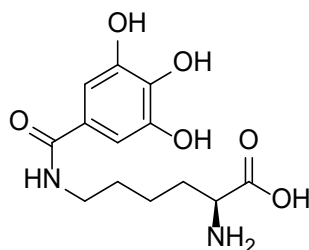
¹H NMR spectra**GA(Boc)₃-OH**

Chemical Formula: C₂₂H₃₀O₁₁
Exact Mass: 470.18

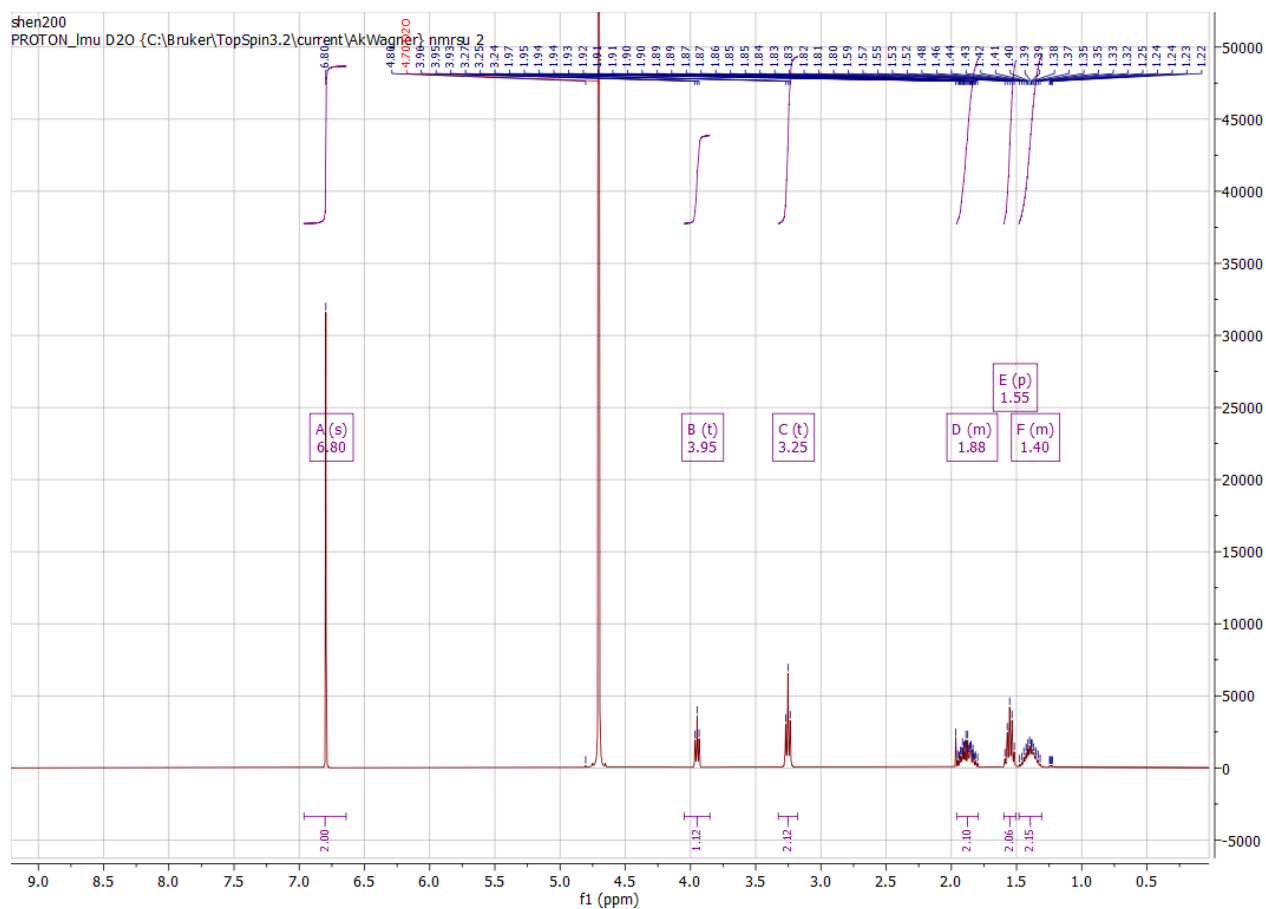


¹H NMR (400 MHz, DMSO-d₆) δ 7.78 (d, J = 0.6 Hz, 2H), 1.49 (s, 18H), 1.48 (s, 9H).

K*

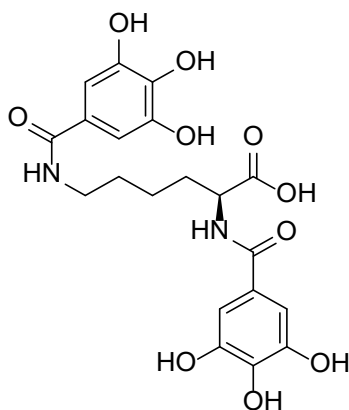


Chemical Formula: $C_{13}H_{18}N_2O_6$
Exact Mass: 298.12

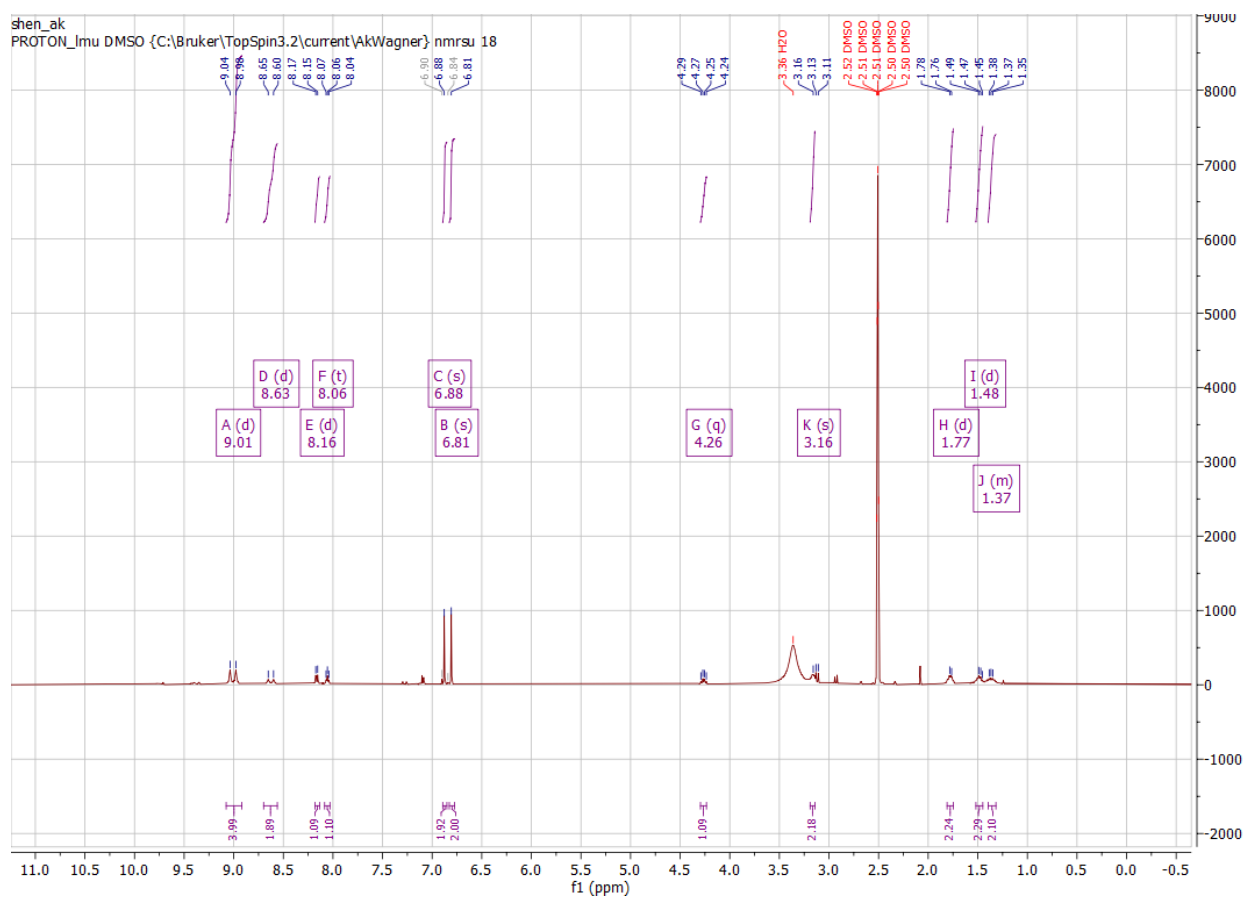


^1H NMR (400 MHz, Deuterium Oxide) δ 6.80 (s, 2H), 3.95 (t, $J = 6.3$ Hz, 1H), 3.25 (t, $J = 6.9$ Hz, 2H), 1.96 - 1.79 (m, 2H), 1.55 (p, $J = 7.2$ Hz, 2H), 1.48 - 1.31 (m, 2H).

K**

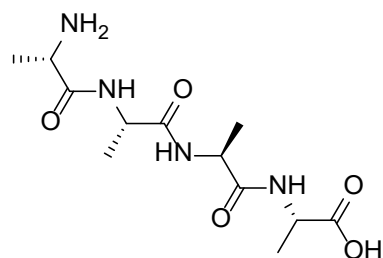


Chemical Formula: C₂₀H₂₂N₂O₁₀
 Exact Mass: 450.13

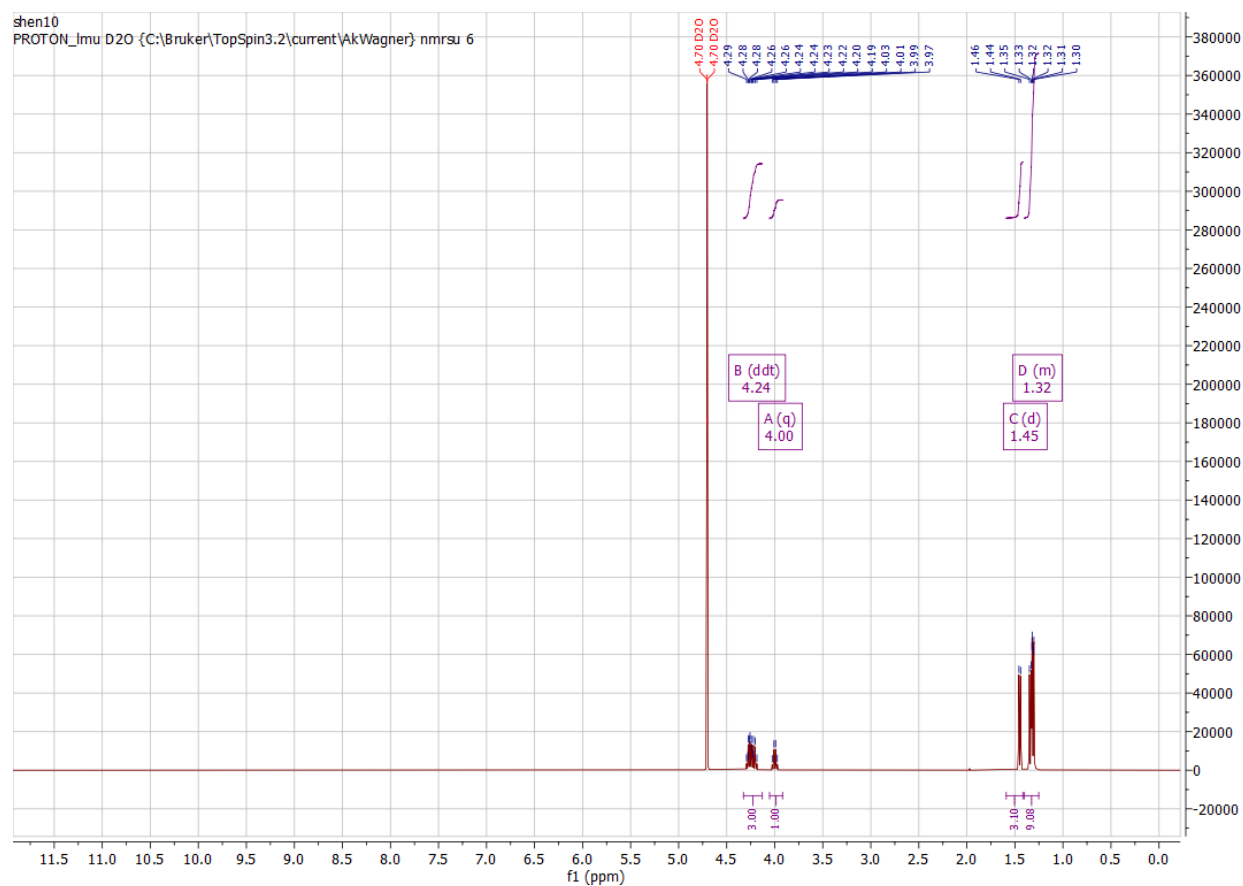


¹H NMR (400 MHz, DMSO-d₆) δ 9.01 (d, *J* = 23.4 Hz, 3H), 8.63 (d, *J* = 21.4 Hz, 2H), 8.16 (d, *J* = 7.6 Hz, 1H), 8.06 (t, *J* = 5.5 Hz, 1H), 6.88 (s, 2H), 6.81 (s, 2H), 4.26 (q, *J* = 7.5 Hz, 1H), 3.16 (s, 2H), 1.77 (d, *J* = 7.6 Hz, 2H), 1.48 (d, *J* = 8.3 Hz, 2H), 1.41 - 1.31 (m, 2H).

A4

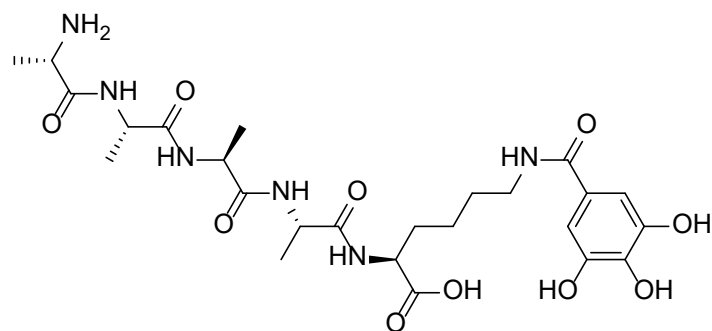


Chemical Formula: $C_{12}H_{22}N_4O_5$
Exact Mass: 302.16

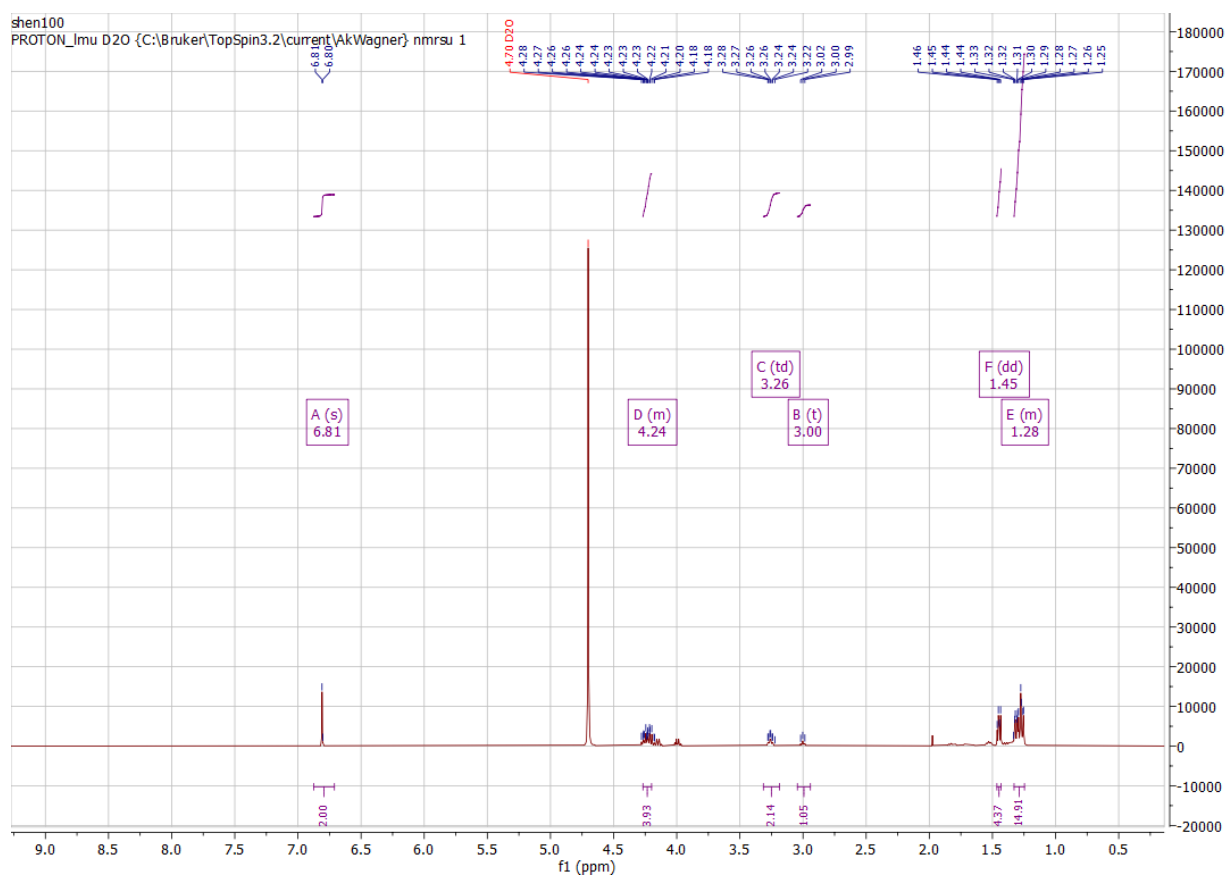


^1H NMR (400 MHz, Deuterium Oxide) δ 4.24 (ddt, $J = 15.9, 14.4, 7.2$ Hz, 3H), 4.00 (q, $J = 7.1$ Hz, 1H), 1.45 (d, $J = 7.1$ Hz, 3H), 1.37 - 1.24 (m, 9H).

A4*

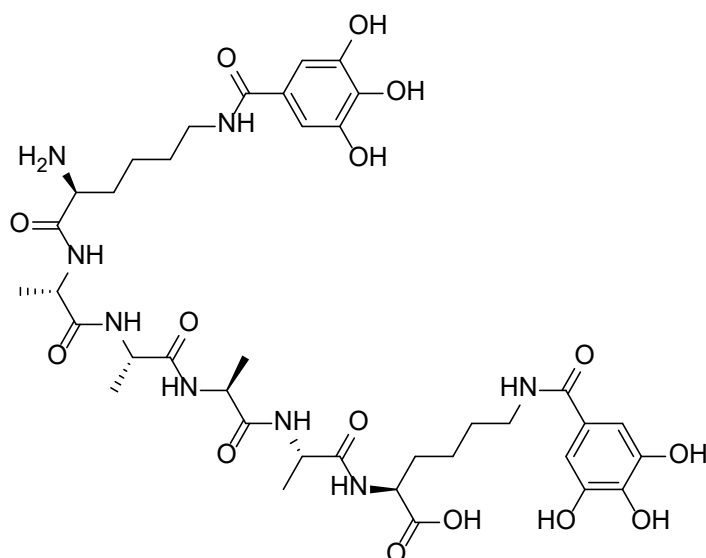
Chemical Formula: C₂₅H₃₈N₆O₁₀

Exact Mass: 582.26

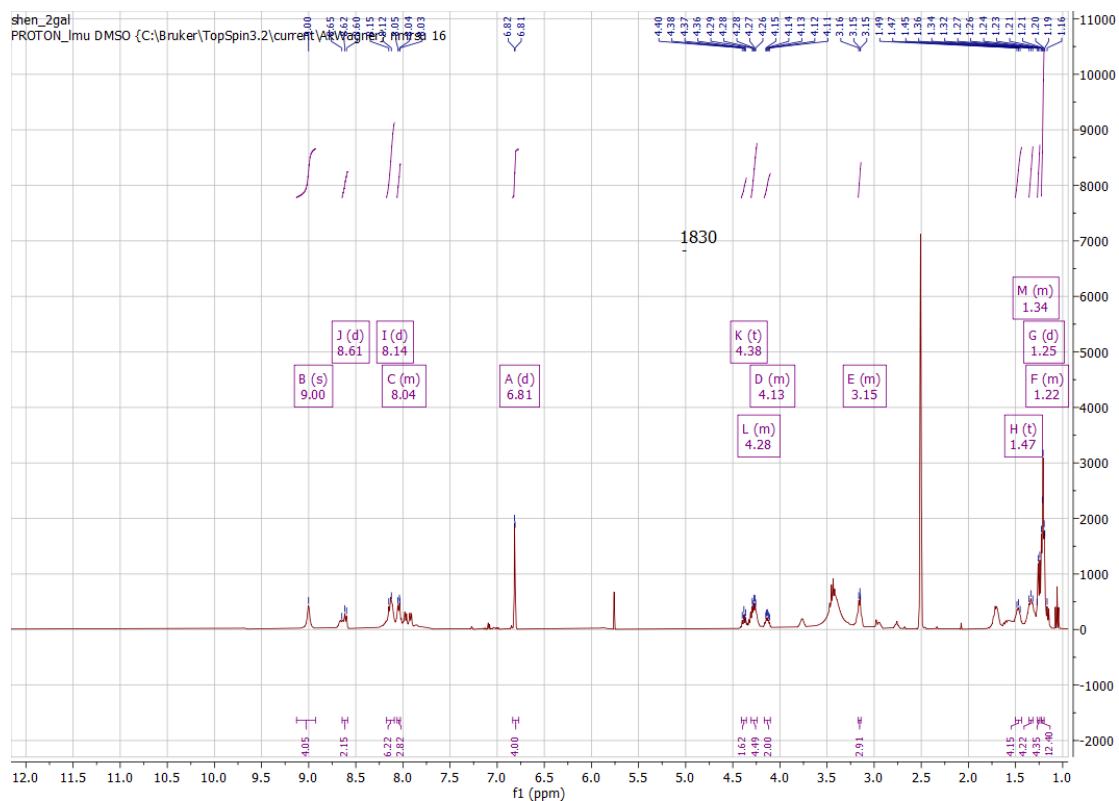


¹H NMR (400 MHz, Deuterium Oxide) δ 6.81 (s, 2H), 4.27 - 4.20 (m, 4H), 3.26 (td, $J = 6.7, 2.3$ Hz, 2H), 3.00 (t, $J = 6.7$ Hz, 1H), 1.45 (dd, $J = 7.1, 3.7$ Hz, 4H), 1.33 - 1.25 (m, 15H).

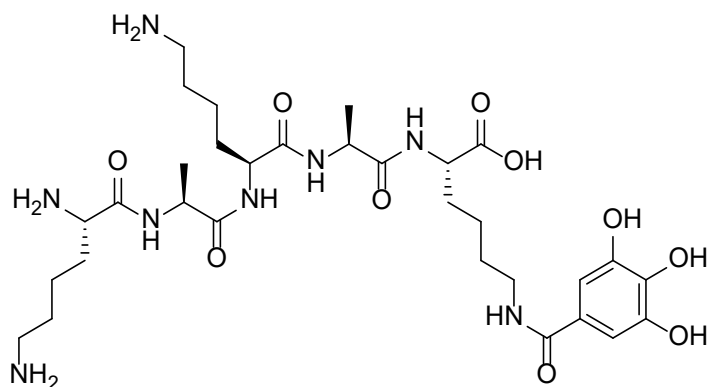
A4**



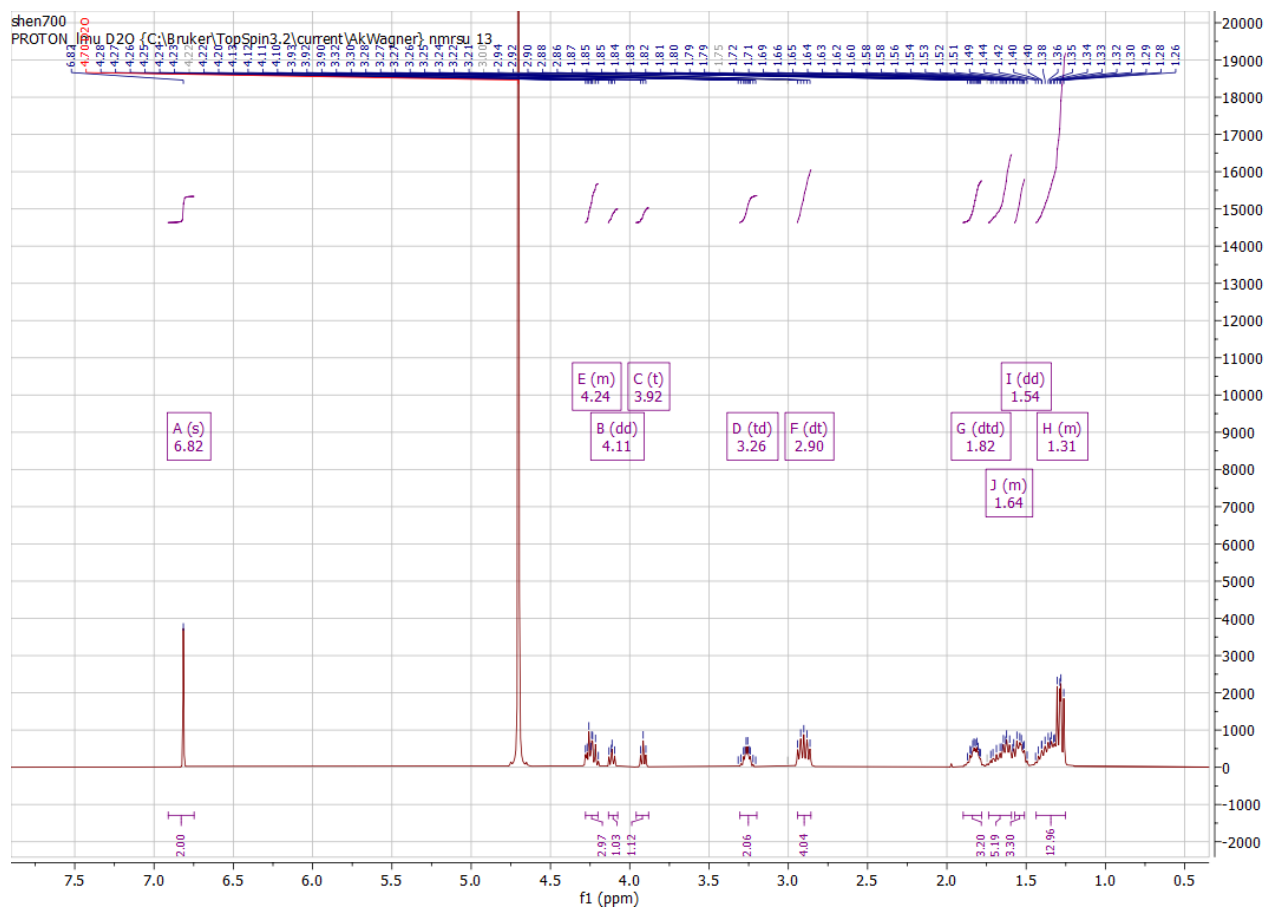
Chemical Formula: $C_{38}H_{54}N_8O_{15}$
Exact Mass: 862.37



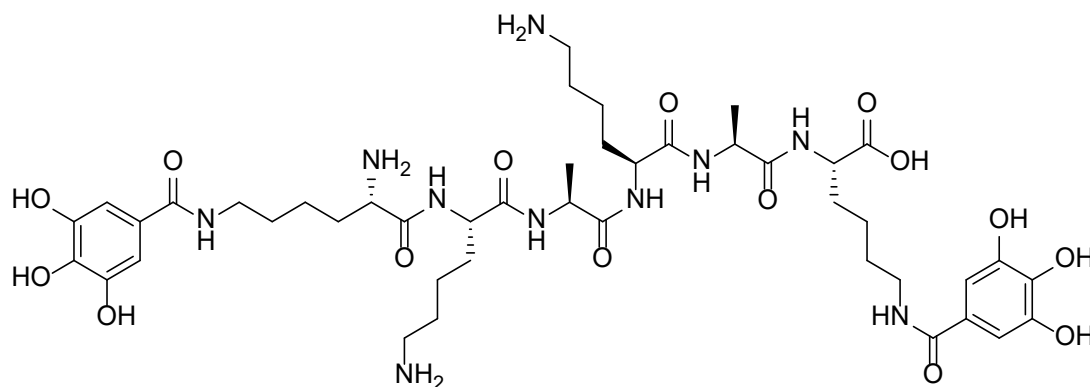
$^1\text{H NMR}$ (400 MHz, $\text{DMSO-}d_6$) δ 9.00 (s, 4H), 8.61 (d, $J = 7.3$ Hz, 2H), 8.14 (d, $J = 10.9$ Hz, 6H), 8.06 - 8.03 (m, 3H), 6.81 (d, $J = 2.4$ Hz, 4H), 4.38 (t, $J = 7.2$ Hz, 2H), 4.31 - 4.24 (m, 4H), 4.17 - 4.10 (m, 2H), 3.17 - 3.14 (m, 3H), 1.47 (t, $J = 6.9$ Hz, 4H), 1.36 - 1.32 (m, 4H), 1.25 (d, $J = 7.0$ Hz, 4H), 1.23 - 1.20 (m, 12H).

(KA)₂*Chemical Formula: C₃₁H₅₂N₈O₁₀

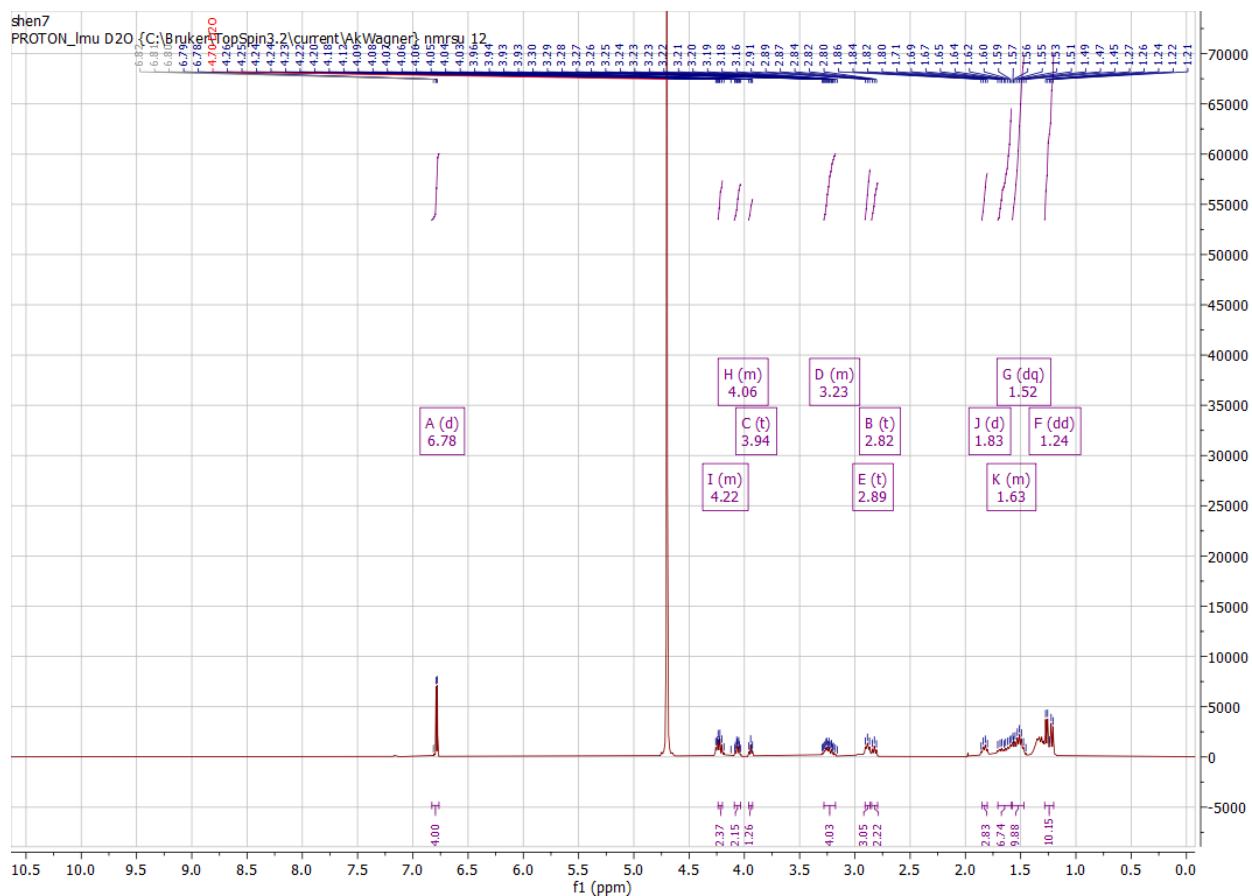
Exact Mass: 696.38



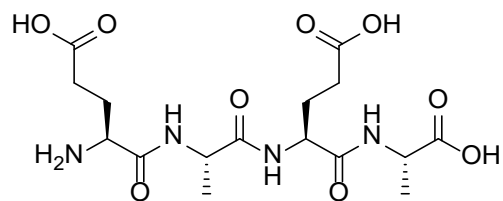
¹H NMR (400 MHz, Deuterium Oxide) δ 6.82 (s, 2H), 4.28 - 4.20 (m, 3H), 4.11 (dd, *J* = 8.0, 6.3 Hz, 1H), 3.92 (t, *J* = 6.7 Hz, 1H), 3.26 (td, *J* = 6.7, 3.6 Hz, 2H), 2.90 (dt, *J* = 15.5, 7.6 Hz, 4H), 1.82 (dtd, *J* = 9.3, 6.3, 2.8 Hz, 3H), 1.74 - 1.59 (m, 5H), 1.54 (dd, *J* = 11.2, 7.4 Hz, 3H), 1.44 - 1.25 (m, 13H).

(KA)₂**

Chemical Formula: $C_{44}H_{68}N_{10}O_{15}$
 Exact Mass: 976.49



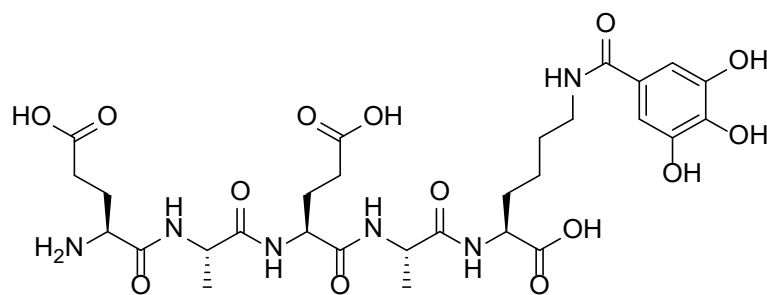
¹H NMR (400 MHz, Deuterium Oxide) δ 6.78 (d, J = 4.5 Hz, 4H), 4.24 - 4.20 (m, 2H), 4.09 - 4.03 (m, 2H), 3.94 (t, J = 6.4 Hz, 1H), 3.28 - 3.18 (m, 4H), 2.89 (t, J = 7.6 Hz, 3H), 2.82 (t, J = 7.7 Hz, 2H), 1.83 (d, J = 7.9 Hz, 3H), 1.71 - 1.58 (m, 7H), 1.52 (dq, J = 15.0, 7.9 Hz, 10H), 1.24 (dd, J = 20.0, 7.2 Hz, 10H).

(EA)₂

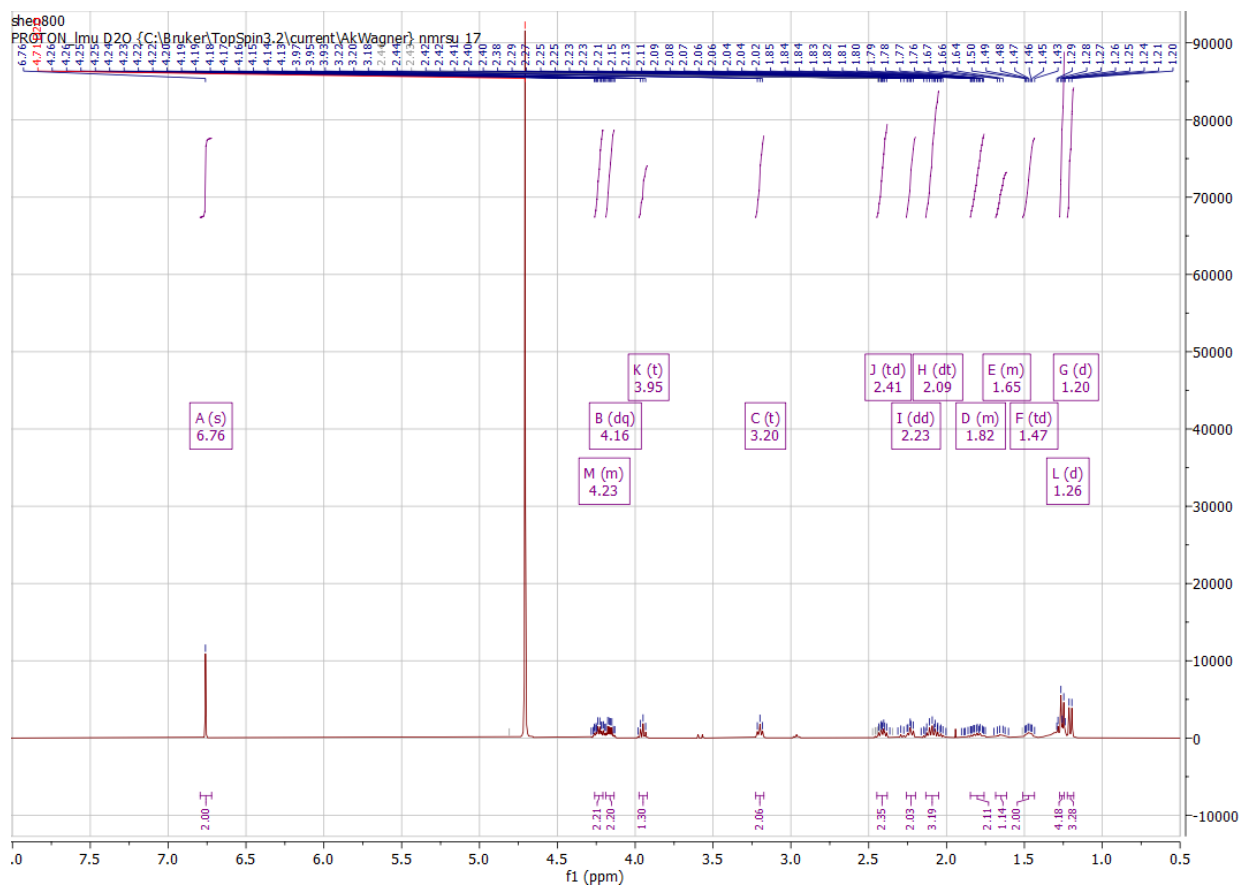
Chemical Formula: C₁₆H₂₆N₄O₉
Exact Mass: 418.17



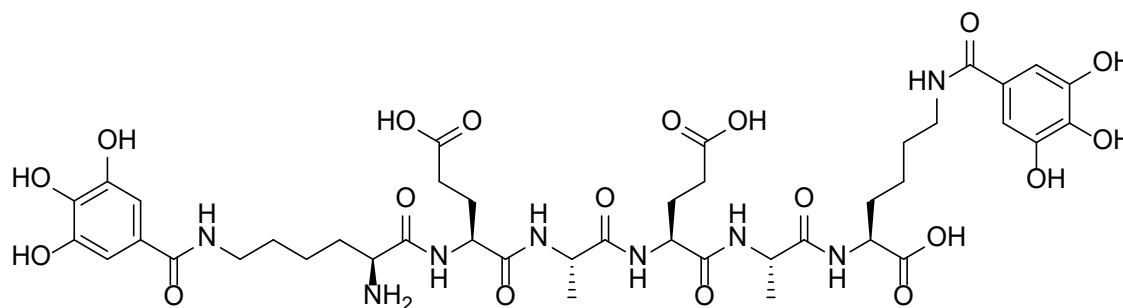
¹H NMR (400 MHz, Deuterium Oxide) δ 4.33 - 4.23 (m, 3H), 4.00 (t, *J* = 6.5 Hz, 1H), 2.54 - 2.38 (m, 4H), 2.14 - 2.00 (m, 3H), 1.91 (ddt, *J* = 14.3, 8.8, 7.2 Hz, 1H), 1.33 (dd, *J* = 12.2, 7.2 Hz, 6H).

(EA)₂*

Chemical Formula: C₂₉H₄₂N₆O₁₄
 Exact Mass: 698.28



¹H NMR (400 MHz, Deuterium Oxide) δ 6.76 (s, 2H), 4.26 - 4.21 (m, 2H), 4.16 (dq, $J = 7.3, 3.9$ Hz, 2H), 3.95 (t, $J = 6.5$ Hz, 1H), 3.20 (t, $J = 6.7$ Hz, 2H), 2.41 (td, $J = 7.4, 5.2$ Hz, 2H), 2.23 (dd, $J = 7.9, 5.9$ Hz, 2H), 2.09 (dt, $J = 14.3, 7.1$ Hz, 3H), 1.85 - 1.76 (m, 2H), 1.68 - 1.61 (m, 1H), 1.47 (td, $J = 7.6, 2.8$ Hz, 2H), 1.26 (d, $J = 7.3$ Hz, 4H), 1.20 (d, $J = 7.2$ Hz, 3H).

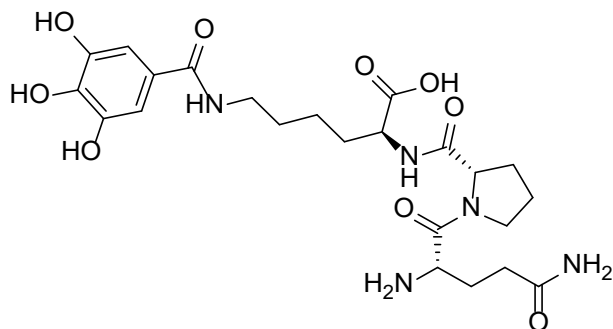
(EA)₂**Chemical Formula: C₄₂H₅₈N₈O₁₉

Exact Mass: 978.38

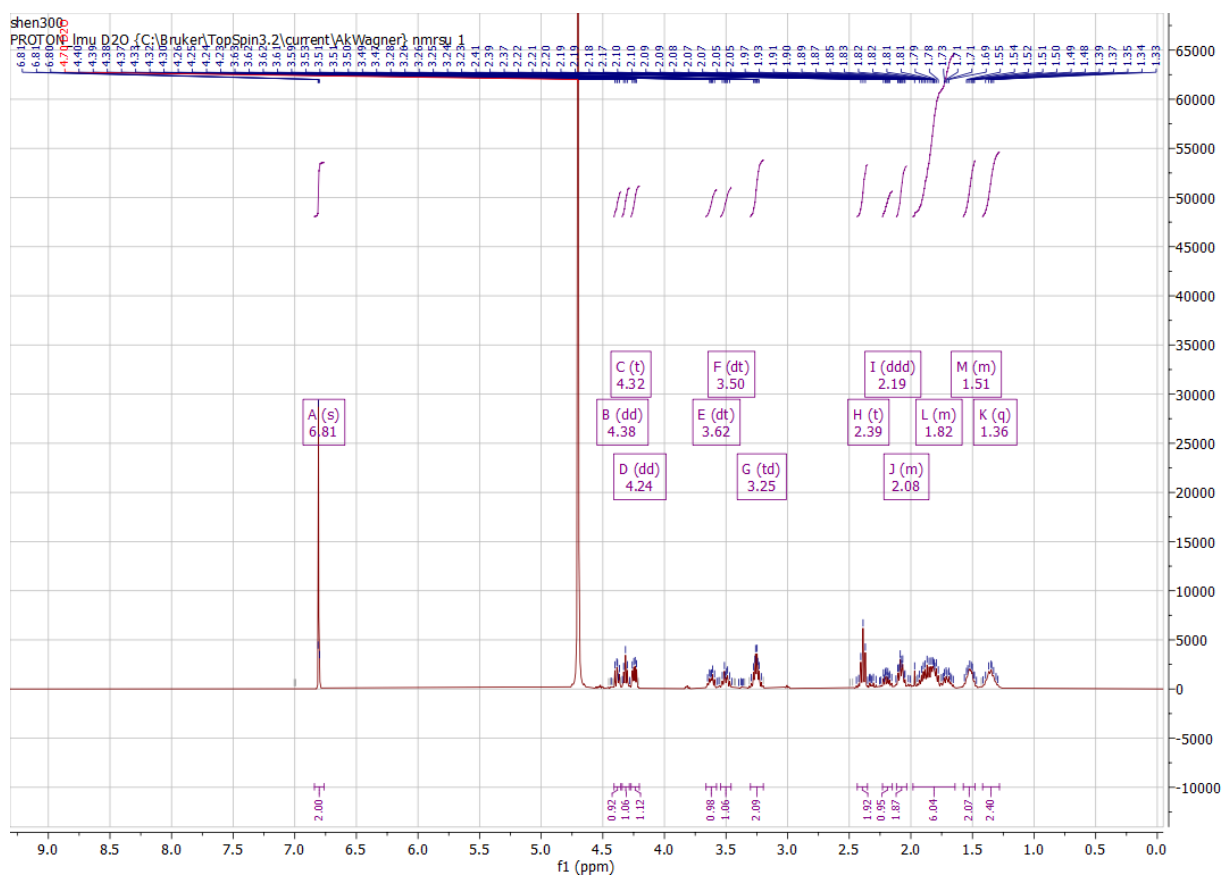


¹H NMR (400 MHz, DMSO-d₆) δ 9.01 (s, 2H), 8.71 (d, *J* = 7.7 Hz, 2H), 8.18 (d, *J* = 7.7 Hz, 3H), 8.11 - 7.99 (m, 5H), 7.95 (dd, *J* = 10.3, 7.5 Hz, 3H), 6.81 (d, *J* = 1.5 Hz, 4H), 4.33 (p, *J* = 7.0 Hz, 4H), 4.24 (dt, *J* = 8.0, 4.2 Hz, 3H), 4.13 (dt, *J* = 12.9, 6.0 Hz, 3H), 2.21 (dd, *J* = 16.2, 8.3 Hz, 5H), 1.74 (d, *J* = 10.9 Hz, 5H), 1.52 - 1.43 (m, 4H), 1.35 (s, 5H), 1.20 (q, *J* = 6.8 Hz, 9H).

SIO*

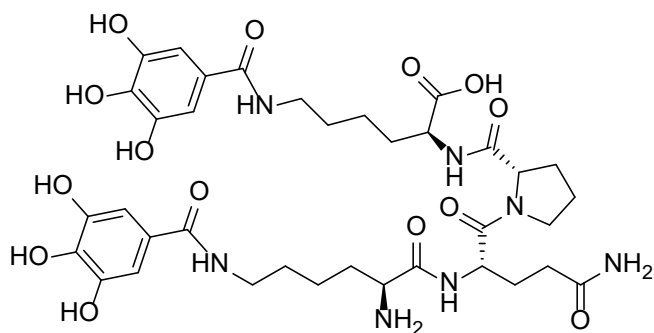
Chemical Formula: $C_{23}H_{33}N_5O_9$

Exact Mass: 523.23

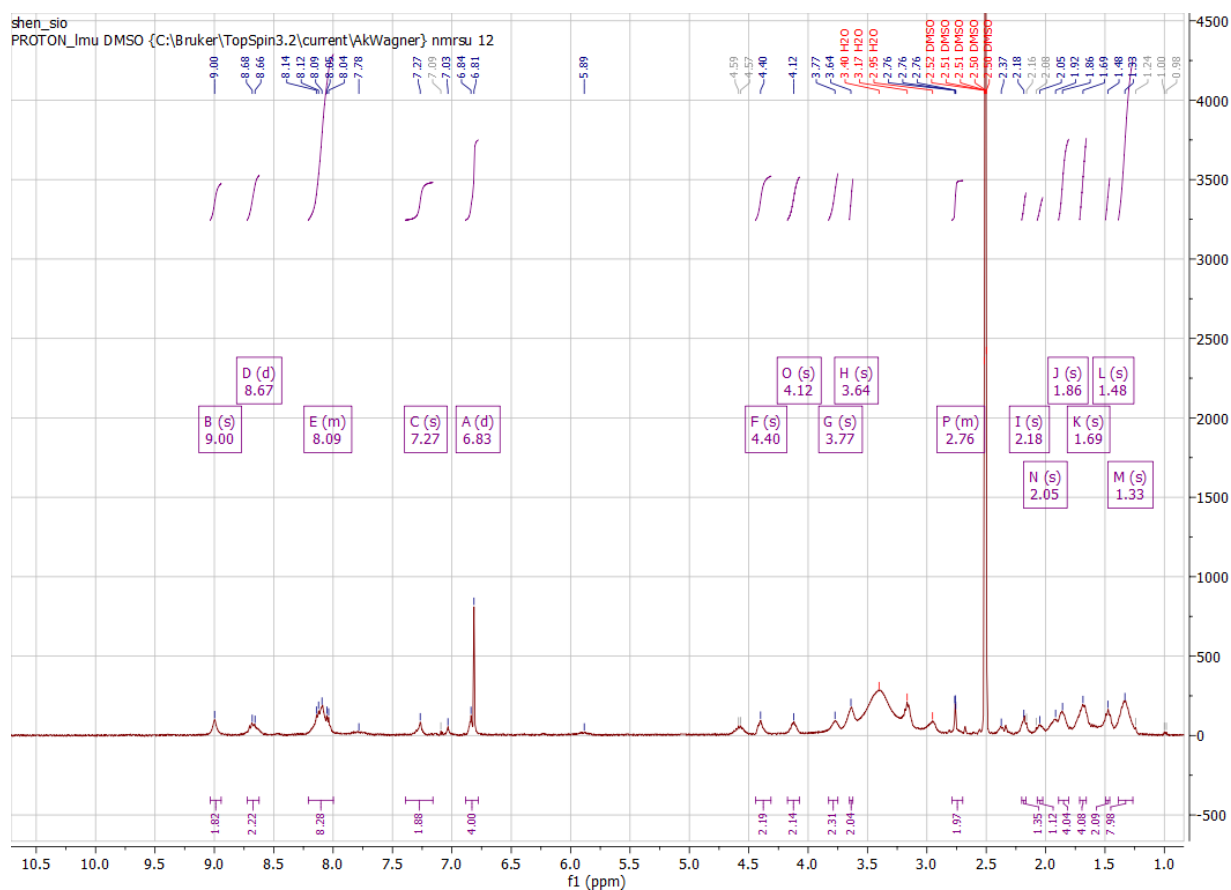


^1H NMR (400 MHz, Deuterium Oxide) δ 6.81 (s, 2H), 4.38 (dd, J = 8.4, 6.1 Hz, 1H), 4.32 (t, J = 5.9 Hz, 1H), 4.24 (dd, J = 9.1, 5.0 Hz, 1H), 3.62 (dt, J = 10.2, 6.4 Hz, 1H), 3.50 (dt, J = 10.1, 7.0 Hz, 1H), 3.25 (td, J = 6.7, 4.9 Hz, 2H), 2.39 (t, J = 7.4 Hz, 2H), 2.19 (ddd, J = 12.5, 8.5, 6.4 Hz, 1H), 2.12 - 2.03 (m, 2H), 1.98 - 1.64 (m, 6H), 1.57 - 1.48 (m, 2H), 1.36 (q, J = 9.3, 8.1 Hz, 2H).

SIO**

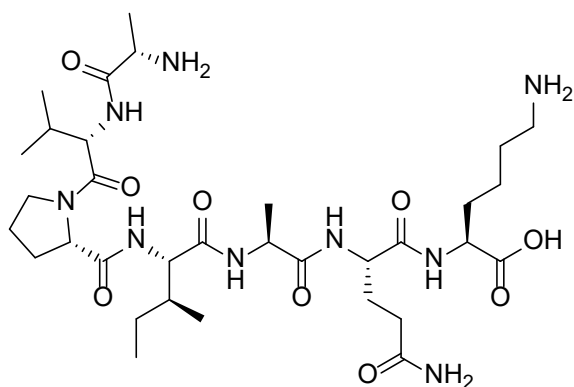
Chemical Formula: $C_{36}H_{49}N_7O_{14}$

Exact Mass: 803.33

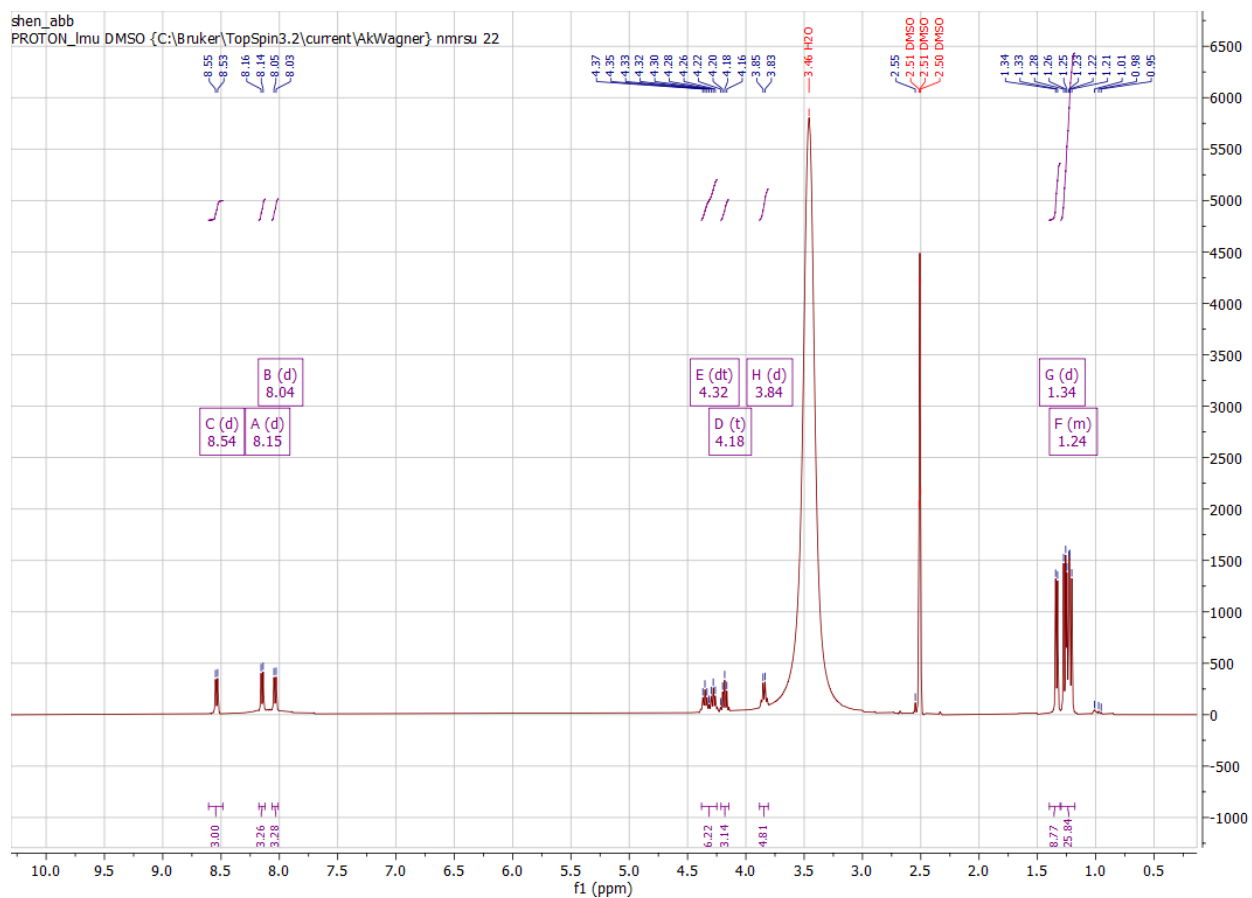


^1H NMR (400 MHz, $\text{DMSO}-d_6$) δ 9.00 (s, 2H), 8.67 (d, $J = 9.4$ Hz, 2H), 8.21 - 8.00 (m, 8H), 7.27 (s, 2H), 6.83 (d, $J = 10.1$ Hz, 4H), 4.40 (s, 2H), 4.12 (s, 2H), 3.77 (s, 2H), 3.64 (s, 2H), 2.79 - 2.70 (m, 2H), 2.18 (s, 1H), 2.05 (s, 1H), 1.86 (s, 4H), 1.69 (s, 4H), 1.48 (s, 2H), 1.33 (s, 8H).

AVP

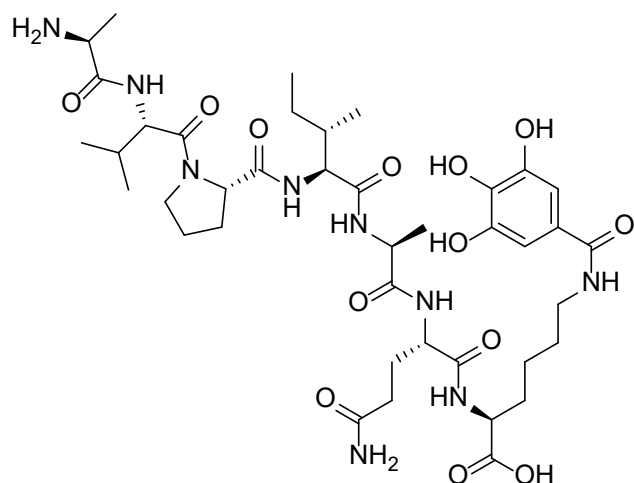


Chemical Formula: $C_{33}H_{59}N_9O_9$
Exact Mass: 725.44

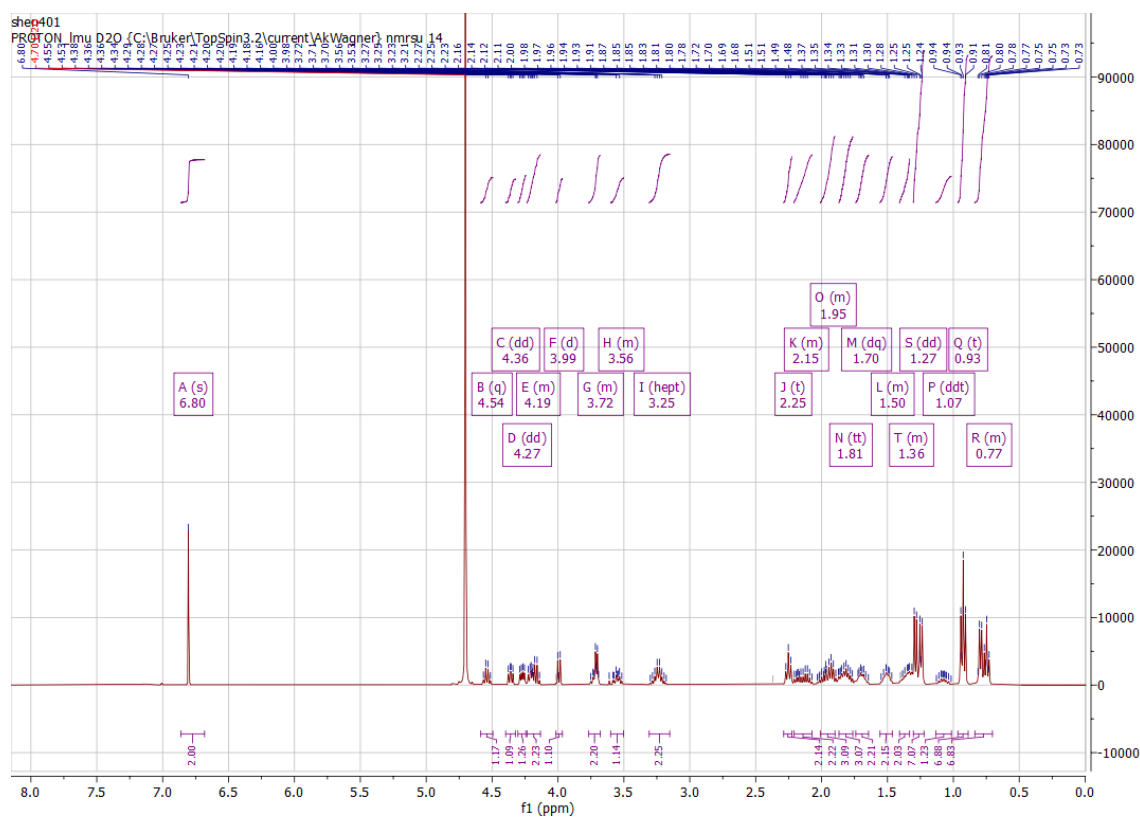


^1H NMR (400 MHz, $\text{DMSO-}d_6$) δ 8.54 (d, $J = 7.5$ Hz, 3H), 8.15 (d, $J = 7.3$ Hz, 3H), 8.04 (d, $J = 7.5$ Hz, 3H), 4.32 (dt, $J = 28.5, 7.2$ Hz, 6H), 4.18 (t, $J = 7.3$ Hz, 3H), 3.84 (d, $J = 7.0$ Hz, 5H), 1.34 (d, $J = 6.9$ Hz, 9H), 1.30 - 1.19 (m, 26H).

AVP*



Chemical Formula: $C_{40}H_{63}N_9O_{13}$
Exact Mass: 877.45

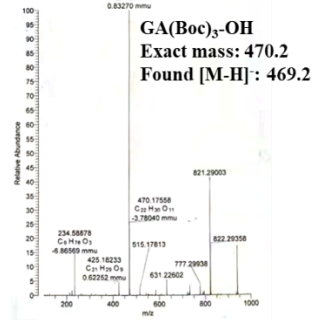


^1H NMR (400 MHz, Deuterium Oxide) δ 6.80 (s, 2H), 4.54 (q, $J = 7.1$ Hz, 1H), 4.36 (dd, $J = 8.4, 5.7$ Hz, 1H), 4.27 (dd, $J = 9.3, 4.6$ Hz, 1H), 4.24 - 4.13 (m, 2H), 3.99 (d, $J = 7.7$ Hz, 1H), 3.77 - 3.68 (m, 2H), 3.60 - 3.50 (m, 1H), 3.25 (hept, $J = 6.7$ Hz, 2H), 2.25 (t, $J = 7.6$ Hz, 2H), 2.21 - 2.07 (m, 2H), 2.01 - 1.90 (m, 3H), 1.81 (tt, $J = 12.5, 6.7$ Hz, 3H), 1.70 (dq, $J = 10.8, 6.0, 4.6$ Hz, 2H), 1.56 - 1.46 (m, 2H), 1.41 - 1.33 (m, 2H), 1.27 (dd, $J = 17.2, 7.2$ Hz, 7H), 1.07 (ddt, $J = 16.3, 14.3, 7.4$ Hz, 1H), 0.93 (t, $J = 7.2$ Hz, 7H), 0.84 - 0.70 (m, 7H).

Mass spectrometry (ESI-MS or MALDI-TOF MS)

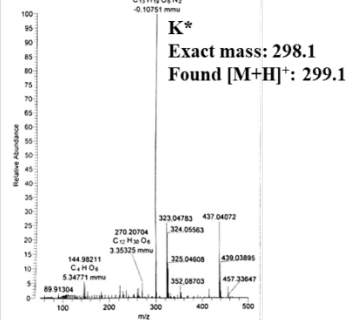
04-fashph-83-#53-221 RT: 0.50-1.98 AV: 22 NL: 2.9965

F: FTMS - p ESI Full ms [100.00-1000.00]



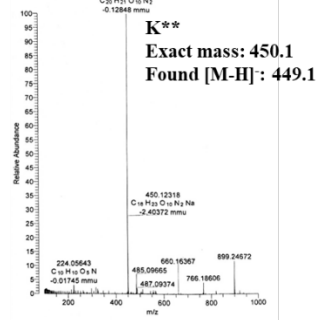
04-fashph-92-220429142224448-245 RT: 0.48-1.96 AV: 25 NL: 2.8265

F: FTMS - p ESI Full ms [50.00-500.00]



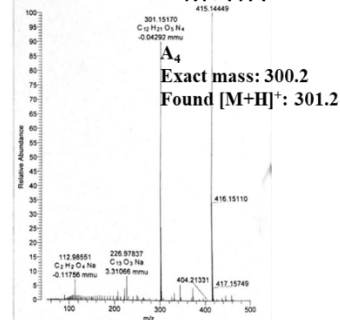
04-fashph-204-2203170951701-#53-221 RT: 0.50-1.97 AV: 22 NL: 2.4065

F: FTMS - p ESI Full ms [100.00-1000.00]



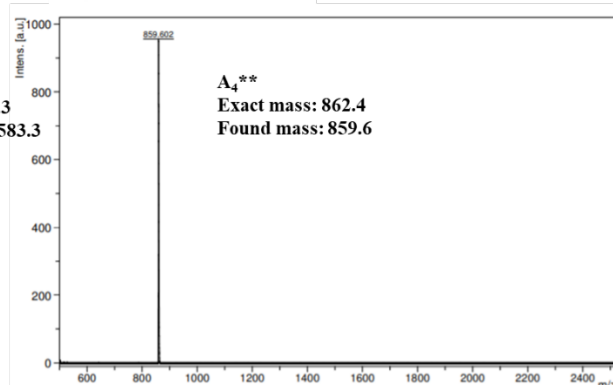
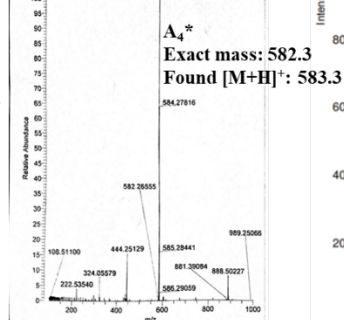
04-fashph-10-220426132221-#48-259 RT: 0.53-1.92 AV: 26 NL: 9.1885

F: FTMS - p ESI Full ms [50.00-500.00]



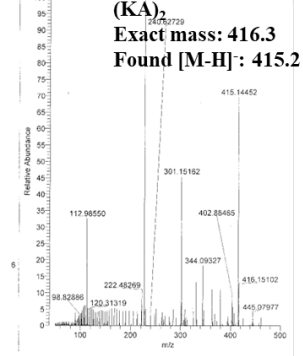
04-fashph-100-#2-324 RT: 0.55-1.96 AV: 23 NL: 7.0065

F: FTMS - p ESI Full ms [100.00-1000.00]



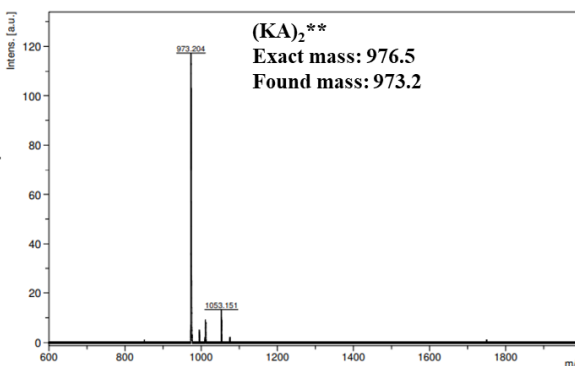
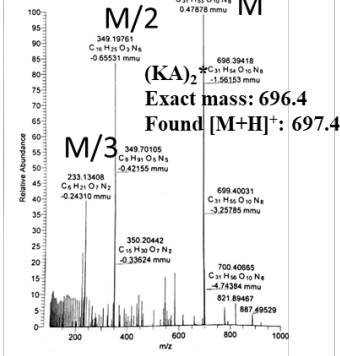
04-fashph-70-#49-249 RT: 0.51-1.94 AV: 25 NL: 1.2455

F: FTMS - p ESI Full ms [50.00-500.00]



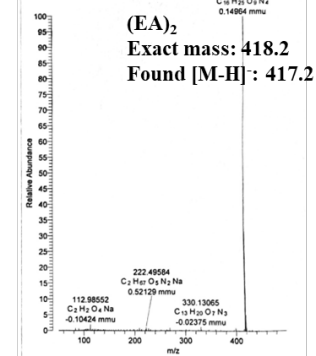
04-fashph-700-#51-253 RT: 0.55-1.97 AV: 25 NL: 3.2766

F: FTMS - p ESI Full ms [100.00-1000.00]



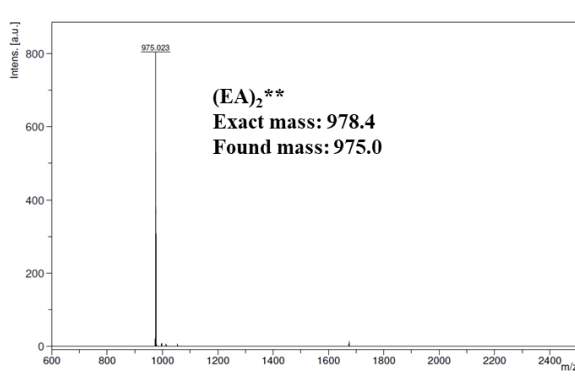
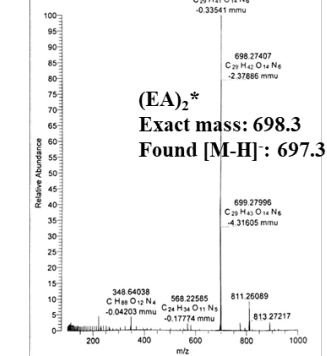
04-fashph-80-#48-256 RT: 0.51-1.94 AV: 26 NL: 1.3266

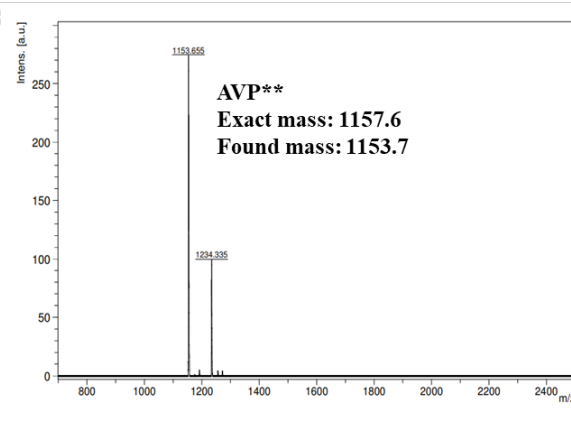
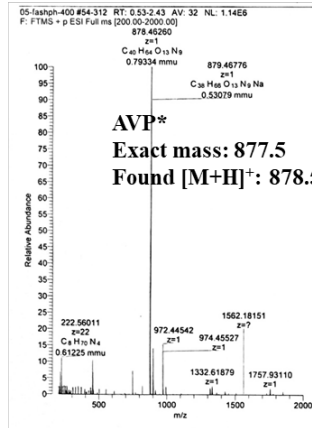
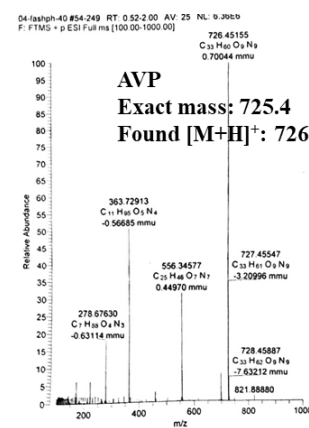
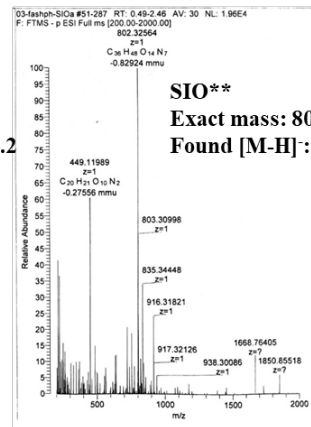
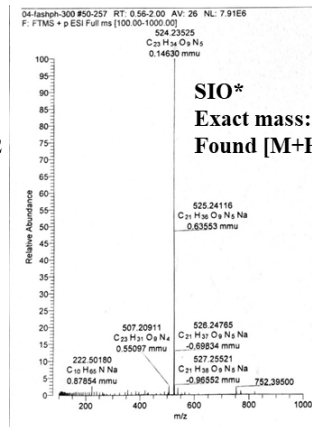
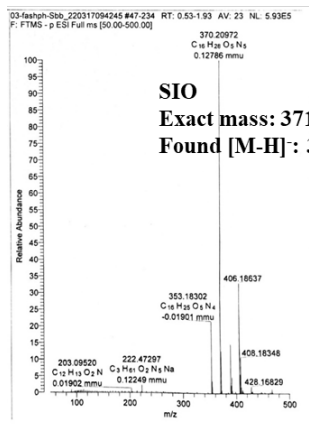
F: FTMS - p ESI Full ms [50.00-500.00]



04-fashph-800-#51-264 RT: 0.52-1.96 AV: 27 NL: 8.8165

F: FTMS - p ESI Full ms [100.00-1000.00]





8 References

- (1) Li, Q.; Dong, Z.; Chen, M.; Feng, L. Phenolic Molecules Constructed Nanomedicine for Innovative Cancer Treatment. *Coord. Chem. Rev.* **2021**, *439*, 213912. <https://doi.org/10.1016/j.ccr.2021.213912>.
- (2) Li, Y.; Miao, Y.; Yang, L.; Zhao, Y.; Wu, K.; Lu, Z.; Hu, Z.; Guo, J. Recent Advances in the Development and Antimicrobial Applications of Metal–Phenolic Networks. *Adv. Sci.* **2022**, *9* (27), 1–22. <https://doi.org/10.1002/advs.202202684>.
- (3) Chen, W.; Liu, M.; Yang, H.; Nezamzadeh-Ejhieh, A.; Lu, C.; Pan, Y.; Liu, J.; Bai, Z. Recent Advances of Fe(III)/Fe(II)-MPNs in Biomedical Applications. *Pharmaceutics* **2023**, *15* (5). <https://doi.org/10.3390/pharmaceutics15051323>.
- (4) Ejima, H.; Richardson, J. J.; Liang, K.; Best, J. P.; Van Koeverden, M. P.; Such, G. K.; Cui, J.; Caruso, F. One-Step Assembly of Coordination Complexes. *Science (80-.)*. **2013**, *341* (6142), 154–157.
- (5) Wang, Y.; Yan, J.; Wen, N.; Xiong, H.; Cai, S.; He, Q.; Hu, Y.; Peng, D.; Liu, Z.; Liu, Y. Metal-Organic Frameworks for Stimuli-Responsive Drug Delivery. *Biomaterials* **2020**, *230*, 119619. <https://doi.org/https://doi.org/10.1016/j.biomaterials.2019.119619>.
- (6) Ejima, H.; Richardson, J. J.; Caruso, F. Metal-Phenolic Networks as a Versatile Platform to Engineer Nanomaterials and Biointerfaces. *Nano Today* **2017**, *12*, 136–148. <https://doi.org/10.1016/j.nantod.2016.12.012>.
- (7) Dai, Y.; Guo, J.; Wang, T. Y.; Ju, Y.; Mitchell, A. J.; Bonnard, T.; Cui, J.; Richardson, J. J.; Hagemeyer, C. E.; Alt, K.; Caruso, F. Self-Assembled Nanoparticles from Phenolic Derivatives for Cancer Therapy. *Adv. Healthc. Mater.* **2017**, *6* (16), 1–7. <https://doi.org/10.1002/adhm.201700467>.

- (8) Xu, W.; Pan, S.; Noble, B. B.; Chen, J.; Lin, Z.; Han, Y.; Zhou, J.; Richardson, J. J.; Yarovsky, I.; Caruso, F. Site-Selective Coordination Assembly of Dynamic Metal-Phenolic Networks. *Angew. Chemie* **2022**, *134* (34), 1–9. <https://doi.org/10.1002/ange.202208037>.
- (9) Dai, Y.; Yang, Z.; Cheng, S.; Wang, Z.; Zhang, R.; Zhu, G.; Wang, Z.; Yung, B. C.; Tian, R.; Jacobson, O.; Xu, C.; Ni, Q.; Song, J.; Sun, X.; Niu, G.; Chen, X. Toxic Reactive Oxygen Species Enhanced Synergistic Combination Therapy by Self-Assembled Metal-Phenolic Network Nanoparticles. *Adv. Mater.* **2018**, *30* (8), 1–8. <https://doi.org/10.1002/adma.201704877>.
- (10) Dabbaghi, A.; Kabiri, K.; Ramazani, A.; Zohuriaan-Mehr, M. J.; Jahandideh, A. Synthesis of Bio-Based Internal and External Cross-Linkers Based on Tannic Acid for Preparation of Antibacterial Superabsorbents. *Polym. Adv. Technol.* **2019**, *30* (11), 2894–2905. <https://doi.org/10.1002/pat.4722>.
- (11) Choubey, S.; Goyal, S.; Varughese, L. R.; Kumar, V.; Sharma, A. K.; Beniwal, V. Probing Gallic Acid for Its Broad Spectrum Applications. *Mini-Reviews Med. Chem.* **2018**, *18* (15), 1283–1293. <https://doi.org/10.2174/1389557518666180330114010>.
- (12) Yu, H.; Ma, M.; Liang, K.; Shen, J.; Lan, Z.; Chen, H. A Self-Assembled Metal-Polyphenolic Nanomedicine for Mild Photothermal-Potentiated Chemodynamic Therapy of Tumors. *Appl. Mater. Today* **2021**, *25*, 101235. <https://doi.org/https://doi.org/10.1016/j.apmt.2021.101235>.
- (13) Moran, J. F.; Klucas, R. V.; Grayer, R. J.; Abian, J.; Becana, M. Complexes of Iron with Phenolic Compounds from Soybean Nodules and Other Legume Tissues: Prooxidant and Antioxidant Properties. *Free Radic. Biol. Med.* **1997**, *22* (5), 861–870. [https://doi.org/10.1016/S0891-5849\(96\)00426-1](https://doi.org/10.1016/S0891-5849(96)00426-1).

- (14) Xie, L.; Li, J.; Wang, L.; Dai, Y. Engineering Metal-Phenolic Networks for Enhancing Cancer Therapy by Tumor Microenvironment Modulation. *Wiley Interdiscip. Rev. Nanomedicine Nanobiotechnology* **2022**, No. September 2022, 1–35. <https://doi.org/10.1002/wnan.1864>.
- (15) Guo, J.; Ping, Y.; Ejima, H.; Alt, K.; Meissner, M.; Richardson, J. J.; Yan, Y.; Peter, K.; Von Elverfeldt, D.; Hagemeyer, C. E.; Caruso, F. Engineering Multifunctional Capsules through the Assembly of Metal-Phenolic Networks. *Angew. Chemie - Int. Ed.* **2014**, *53* (22), 5546–5551. <https://doi.org/10.1002/anie.201311136>.
- (16) White, P. J.; Broadley, M. R. Biofortification of Crops with Seven Mineral Elements Often Lacking in Human Diets - Iron, Zinc, Copper, Calcium, Magnesium, Selenium and Iodine. *New Phytol.* **2009**, *182* (1), 49–84. <https://doi.org/10.1111/j.1469-8137.2008.02738.x>.
- (17) Chang, S. S.; Lee, V. S. Y.; Tseng, Y. L.; Chang, K. C.; Chen, K. B.; Chen, Y. L.; Li, C. Y. Gallic Acid Attenuates Platelet Activation and Platelet-Leukocyte Aggregation: Involving Pathways of Akt and GSK3 β . *Evidence-based Complement. Altern. Med.* **2012**, 2012. <https://doi.org/10.1155/2012/683872>.
- (18) Bai, J.; Zhang, Y.; Tang, C.; Hou, Y.; Ai, X.; Chen, X.; Zhang, Y.; Wang, X.; Meng, X. Gallic Acid: Pharmacological Activities and Molecular Mechanisms Involved in Inflammation-Related Diseases. *Biomed. Pharmacother.* **2021**, *133* (September 2020), 110985. <https://doi.org/10.1016/j.biopha.2020.110985>.
- (19) Hsieh, C.-L.; Lin, Y.-C.; Yen, G.-C.; Chen, H.-Y. Preventive Effects of Guava (*Psidium Guajava* L.) Leaves and Its Active Compounds against α -Dicarbonyl Compounds-Induced Blood Coagulation. *Food Chem.* **2007**, *103* (2), 528–535. <https://doi.org/https://doi.org/10.1016/j.foodchem.2006.08.022>.
- (20) de Mejía, E. G.; Chandra, S.; Ramírez-Mares, M. V.; Wang, W. Catalytic Inhibition of Human DNA Topoisomerase by Phenolic Compounds in *Ardisia Compressa*

- Extracts and Their Effect on Human Colon Cancer Cells. *Food Chem. Toxicol.* **2006**, *44* (8), 1191–1203. <https://doi.org/10.1016/j.fct.2006.01.015>.
- (21) Kubola, J.; Siriamornpun, S. Phenolic Contents and Antioxidant Activities of Bitter Gourd (*Momordica Charantia* L.) Leaf, Stem and Fruit Fraction Extracts in Vitro. *Food Chem.* **2008**, *110* (4), 881–890. <https://doi.org/https://doi.org/10.1016/j.foodchem.2008.02.076>.
- (22) Uozaki, M.; Yamasaki, H.; Katsuyama, Y.; Higuchi, M.; Higuti, T.; Koyama, A. H. Antiviral Effect of Octyl Gallate against DNA and RNA Viruses. *Antiviral Res.* **2007**, *73* (2), 85–91. <https://doi.org/10.1016/j.antiviral.2006.07.010>.
- (23) Yang, J.; Dai, D.; Zhang, X.; Teng, L.; Ma, L.; Yang, Y. W. Multifunctional Metal-Organic Framework (MOF)-Based Nanoplatfoms for Cancer Therapy: From Single to Combination Therapy. *Theranostics* **2023**, *13* (1), 295–323. <https://doi.org/10.7150/thno.80687>.
- (24) van Driel, W. J.; Koole, S. N.; Sikorska, K.; Schagen van Leeuwen, J. H.; Schreuder, H. W. R.; Hermans, R. H. M.; de Hingh, I. H. J. T.; van der Velden, J.; Arts, H. J.; Massuger, L. F. A. G.; Aalbers, A. G. J.; Verwaal, V. J.; Kieffer, J. M.; Van de Vijver, K. K.; van Tinteren, H.; Aaronson, N. K.; Sonke, G. S. Hyperthermic Intraperitoneal Chemotherapy in Ovarian Cancer. *N. Engl. J. Med.* **2018**, *378* (3), 230–240. <https://doi.org/10.1056/nejmoa1708618>.
- (25) Meyers, B. M.; Cosby, R.; Quereshy, F.; Jonker, D. Adjuvant Chemotherapy for Stage II and III Colon Cancer Following Complete Resection: A Cancer Care Ontario Systematic Review. *Clin. Oncol.* **2017**, *29* (7), 459–465. <https://doi.org/https://doi.org/10.1016/j.clon.2017.03.001>.
- (26) Tierney, J. F.; Chivukula, S. V.; Wang, X.; Pappas, S. G.; Schadde, E.; Hertl, M.; Poirier, J.; Keutgen, X. M. Resection of Primary Tumor May Prolong Survival in Metastatic Gastroenteropancreatic Neuroendocrine Tumors. *Surg. (United States)*

- 2019**, *165* (3), 644–651. <https://doi.org/10.1016/j.surg.2018.09.006>.
- (27) Craik, D. J.; Fairlie, D. P.; Liras, S.; Price, D. The Future of Peptide-Based Drugs. *Chem. Biol. Drug Des.* **2013**, *81* (1), 136–147. <https://doi.org/10.1111/cbdd.12055>.
- (28) Weichselbaum, R. R.; Liang, H.; Deng, L.; Fu, Y. X. Radiotherapy and Immunotherapy: A Beneficial Liaison? *Nat. Rev. Clin. Oncol.* **2017**, *14* (6), 365–379. <https://doi.org/10.1038/nrclinonc.2016.211>.
- (29) Ribas, A.; Wolchok, J. D. Cancer Immunotherapy Using Checkpoint Blockade. *Science (80-.)*. **2018**, *359* (6382), 1350–1355. <https://doi.org/10.1126/science.aar4060>.
- (30) Zheng, D. W.; Lei, Q.; Zhu, J. Y.; Fan, J. X.; Li, C. X.; Li, C.; Xu, Z.; Cheng, S. X.; Zhang, X. Z. Switching Apoptosis to Ferroptosis: Metal-Organic Network for High-Efficiency Anticancer Therapy. *Nano Lett.* **2017**, *17* (1), 284–291. <https://doi.org/10.1021/acs.nanolett.6b04060>.
- (31) Zhang, C.; Bu, W.; Ni, D.; Zhang, S.; Li, Q.; Yao, Z.; Zhang, J.; Yao, H.; Wang, Z.; Shi, J. Synthesis of Iron Nanometallic Glasses and Their Application in Cancer Therapy by a Localized Fenton Reaction. *Angew. Chemie - Int. Ed.* **2016**, *55* (6), 2101–2106. <https://doi.org/10.1002/anie.201510031>.
- (32) Zhou, Z.; Song, J.; Tian, R.; Yang, Z.; Yu, G.; Lin, L.; Zhang, G.; Fan, W.; Zhang, F.; Niu, G.; Nie, L.; Chen, X. Activatable Singlet Oxygen Generation from Lipid Hydroperoxide Nanoparticles for Cancer Therapy. *Angew. Chemie - Int. Ed.* **2017**, *56* (23), 6492–6496. <https://doi.org/10.1002/anie.201701181>.
- (33) Ushio-Fukai, M.; Nakamura, Y. Reactive Oxygen Species and Angiogenesis NADPH Oxidase As. *Cancer Lett.* **2008**, *266* (1), 37–52. <https://doi.org/10.1016/j.canlet.2008.02.044.Reactive>.

- (34) Dixon, S. J.; Stockwell, B. R. The Role of Iron and Reactive Oxygen Species in Cell Death. *Nat. Chem. Biol.* **2014**, *10* (1), 9–17.
<https://doi.org/10.1038/nchembio.1416>.
- (35) Zhang, L.; Wan, S. S.; Li, C. X.; Xu, L.; Cheng, H.; Zhang, X. Z. An Adenosine Triphosphate-Responsive Autocatalytic Fenton Nanoparticle for Tumor Ablation with Self-Supplied H₂O₂ and Acceleration of Fe(III)/Fe(II) Conversion. *Nano Lett.* **2018**, *18* (12), 7609–7618. <https://doi.org/10.1021/acs.nanolett.8b03178>.
- (36) Ozben, T. Oxidative Stress and Apoptosis: Impact on Cancer Therapy. *J. Pharm. Sci.* **2007**, *96* (9), 2181–2196. <https://doi.org/10.1002/jps.20874>.
- (37) Wang, J.; Yi, J. Cancer Cell Killing via ROS: To Increase or Decrease, That Is a Question. *Cancer Biol. Ther.* **2008**, *7* (12), 1875–1884.
<https://doi.org/10.4161/cbt.7.12.7067>.
- (38) Guo, Y.; Zhang, X.; Sun, W.; Jia, H. R.; Zhu, Y. X.; Zhang, X.; Zhou, N.; Wu, F. G. Metal-Phenolic Network-Based Nanocomplexes That Evoke Ferroptosis by Apoptosis: Promoted Nuclear Drug Influx and Reversed Drug Resistance of Cancer. *Chem. Mater.* **2019**, *31* (24), 10071–10084.
<https://doi.org/10.1021/acs.chemmater.9b03042>.
- (39) Dong, Z.; Feng, L.; Chao, Y.; Hao, Y.; Chen, M.; Gong, F.; Han, X.; Zhang, R.; Cheng, L.; Liu, Z. Amplification of Tumor Oxidative Stresses with Liposomal Fenton Catalyst and Glutathione Inhibitor for Enhanced Cancer Chemotherapy and Radiotherapy. *Nano Lett.* **2019**, *19* (2), 805–815.
<https://doi.org/10.1021/acs.nanolett.8b03905>.
- (40) Chen, X.; Ma, R.; Fu, Z.; Su, Q.; Luo, X.; Han, Y.; Yang, Y.; Deng, Q. Metal-Phenolic Networks-Encapsulated Cascade Amplification Delivery Nanoparticles Overcoming Cancer Drug Resistance via Combined Starvation/Chemodynamic/Chemo Therapy. *Chem. Eng. J.* **2022**, *442*, 136221.

- <https://doi.org/https://doi.org/10.1016/j.cej.2022.136221>.
- (41) Apostolopoulos, V.; Bojarska, J.; Chai, T. T.; Elnagdy, S.; Kaczmarek, K.; Matsoukas, J.; New, R.; Parang, K.; Lopez, O. P.; Parhiz, H.; Perera, C. O.; Pickholz, M.; Remko, M.; Saviano, M.; Skwarczynski, M.; Tang, Y.; Wolf, W. M.; Yoshiya, T.; Zabrocki, J.; Zielenkiewicz, P.; Alkhazindar, M.; Barriga, V.; Kelaidonis, K.; Sarasia, E. M.; Toth, I. A Global Review on Short Peptides: Frontiers and Perspectives. *Molecules* **2021**, *26* (2).
<https://doi.org/10.3390/molecules26020430>.
- (42) Cooper, B. M.; Iegre, J.; O'Donovan, D. H.; Ölwegård Halvarsson, M.; Spring, D. R. Peptides as a Platform for Targeted Therapeutics for Cancer: Peptide-Drug Conjugates (PDCs). *Chem. Soc. Rev.* **2021**, *50* (3), 1480–1494.
<https://doi.org/10.1039/d0cs00556h>.
- (43) Holz, E.; Darwish, M.; Tesar, D. B.; Shatz-Binder, W. A Review of Protein- and Peptide-Based Chemical Conjugates: Past, Present, and Future. *Pharmaceutics* **2023**, *15* (2). <https://doi.org/10.3390/pharmaceutics15020600>.
- (44) Hartrampf, N.; Saebi, A.; Poskus, M.; Gates, Z. P.; Callahan, A. J.; Cowfer, A. E.; Hanna, S.; Antilla, S.; Schissel, C. K.; Quartararo, A. J.; Ye, X.; Mijalis, A. J.; Simon, M. D.; Loas, A.; Liu, S.; Jessen, C.; Nielsen, T. E.; Pentelute, B. L. Synthesis of Proteins by Automated Flow Chemistry. *Science* (80-.). **2020**, *368* (6494), 980–987. <https://doi.org/10.1126/science.abb2491>.
- (45) Henninot, A.; Collins, J. C.; Nuss, J. M. The Current State of Peptide Drug Discovery: Back to the Future? *Journal of Medicinal Chemistry*. American Chemical Society February 22, 2018, pp 1382–1414.
<https://doi.org/10.1021/acs.jmedchem.7b00318>.
- (46) Vinogradov, A. A.; Yin, Y.; Suga, H. Macrocyclic Peptides as Drug Candidates: Recent Progress and Remaining Challenges. *J. Am. Chem. Soc.* **2019**, *141* (10),

- 4167–4181. <https://doi.org/10.1021/jacs.8b13178>.
- (47) Yudin, A. K. Macrocycles: Lessons from the Distant Past, Recent Developments, and Future Directions. *Chem. Sci.* **2015**, *6* (1), 30–49. <https://doi.org/10.1039/c4sc03089c>.
- (48) Lau, J. L.; Dunn, M. K. Therapeutic Peptides: Historical Perspectives, Current Development Trends, and Future Directions. *Bioorganic Med. Chem.* **2018**, *26* (10), 2700–2707. <https://doi.org/10.1016/j.bmc.2017.06.052>.
- (49) Baradaran, M. Current Status of Peptide Medications and the Position of Active Therapeutic Peptides with Scorpion Venom Origin. *Jundishapur J. Nat. Pharm. Prod.* **2023**, *In Press* (In Press), 1–12. <https://doi.org/10.5812/jjnpp-134049>.
- (50) Wang, L.; Wang, N.; Zhang, W.; Cheng, X.; Yan, Z.; Shao, G.; Wang, X.; Wang, R.; Fu, C. Therapeutic Peptides: Current Applications and Future Directions. *Signal Transduct. Target. Ther.* **2022**, *7* (1). <https://doi.org/10.1038/s41392-022-00904-4>.
- (51) Otvos, L.; Wade, J. D. Current Challenges in Peptide-Based Drug Discovery. *Front. Chem.* **2014**, *2* (AUG), 8–11. <https://doi.org/10.3389/fchem.2014.00062>.
- (52) Muttenthaler, M.; King, G. F.; Adams, D. J.; Alewood, P. F. Trends in Peptide Drug Discovery. *Nat. Rev. Drug Discov.* **2021**, *20* (4), 309–325. <https://doi.org/10.1038/s41573-020-00135-8>.
- (53) Lau, J. L.; Dunn, M. K. Therapeutic Peptides: Historical Perspectives, Current Development Trends, and Future Directions. *Bioorganic Med. Chem.* **2018**, *26* (10), 2700–2707. <https://doi.org/10.1016/j.bmc.2017.06.052>.
- (54) Merrifield, R. B. Solid Phase Peptide Synthesis. *Excerpta Med., I.C.S.* **1976**, *No.374*, 29–39. <https://doi.org/10.1201/9781003069225-2>.

- (55) Vlieghe, P.; Lisowski, V.; Martinez, J.; Khrestchatisky, M. Synthetic Therapeutic Peptides: Science and Market. *Drug Discov. Today* **2010**, *15* (1–2), 40–56. <https://doi.org/10.1016/j.drudis.2009.10.009>.
- (56) Imai, K.; Takaoka, A. Comparing Antibody and Small-Molecule Therapies for Cancer. *Nat. Rev. Cancer* **2006**, *6* (9), 714–727. <https://doi.org/10.1038/nrc1913>.
- (57) Lawson, A. D. G. Antibody-Enabled Small-Molecule Drug Discovery. *Nat. Rev. Drug Discov.* **2012**, *11* (7), 519–525. <https://doi.org/10.1038/nrd3756>.
- (58) Smith, A. J. New Horizons in Therapeutic Antibody Discovery: Opportunities and Challenges versus Small-Molecule Therapeutics. *J. Biomol. Screen.* **2015**, *20* (4), 437–453. <https://doi.org/10.1177/1087057114562544>.
- (59) Pelay-Gimeno, M.; Glas, A.; Koch, O.; Grossmann, T. N. Structure-Based Design of Inhibitors of Protein-Protein Interactions: Mimicking Peptide Binding Epitopes. *Angew. Chemie - Int. Ed.* **2015**, *54* (31), 8896–8927. <https://doi.org/10.1002/anie.201412070>.
- (60) Smith, M. C.; Gestwicki, J. E. Features of Protein-Protein Interactions That Translate into Potent Inhibitors: Topology, Surface Area and Affinity. *Expert Rev. Mol. Med.* **2012**, *14* (July), 1–20. <https://doi.org/10.1017/erm.2012.10>.
- (61) Wilhelm, S.; Carter, C.; Lynch, M.; Lowinger, T.; Dumas, J.; Smith, R. A.; Schwartz, B.; Simantov, R.; Kelley, S. Discovery and Development of Sorafenib: A Multikinase Inhibitor for Treating Cancer. *Nat. Rev. Drug Discov.* **2006**, *5* (10), 835–844. <https://doi.org/10.1038/nrd2130>.
- (62) Diao, L.; Meibohm, B. Pharmacokinetics and Pharmacokinetic-Pharmacodynamic Correlations of Therapeutic Peptides. *Clinical Pharmacokinetics*. October 2013, pp 855–868. <https://doi.org/10.1007/s40262-013-0079-0>.

- (63) Acar, H.; Ting, J. M.; Srivastava, S.; LaBelle, J. L.; Tirrell, M. V. Molecular Engineering Solutions for Therapeutic Peptide Delivery. *Chem. Soc. Rev.* **2017**, *46* (21), 6553–6569. <https://doi.org/10.1039/c7cs00536a>.
- (64) Rong, G.; Wang, C.; Chen, L.; Yan, Y.; Cheng, Y. Fluoroalkylation Promotes Cytosolic Peptide Delivery. *Sci. Adv.* **2020**, *6* (33). <https://doi.org/10.1126/sciadv.aaz1774>.
- (65) Soudy, R.; Kimura, R.; Patel, A.; Fu, W.; Kaur, K.; Westaway, D.; Yang, J.; Jhamandas, J. Short Amylin Receptor Antagonist Peptides Improve Memory Deficits in Alzheimer's Disease Mouse Model. *Sci. Rep.* **2019**, *9* (1), 1–11. <https://doi.org/10.1038/s41598-019-47255-9>.
- (66) Hamley, I. W. Small Bioactive Peptides for Biomaterials Design and Therapeutics. *Chem. Rev.* **2017**, *117* (24), 14015–14041. <https://doi.org/10.1021/acs.chemrev.7b00522>.
- (67) Liu, X.; Wu, F.; Ji, Y.; Yin, L. Recent Advances in Anti-Cancer Protein/Peptide Delivery. *Bioconjug. Chem.* **2019**, *30* (2), 305–324. <https://doi.org/10.1021/acs.bioconjchem.8b00750>.
- (68) Henninot, A.; Collins, J. C.; Nuss, J. M. The Current State of Peptide Drug Discovery: Back to the Future? *J. Med. Chem.* **2018**, *61* (4), 1382–1414. <https://doi.org/10.1021/acs.jmedchem.7b00318>.
- (69) Bhat, A.; Roberts, L. R.; Dwyer, J. J. Lead Discovery and Optimization Strategies for Peptide Macrocycles. *Eur. J. Med. Chem.* **2015**, *94*, 471–479. <https://doi.org/10.1016/j.ejmech.2014.07.083>.
- (70) Naylor, M. R.; Bockus, A. T.; Blanco, M. J.; Lokey, R. S. Cyclic Peptide Natural Products Chart the Frontier of Oral Bioavailability in the Pursuit of Undruggable Targets. *Curr. Opin. Chem. Biol.* **2017**, *38*, 141–147.

- <https://doi.org/10.1016/j.cbpa.2017.04.012>.
- (71) Vorherr, T. Modifying Peptides to Enhance Permeability. *Future Med. Chem.* **2015**, *7* (8), 1009–1021. <https://doi.org/10.4155/fmc.15.43>.
- (72) Qvit, N.; Rubin, S. J. S.; Urban, T. J.; Mochly-Rosen, D.; Gross, E. R. Peptidomimetic Therapeutics: Scientific Approaches and Opportunities. *Drug Discov. Today* **2017**, *22* (2), 454–462. <https://doi.org/10.1016/j.drudis.2016.11.003>.
- (73) Blackwell, H. E.; Grubbs, R. H. Highly Efficient Synthesis of Covalently Cross-Linked Peptide Helices by Ring-Closing Metathesis. *Angew. Chemie - Int. Ed.* **1998**, *37* (23), 3281–3284. [https://doi.org/10.1002/\(SICI\)1521-3773\(19981217\)37:23<3281::AID-ANIE3281>3.0.CO;2-V](https://doi.org/10.1002/(SICI)1521-3773(19981217)37:23<3281::AID-ANIE3281>3.0.CO;2-V).
- (74) Heinis, C.; Rutherford, T.; Freund, S.; Winter, G. Phage-Encoded Combinatorial Chemical Libraries Based on Bicyclic Peptides. *Nat. Chem. Biol.* **2009**, *5* (7), 502–507. <https://doi.org/10.1038/nchembio.184>.
- (75) Vu, Q. N.; Young, R.; Sudhakar, H. K.; Gao, T.; Huang, T.; Tan, Y. S.; Lau, Y. H. Cyclisation Strategies for Stabilising Peptides with Irregular Conformations. *RSC Med. Chem.* **2021**, *12* (6), 887–901. <https://doi.org/10.1039/d1md00098e>.
- (76) Lau, Y. H.; De Andrade, P.; Wu, Y.; Spring, D. R. Peptide Stapling Techniques Based on Different Macrocyclisation Chemistries. *Chem. Soc. Rev.* **2015**, *44* (1), 91–102. <https://doi.org/10.1039/c4cs00246f>.
- (77) Lamers, C. Overcoming the Shortcomings of Peptide-Based Therapeutics. *Futur. Drug Discov.* **2022**, *4* (2). <https://doi.org/10.4155/fdd-2022-0005>.
- (78) Di, L. Strategic Approaches to Optimizing Peptide ADME Properties. *AAPS J.* **2015**, *17* (1), 134–143. <https://doi.org/10.1208/s12248-014-9687-3>.

- (79) Werle, M.; Bernkop-Schnürch, A. Strategies to Improve Plasma Half Life Time of Peptide and Protein Drugs. *Amino Acids* **2006**, *30* (4), 351–367. <https://doi.org/10.1007/s00726-005-0289-3>.
- (80) Xue, Y. P.; Cao, C. H.; Zheng, Y. G. Enzymatic Asymmetric Synthesis of Chiral Amino Acids. *Chem. Soc. Rev.* **2018**, *47* (4), 1516–1561. <https://doi.org/10.1039/c7cs00253j>.
- (81) Stevenazzi, A.; Marchini, M.; Sandrone, G.; Vergani, B.; Lattanzio, M. Amino Acidic Scaffolds Bearing Unnatural Side Chains: An Old Idea Generates New and Versatile Tools for the Life Sciences. *Bioorganic Med. Chem. Lett.* **2014**, *24* (23), 5349–5356. <https://doi.org/10.1016/j.bmcl.2014.10.016>.
- (82) Narancic, T.; Almahboub, S. A.; O'Connor, K. E. Unnatural Amino Acids: Production and Biotechnological Potential. *World J. Microbiol. Biotechnol.* **2019**, *35* (4), 1–11. <https://doi.org/10.1007/s11274-019-2642-9>.
- (83) Ding, Y.; Ting, J. P.; Liu, J.; Al-Azzam, S.; Pandya, P.; Afshar, S. Impact of Non-Proteinogenic Amino Acids in the Discovery and Development of Peptide Therapeutics. *Amino Acids* **2020**, *52* (9), 1207–1226. <https://doi.org/10.1007/s00726-020-02890-9>.
- (84) Wu, H.; Huang, J. Optimization of Protein and Peptide Drugs Based on the Mechanisms of Kidney Clearance. *Protein Pept. Lett.* **2018**, *25* (6), 514–521.
- (85) Zhou, K.; Zheng, X.; Xu, H.; Zhang, J.; Chen, Y.; Xi, T.; Feng, T. Studies of Poly (Ethylene Glycol) Modification of HM-3 Polypeptides. **2009**, 932–936.
- (86) Hoppenz, P.; Els-Heindl, S.; Beck-Sickinger, A. G. Peptide-Drug Conjugates and Their Targets in Advanced Cancer Therapies. *Front. Chem.* **2020**, *8* (July), 1–24. <https://doi.org/10.3389/fchem.2020.00571>.

- (87) Vrettos, E. I.; Mező, G.; Tzakos, A. G. On the Design Principles of Peptide–Drug Conjugates for Targeted Drug Delivery to the Malignant Tumor Site. *Beilstein J. Org. Chem.* **2018**, *14*, 930–954. <https://doi.org/10.3762/BJOC.14.80>.
- (88) Ruan, H.; Chen, X.; Xie, C.; Li, B.; Ying, M.; Liu, Y.; Zhang, M.; Zhang, X.; Zhan, C.; Lu, W.; Lu, W. Stapled RGD Peptide Enables Glioma-Targeted Drug Delivery by Overcoming Multiple Barriers. *ACS Appl. Mater. Interfaces* **2017**, *9* (21), 17745–17756. <https://doi.org/10.1021/acsami.7b03682>.
- (89) Kalimuthu, K.; Lubin, B. C.; Bazylevich, A.; Gellerman, G.; Shpilberg, O.; Luboshits, G.; Firer, M. A. Gold Nanoparticles Stabilize Peptide-Drug-Conjugates for Sustained Targeted Drug Delivery to Cancer Cells. *J. Nanobiotechnology* **2018**, *16* (1), 1–13. <https://doi.org/10.1186/s12951-018-0362-1>.
- (90) Mitchell, M. J.; Billingsley, M. M.; Haley, R. M.; Wechsler, M. E.; Peppas, N. A.; Langer, R. Engineering Precision Nanoparticles for Drug Delivery. *Nat. Rev. Drug Discov.* **2021**, *20* (2), 101–124. <https://doi.org/10.1038/s41573-020-0090-8>.
- (91) Röder, R.; Preiß, T.; Hirschle, P.; Steinborn, B.; Zimpel, A.; Höhn, M.; Rädler, J. O.; Bein, T.; Wagner, E.; Wuttke, S.; Lächelt, U. Multifunctional Nanoparticles by Coordinative Self-Assembly of His-Tagged Units with Metal-Organic Frameworks. *J. Am. Chem. Soc.* **2017**, *139* (6), 2359–2368. <https://doi.org/10.1021/jacs.6b11934>.
- (92) Navarro-Sánchez, J.; Argente-García, A. I.; Moliner-Martínez, Y.; Roca-Sanjuán, D.; Antypov, D.; Campíns-Falcó, P.; Rosseinsky, M. J.; Martí-Gastaldo, C. Peptide Metal-Organic Frameworks for Enantioselective Separation of Chiral Drugs. *J. Am. Chem. Soc.* **2017**, *139* (12), 4294–4297. <https://doi.org/10.1021/jacs.7b00280>.
- (93) Martí-Gastaldo, C.; Warren, J. E.; Stylianou, K. C.; Flack, N. L. O.; Rosseinsky, M. J. Enhanced Stability in Rigid Peptide-Based Porous Materials. *Angew. Chemie - Int. Ed.* **2012**, *51* (44), 11044–11048. <https://doi.org/10.1002/anie.201203929>.

- (94) Katsoulidis, A. P.; Park, K. S.; Antypov, D.; Martí-Gastaldo, C.; Miller, G. J.; Warren, J. E.; Robertson, C. M.; Blanc, F.; Darling, G. R.; Berry, N. G.; Purton, J. A.; Adams, D. J.; Rosseinsky, M. J. Guest-Adaptable and Water-Stable Peptide-Based Porous Materials by Imidazolate Side Chain Control. *Angew. Chemie - Int. Ed.* **2014**, *53* (1), 193–198. <https://doi.org/10.1002/anie.201307074>.
- (95) Ren, L.; Lv, J.; Wang, H.; Cheng, Y. A Coordinative Dendrimer Achieves Excellent Efficiency in Cytosolic Protein and Peptide Delivery. *Angew. Chemie - Int. Ed.* **2020**, *59* (12), 4711–4719. <https://doi.org/10.1002/anie.201914970>.
- (96) Yu, X.; Gou, X.; Wu, P.; Han, L.; Tian, D.; Du, F.; Chen, Z.; Liu, F.; Deng, G.; Chen, A. T.; Ma, C.; Liu, J.; Hashmi, S. M.; Guo, X.; Wang, X.; Zhao, H.; Liu, X.; Zhu, X.; Sheth, K.; Chen, Q.; Fan, L.; Zhou, J. Activatable Protein Nanoparticles for Targeted Delivery of Therapeutic Peptides. *Adv. Mater.* **2018**, *1705383* (30), 1–7. <https://doi.org/10.1002/adma.201705383>.
- (97) Tomoya Suma, Jiwei Cui, Markus Müllner, Shiwei Fu, Jenny Tran, Ka Fung Noi, Yi Ju, and F. C. Modulated Fragmentation of Proapoptotic Peptide Nanoparticles Regulates Cytotoxicity. *J. Am. Chem. Soc.* **2017**, *139* (10), 4009–4018. <https://doi.org/10.1021/jacs.6b11302>.
- (98) Chrysafis, C.; Said, A.; Drukarev, A.; Islam, A.; Pearlman, W. A. POLYHYDROXY PHENOLS AND THEIR USE IN BINDING P-SELECTIN. *Int. Pat.* **2017**, *1* (12), 8.
- (99) Zhang, Z.; Sun, L.; Zhou, G.; Xie, P.; Ye, J. Sepia Ink Oligopeptide Induces Apoptosis and Growth Inhibition in Human Lung Cancer Cells. *Oncotarget* **2017**, *8* (14), 23202–23212. <https://doi.org/10.18632/oncotarget.15539>.
- (100) Yang, L.; Mashima, T.; Sato, S.; Mochizuki, M.; Sakamoto, H.; Yamori, T.; Ohhara, T.; Tsuruo, T. Predominant Suppression of Apoptosome by Inhibitor of Apoptosis Protein in Non-Small Cell Lung Cancer H460 Cells: Therapeutic Effect of a Novel Polyarginine-Conjugated Smac Peptide. *Cancer Res.* **2003**, *63* (4),

831–837.

- (101) Wang, Q.; Tian, S.; Ning, P. Degradation Mechanism of Methylene Blue in a Heterogeneous Fenton-like Reaction Catalyzed by Ferrocene. *Ind. Eng. Chem. Res.* **2014**, *53* (2), 643–649. <https://doi.org/10.1021/ie403402q>.
- (102) Jin, Q.; Zhu, W.; Jiang, D.; Zhang, R.; Kutyreff, C. J.; Engle, J. W.; Huang, P.; Cai, W.; Liu, Z.; Cheng, L. Ultra-Small Iron-Gallic Acid Coordination Polymer Nanoparticles for Chelator-Free Labeling of ^{64}Cu and Multimodal Imaging-Guided Photothermal Therapy. *Nanoscale* **2017**, *9* (34), 12609–12617. <https://doi.org/10.1039/c7nr03086j>.
- (103) Fazary, A. E.; Taha, M.; Ju, Y. H. Iron Complexation Studies of Gallic Acid. *J. Chem. Eng. Data* **2009**, *54* (1), 35–42. <https://doi.org/10.1021/je800441u>.
- (104) Koczur, K. M.; Mourdikoudis, S.; Polavarapu, L.; Skrabalak, S. E. Polyvinylpyrrolidone (PVP) in Nanoparticle Synthesis. *Dalt. Trans.* **2015**, *44* (41), 17883–17905. <https://doi.org/10.1039/c5dt02964c>.
- (105) Stopford, W.; Turner, J.; Cappellini, D.; Brock, T. Bioaccessibility Testing of Cobalt Compounds. *J. Environ. Monit.* **2003**, *5* (4), 675–680. <https://doi.org/10.1039/b302257a>.

9 Publication

F Shen, Y Lin, M Höhn, X Luo, M Döblinger, E Wagner, U Lächelt (2023) Iron-Gallic Acid Peptide Nanoparticles as a Versatile Platform for Cellular Delivery with Synergistic ROS Enhancement Effect. *Pharmaceutics* **15** (7), 1789.

10 Acknowledgements

I would like to express my deep gratitude to the people who have supported and encouraged me throughout my journey in completing this PhD thesis.

First of all, I would like to thank Prof. Dr. Ernst Wagner for the opportunities he has provided me to grow and learn as a researcher in his group. I greatly appreciate his support and professional guidance.

Next, I would like to thank Ass-Prof. Dr. Ulrich Lächelt for his invaluable guidance, unwavering support, and constructive feedback throughout my research. I have learned a lot from him and his passion for the chemistry and the science motivated me a lot during the past four years. I am truly grateful for the time and effort he has invested in me.

I also especially want to thank Dr. Yi Lin, Paul Folda, Fengrong Zhang and Xianjin Luo for spending so much time on cell culture work to test my synthesized nanoparticles, and we have very great collaboration. All synthetic work would be irrelevant without your contribution! It was great teamwork that added up perfectly within different projects.

I thank Teoman Benli-Hoppe, Simone Berger, Tobias Burghardt and Melina Grau and for the MALDI-TOF-MS measurements. They really support my work on this very important characterization. I would like to thank Dr. Lun Peng, for teaching me solid-phase synthesis during my first weeks in the lab and for providing scientific advice whenever needed.

I would like to thank my colleagues, Anna-Lina Lessl, Özgür Öztürk for every week's discussion. Many thanks to Wolfgang Rödl for the support with our technical equipment, for repairing almost any broken instrument or computer and for ensuring the technical maintenance, as well as Olga Brück, Miriam Höhn, Ursula Biebl and Melinda Kiss for keeping the lab running, so that we could focus on science issues due to their contributions to the group.

I would also like to thank our lunch group (Dr. Jie Luo, Dr. Yanfang, Dr. Yi Lin, Dr. Lun Peng, Dr. Meng Lyu, Fengrong Zhang and Xianjin Luo) for the interesting and extensive discussions about science and life.

I also owe my sincere gratitude to my friends (Chenglong Guo, Yongsheng Han, Xueyin Liu, Hongcheng Mai, Zhouyi Rong) who gave me their help and time by listening to me and helping me work out my problems during the difficulties in my PhD study.

Many thanks to all the AK Wagner members for giving me a comfortable learning atmosphere and an unforgettable time we spent together. Special thanks to China Scholarship Council for supporting my study and life in Munich.

Then, my thanks would go to my beloved family for their loving consideration and great confidence in me all through these years. Their silent support gave me the courage and confidence to face whatever happens.

Finally, I really want to thank my wife who created a comfortable environment that allowed me to focus on my work without any worries, and gave me some great advice in study and life.

Thank you all for your support and encouragement, and for making this journey a truly unforgettable experience.